MEHMET AYAR

METU 2005

DESIGN OF
AN ELECTROMAGNETIC CLASSIFIER
FOR SPHERICAL TARGETS

MEHMET AYAR

APRIL 2005

DESIGN OF
AN ELECTROMAGNETIC CLASSIFIER
FOR SPHERICAL TARGETS

A THESIS SUBMITTED TO
THE GRADUATE SCHOOL OF NATURAL AND APPLIED SCIENCES
OF
MIDDLE EAST TECHNICAL UNIVERSITY

BY

MEHMET AYAR

IN PARTIAL FULFILLMENT OF THE REQUIREMENTS
FOR THE DEGREE OF MASTER OF SCIENCE
IN
ELECTRICAL AND ELECTRONICS ENGINEERING

APRIL 2005

Approval of the Graduate School of Natural and Applied Sciences

Prof. Dr. Canan ÖZGEN
Director

I certify that this thesis satisfies all the requirements as a thesis for the degree of Master of Science.

Prof. Dr. İsmet ERKMEN
Head of Department

This is to certify that we have read this thesis and that in our opinion it is fully adequate, in scope and quality, as a thesis for the degree of Master of Science.

Prof. Dr. Gönül TURHAN SAYAN
Supervisor

Examining Committee Members

Prof. Dr. Canan TOKER	(METU,EE)	
Prof. Dr. Gönül TURHAN-SAYAN	(METU,EE)	
Prof. Dr. Mustafa KUZUOĞLU	(METU,EE)	
Prof. Dr. Kemal LEBLEBİCİOĞLU	(METU,EE)	
Yakup TAŞDELEN, M.S.	(Sav.San.Müst.)	

I hereby declare that all information in this document has been obtained and presented in accordance with academic rules and ethical conduct. I also declare that, as required by these rules and conduct, I have fully cited referenced all material and results that are not original to this work.

Name, Last name: Mehmet AYAR

Signature :

ABSTRACT

DESIGN OF
AN ELECTROMAGNETIC CLASSIFIER FOR SPHERICAL TARGETS

AYAR, Mehmet
M.S., Department of Electrical and Electronics Engineering
Supervisor :Prof. Dr. Gönül TURHAN SAYAN

APRIL 2005, 92 pages

This thesis applies an electromagnetic feature extraction technique to design electromagnetic target classifiers for conductors, dielectrics and dielectric coated conductors using their natural resonance related late-time scattered responses. Classifier databases contain scattered data at only a few aspects for each candidate target. The targets are dielectric spheres of varying sizes and refractive indices, perfectly conducting spheres varying sizes and dielectric coated conducting spheres of varying refractive indices and thickness in coating. The applied classifier design technique is suitable for real-time target classification because of the computational efficiency of feature extraction and decision making approaches. The Wigner-Ville Distribution (WD) is employed in this study in addition to the Principal Components Analysis (PCA) technique to extract target features mainly from late-time target responses. WD is applied to the back-scattered responses at different aspects. To decrease aspect dependency, feature vectors are extracted from selected late-time portions of the WD outputs that include natural resonance related information. Principal components analysis is also used to fuse the feature vectors and/or late-time target responses extracted from reference aspects of a given target into a single characteristic feature vector for each target to further reduce aspect dependency.

Keywords: Electromagnetic target classification, time-frequency analysis, Wigner-Ville distribution, principal component analysis, feature extraction.

ÖZ

KÜRESEL HEDEFLER İÇİN ELEKTROMANYETİK SINIFLANDIRICI TASARIMI

AYAR, Mehmet
Y. Lisans, Elektrik ve Elektronik Mühendisliği Bölümü
Tez Yöneticisi : Prof. Dr. Gönül TURHAN SAYAN

APRIL 2005, 92 sayfa

Bu tez iletkenler, dielektrikler ve dielektrik kaplı iletkenler için bir hedeflerin saçılan sinyallerinin geç zamanlarındaki doğal salınımlarını kullanan elektromanyetik hedef sınıflandırıcılar tasarlamak için bir elektromanyetik hedef özçıkarım tekniği kullanır. Sınıflandırıcı veri bankaları her muhtemel hedefin sadece bir kaç açıdaki saçılım verilerini içerir. Hedefler büyüklükleri ve kırınım indeksleri farklı küreler, büyüklükleri farklı iletken küreler, kırınım indeksleri ve kaplama kalınlığı farklı dielektrik madde kaplı iletken kürelerdir. Uygulanan sınıflandırıcı tasarım tekniği nitelik özçıkarım ve karar verme yaklaışmları verimliliği sebebiyle gerçek zamanlı sınıflandırma için uygundur. Bu çalışmada, hedeflerin geç zaman tepkilerinden özniteliklerini çıkarmak amacıyla Wigner-Ville Dağılımı (WD) hedeflerin geç zaman Esas Bileşenler Analizi (PCA) tekniğine ilave olarak kullanılmıştır. WD değişik açılardan gelen geri saçılan tepkilere uygulanmıştır. Açısal bağımlılığı azaltmak maksadıyla, öz nitelik vektörleri WD çıktılarının doğal rezonanslarla ilgili bilgileri içeren seçilmiş geç zaman bölümlerinden çıkartılmıştır. Esas Bileşenler Analizi tekniği, açısal bağımlılığı daha da düşürmek amacıyla, herbir hedef için referans açılarında üretilmiş öz nitelik vektörlerinin ve/veya geç zaman hedef tepkilerinin, hedefi tanımlayan tek bir öz nitelik vektöründe toplanmasında kullanılmıştır.

Anahtar sözcükler: Elektromanyetik hedef sınıflandırma, zaman-frekans analizi, Wigner-Ville dağılımı, esas bileşenler analizi, öznitelik çıkarımı.

To My Daughter Meryem

ACKNOWLEDGEMENTS

I wish to express my deepest gratitude to my supervisor Prof. Dr. Gönül TURHAN SAYAN for her guidance, advices, criticism and encouragements and insight throughout the research. I would like to thank also for giving me the opportunity to work on this issue. She has been a great source of inspiration and her invaluable guidance and timely input has helped me throughout my Masters Degree program at the METU.

My special thanks and appreciation goes to my wife Mehtap AYAR who has shared the entire burden of the study with me and provided constant encouragement. Without her encouragement and support, it would not be possible for me to complete this study.

TABLE OF CONTENTS

LIST OF TABLES

LIST OF FIGURES

LIST OF ABBREVIATIONS AND ACRONYMS

CCF	Correct Classification Factor
CCM	Complete Class Match
CFR	Complex Frequency Response
CNR	Complex Natural Resonance
EW	Electronic Warfare
FFV	Fused Feature Vector
FSS	Fused Scattered Signal
IFFT	Inverse Fast Fourier Transformation
LTFV	Late-Time Feature Vector
LTSS	Late-Time Scattered Signal
MRM	Maximum Reference Match
NN	Neural Network
PC	Principal Component
PCA	Principal Component Analysis
RDc	Correct Decision Rate
SEM	Singularity Expansion Method
SNR	Signal to Noise Ratio
UWB	Ultra-Wide Band
WD	Wigner-Ville Distribution

CHAPTER I

INTRODUCTION

Design of an electromagnetic target classifier using the scattered electromagnetic fields for target characterization is a difficult task. Since the related scattering mechanisms are very complicated with signals being strongly dependent on frequency, polarization and aspect angle of the transmittance and reception, classification of targets is almost impossible without using feature extraction. In particular, the aspect dependency makes the recognition problem quite complex. Therefore, intelligent feature extraction techniques should be used to characterize targets with minimized sensitivity to aspect variations.

Two important problems exist in target classification. One is the feature extraction problem from the input signals, and the other is the decision problem based on the extracted features. The feature extraction can also be called as the target characterization; its purpose is to extract some distinctive features of a given target from its unprocessed scattered data. Collecting of such features lead to construction of a feature vector.

The simplest feature vector associated with a scattered signal consists of its linear expansion coefficients with respect to a basis, and the most common expansion of this sort is the Fourier transform. However, the Fourier transform does not provide localization both in time and frequency. Recently, there has been an increasing interest in joint time-frequency analysis (e.g., short-time Fourier transform, Wigner- Ville distribution, Gabor expansion, wavelet transform, etc.) as feature extractors to fill this gap in signal analysis [1]–[15].

The time-frequency techniques, which can be used for feature extraction, can be classified into two main categories: linear transforms (e.g., Short-Time Fourier Transform, Gabor expansion, Wavelet Transform) and quadratic transforms (e.g., Wigner-Ville Distribution, Page Distribution, Choi-Williams Distribution, etc.).

In the area of electromagnetic target recognition, various target classification techniques have been proposed in literature. A considerable amount of techniques make use of natural scattered response of a target [2], [3], [16], [17], [18], [19]. Neural Network (NN) analysis based techniques [1], [4], [12], [20], [21], [22], [23] are also very common. However, NN based feature extraction techniques have two main disadvantages; first of all NN needs a large set of scattering data at many different aspects for each target in the database. A large database for each target is not desirable, because generally it is neither feasible nor practical as in real world applications obtaining data for practical targets may be very difficult. Secondly, improving the database or adding a new target or a new reference data in the case of a NN type classifier requires training the whole network possibly with a new structure according to this new reference database [2], [3]. Because of the disadvantages just mentioned, NN type feature extraction techniques are not preferred in this thesis.

The main objective of the overall signal processing scheme used in this work is to design a classifier which identifies spherical targets that has different physical (material composition) properties or geometrical parameters. To fulfill this objective, each target of concern will be represented by a single characteristic feature vector in an almost aspect independent manner [2], [3].

For this purpose first, moderately aspect dependent late-time energy feature vectors are extracted from the extremely aspect-variant time-domain scattered signals of a given target class at several designated reference aspects. The Wigner-Ville Distribution (WD) is used as the main signal processing tool for feature extraction as discussed in [2], [3] as distribution of the target's natural-resonance related scattered energy over a selected late time segment of the joint time frequency plane can be characterized in this way. Feature extraction scheme employed in this procedure is inspired by the Singularity Expansion Method (SEM) [24] which describes the resonant behavior of scattered electromagnetic field when the target is represented by a linear, time-invariant system model [25]. The WD-based feature extraction technique is based on the resonance features of target signatures when it makes use of sufficiently late-time scattered response data. In this way, utilization of the highly dominant natural resonance mechanisms of the targets become possible and leads to significantly increased correct classification rates as demonstrated by Turhan-Sayan in [2], [3]. Additional to the use of WD, Principal Component Analysis (PCA) is also applied in the feature extraction procedure as the second step. Late-time feature vectors (LTFV) obtained for a given target at different design aspects are fused by using the PCA technique to obtain a single characteristic late-time feature vector called the fused feature vector (FFV) to represent this target. The resulting WD/PCA based feature extraction/target recognition technique [3] offers a simple, easily repeatable and a computationally efficient classifier design approach as compared to the alternative electromagnetic target recognition techniques, including techniques such as the E-pulse and K-pulse techniques which are also based on natural resonance concept [17,19,26,27].

In this thesis, we will focus on designing an electromagnetic target classifier to identify perfectly conducting spheres, perfect dielectric, and dielectric coated conducting spheres using the WD/PCA based natural resonance based feature extraction technique shortly explained using scattered data at only a few reference aspects. This approach will provide high correct classification rates, low memory consumption, and high detection speed as well as high correct classification rates and robustness even under excessive noise.

The organization of the thesis is as follows:

Chapter 2 describes the details of the WD/PCA and natural resonance based feature extraction technique used in this thesis.

In Chapter 3, the process of the generation of back-scattering electromagnetic signals in frequency domain will be discussed. The design of classifiers for different target sets of perfectly conducting spheres, perfect dielectric spheres, and dielectric coated conducting spheres will be demonstrated. The noise performance of the classification technique will also be investigated.

Finally, in Chapter 4, the concluding remarks will be presented.

CHAPTER II

BASIC THEORY AND A NATURAL-RESONANCE BASED FEATURE EXTRACTION TECHNIQUE

2.1. Basics

The natural-resonance based feature extraction technique that is used in this thesis for target recognition will be explained in this chapter with its theoretical foundation. We will call this specific technique as the "core technique" throughout this thesis. Following the preliminary research reported in [2], the core technique has been introduced for the first time by Turhan-Sayan [3] and applied for dielectric targets. Recently, its application is extended to targets modeled by perfectly conducting wire structures by Ersoy and Turhan-Sayan in [13]. In the present study, our main goal is to investigate the applicability of this technique to large number of targets, which differ from each other by their material composition, such as perfectly conducting, dielectric and dielectric coated conducting spheres.

Shape, size and material properties of a target determine the values of complex natural resonance (CNR) frequencies (or system poles as also called) of a target. Target poles are known to be independent of aspect and polarization conditions [24]. In the core technique utilized in this work, CNR frequencies are not used directly, but their effects will be used indirectly over the late-time region of time-domain scattered signals.

The well-known singularity expansion (SEM) method formulates the complex natural resonance mechanism in linear system models of targets

[24, 35, 36]. In this context, in the complex frequency domain, the aspect-dependent system function of the target which is modeled as a distributed linear, time-invariant system, can be given as

$$H(s,\Omega) = A(s,\Omega) + \sum_{n=1}^{\infty} \frac{R_n(s,\Omega)}{(s-s_n)(s-s_n^*)} \tag{2.1}$$

where

$$s = \sigma + jw \tag{2.2}$$

is the complex frequency variable

with $w = 2\pi f$ (2.3)

being the angular frequency. $A(s,\Omega)$ is the an entire function having no singularities in the complex frequency plane. The s_n's are complex-valued system poles occurring in complex conjugate pairs. $R_n(s,\Omega)$'s are the residue system poles.

The Inverse Laplace transform of this expression can be expressed in the general form,

$$h(t,\Omega) = a(t,\Omega) + \sum_{n=1}^{\infty} b_n(\Omega) e^{-\sigma_n t} \cos(w_n t + \theta_n) \tag{2.4}$$

where h(t,Ω) is the aspect dependent impulse response of the target. The symbol Ω represents the aspect dependency in Equations (2.1) and (2.4).

The function $a(t,\Omega)$ is needed to represent the forced response stemming from the direct interaction of the excitation (the impulse function) with the target. When the target is of finite size, the function $a(t,\Omega)$ is strictly an early-time contribution lasting as long as the transition time of the excitation over the target.

The summation in Equation (2.4), which is composed of damped sinusoidal signals, is the natural impulse response of the target. The contribution of each target pole pair (s_n and s_n*) to the target response depends on the value of the associated residues, R_n's in Equation (2.1). As the aspect of scattered signal changes, the residues of the target poles change accordingly. Therefore, a pole pair which is very dominant at one aspect may be weakly excited at another aspect contributing to the overall response at a negligible level. On the other hand, a target pole pair leads to a long lasting oscillation in time, if σ_n (the negative real parts of s_n and s_n*) which is called the attenuation constant (or damping coefficient), is small in magnitude. For these reasons, the scattering data of a target must be used at a sufficiently large set of different aspects to capture information about most of the dominant CNR frequencies available in late-time responses at various aspect angles. This procedure helps reducing the aspect dependency of the scattered data that complicates the problem of target classification. To extract target specific information from the target response in the late time region, we can use a joint time-frequency representation. Theoretically, localization of the natural response over the joint time-frequency domain is closely related to the real and imaginary parts of target poles [2]. To avoid the effects of the highly aspect dependent nature of early-time (forced) part of the target's scattered response, the relatively late-time portions of the time-frequency distribution matrices will be used in the feature extraction process.

2.2. The Usage of WD in Feature Extraction Process

The auto Wigner-Ville Distribution (WD) is used to get useful energy related information from the selected late-time portion of the target response signal at every predefined aspect angle. The WD is considered to be more useful than the other time-frequency distributions as it satisfies a large set of desired properties including the important marginal properties. It is important to note that the late-time feature vectors obtained by using this WD based feature extraction technique, was found considerably less sensitive to aspect variations as compared to the corresponding time-domain scattered signals for spherical dielectric structures by Turhan-Sayan in [2].

For a classification problem, extracting feature vectors using a common time interval and a common frequency-band for all candidate targets and for all aspects is very important. For gain invariant classification, the total energy of all the signals, used in classification database, are normalized to unity at the beginning of the feature extraction process. The time-frequency analysis of these normalized signals will be carried on by evaluating the auto WD of each signal. The auto WD of a time signal $x(t)$ is defined as,

$$W_x(t,f) = \int_{\tau} x(t+\frac{\tau}{2})x^*(t-\frac{\tau}{2})e^{-j2\pi f\tau}d\tau \tag{2.5}$$

where the superscript (*) shows complex conjugation. WD satisfies marginal properties

$$\int_{f} W_x(t,f)df = p_x(t) = |x(t)|^2 \tag{2.6}$$

$$\int_{t} W_x(t,f)dt = P_x(f) = |X(f)|^2 \tag{2.7}$$

where X(f) is the Fourier transform of the signal x(t), $p_x(t)$ and $P_x(f)$ denotes the instantaneous power and the spectral energy density of the signal, respectively. Satisfaction of marginal properties do not mean that the WD output gives an exact time-frequency energy density defined at every point in the time-frequency plane as explained by uncertainty principle which does not allow infinite resolution in both time and frequency simultaneously [37]. Since WD outputs have very strong and highly oscillatory interference terms that may seriously deteriorate the identification capability of the classifier [3]. Although no negative energy exists in real world, the WD outputs may have negative values due to interference terms in joint time-frequency plane. Getting rid of such unwanted negative entries by replacing the negative entries by zeros in the WD output matrix is an empirical remedy used to improve the classification performance remarkably as discussed in [2].

The modified auto WD of a signal is constructed by taking only its non-negative entries by using the formula in Equation (2.8).

$$\widetilde{W}_x(t,f) = \frac{W_x(t,f) + abs(W_x(t,f))}{2} \tag{2.8}$$

Even after getting rid of such negative WD values, the discrete WD output utilized in the matrix form is not found to be useful enough for target classification.

2.3. Construction of Late-Time Feature Vectors

WD values needs to be further processed to obtain a partitioned energy density vector for better characterization of the target.

Because, for all real-valued signals, the WD output matrix has even symmetry with respect to frequency, it is enough to process on the non-negative frequency portion of WD matrix which has a size of (N/2 x N). Before WD calculations, the time-domain signal x(t) is normalized such that its total energy is equal to unity. Then, the total time span T_0, is divided into Q time bands which have equal length of T_0/Q seconds. The amount of energy contributed to each time bands q by a spectral component f_m is given by [2] as

$$E_q(f_m) = \int_{(q-1)\Delta}^{q\Delta} W_x(t, f_m)dt \quad \text{for q=1,2,3,......Q} \tag{2.9}$$

where $\Delta = T_0$/Q , m =1,2,....,N/2 and $f_m = (m-1)/(2T_0)$.

Energies provided by each spectral component f_m into q^{th} subinterval, can be put into a vector form,

$$\overline{E_q} = [\, E_q(f_1) \quad E_q(f_2) \,.......\, E_q(f_{N/2}) \,] \tag{2.10}$$

Because there are Q bands at all, the partitioned energy density vector $\overline{E}$ is given as a combined form of Equation (2.10) for each subinterval q;

$$\overline{E} = [\, \overline{E_1} \quad \overline{E_2} \,.............\, \overline{E_Q} \,] \tag{2.11}$$

that has the length of N/2 x Q. This process is performed on total time span. Since, we need to get natural resonance components that appear in late-time region of data, taking two successive time bands (q*and q*+1) in feature vector construction is useful to seize some discerning information about the real parts of the natural resonance frequencies. By this way, target characterization capability of the classifier can be enhanced significantly as discussed in [3].

Selecting Q value which is the number of time bands that total time span T_0 would be divided into, and selecting discerning bands (q* and q*+1) are two major milestones for designing a classifier based on technique discussed in this thesis. Using late-time scattered field information is essential to utilize feature extraction successfully. Because the feature extraction technique used in this thesis is intended to utilize the target's natural resonance mechanisms.

We need to obtain a Late-Time Feature Vectors (LTFV) as to be demonstrated in next chapter to construct the reference database of the classifier using the LTFVs reduce aspect dependency of the classifier.

Q and q* are chosen by using scattered data only at the reference aspects. In this work, five aspects are selected same as in reference [2] and [3]. The optimum value of Q for a classifier design will be selected as follows:

First of all for a specific target, a set of partitioned energy density vectors is computed for a given Q value, at all K reference aspects using (2.11). In this work K is selected as 5 and the reference aspects are 180-5, 180-45, 180-90, 180-135 and 180-179. Secondly, the pair-wise correlation coefficients between the resulting full-time feature vectors are computed within this set. By this process, we construct a sequence of correlation coefficients. Finally, the variance of this sequence is computed. The process repeated for the same target for each candidate value of Q. We need these computed variances to be as small as possible to determine the best value of Q that provides the smallest aspect dependency. The Q value that corresponds to the smallest varience should be chosen as the optimum Q value for that target. The same procedure can be repeated for all targets in the classifier to make sure that the selected Q value is suitable for all targets.

After selection of the optimum value of Q, the optimum value of q*, determined as follows:

The value of q* is selected using Correct Classification Factor (CCF) introduced in [2]. CCF can be computed by Equation (2.12) below,

$$CCF\ (q^*) = \frac{1}{M_{tar}K^2}\sum_{i,j} r_{i,j}^{matched} - \frac{1}{(M_{tar}{}^2 - M_{tar})K^2}\sum_{i,j} r_{i,j}^{mismatched} \tag{2.12}$$

where M_{tar} is the number of targets and K is the number of reference aspects, $r_{i,j}^{matched}$ is the correlation coefficient between any two LTFVs which belong to the same target at different aspects (matched case), $r_{i,j}^{mismatched}$ is the correlation coefficient between any two LTFVs which belong to different targets (mismatched case).

Since high correlation coefficients between the matched feature vectors and low correlation coefficients between the mismatched feature vectors are expected, the factor CCF must be as large as possible to satisfy our design objectives. The optimal value of q* is selected to get the largest CCF value. To stay away from the low SNR, which happens at the very late time zone of the scattered data, and to keep as much of the useful resonance information as possible the optimal value for q* is selected at a value for which the CCF makes a big jump. The LTFVs are constructed for this optimum q*.

2.4. Usage of PCA on extracted features

To reduce aspect dependency, principal component analysis (PCA) is used for obtaining a single characteristic feature vector for each target from the late-time feature vectors extracted at the reference aspects. The resulting feature vector can effectively represent the target over a broad range of aspects.

In general, PCA is a method for identifying patterns in data, and expressing different sets of data in such a way as to highlight their similarities and differences. Since patterns in data can be hard to find in data of high dimension, where the luxury of graphical representation is not available, PCA is a powerful tool for analysing data. The other main advantage of PCA is data by reducing the number of dimensions, without much loss of information. In this study, we will use the PCA technique for feature extraction through multi-aspect feature fusion as introduced by Turhan-Sayan in [3].

In the previous sections, we described how to select our design parameters and construct LTFVs. Now, we will use Principal Component Analysis (PCA) to reduce the computational time and to increase the classification accuracy.

Owing to PCA, for a target, LTFVs of all reference aspects can be integrated into a single vector which is called ‘Fused Feature Vector’ (FFV). Test process can be done by comparing test LTFV with only FFVs of each target. Because of that, dimensionality and consequently computational time is reduced by a factor of number of reference aspects K. More importantly, b using the PCA, we can further decrease aspect dependency and increase accuracy performance of the classifier.

We will describe the basic procedure of this PCA-based multi-aspect feature fusion technique as follows: Assume that we have K reference aspects, N is the length of each corresponding LTFVs, and F is feature matrix of size K x N whose rows are LTFVs of size 1xN each, belonging to a given target class at K reference aspect.

$$F^T = [\overline{e}_1^T \quad \overline{e}_2^T \ .... \ \overline{e}_K^T] \tag{2.13}$$

where T denotes the transpose operator.

The covariance matrix S_F of the feature matrix F, is a symmetric matrix (of size K x K) is given as;

$$S_F = \begin{bmatrix} s_1^{\ 2} & s_{12} & \cdots & s_{1K} \\ s_{21} & s_2^{\ 2} & \cdots & s_{2K} \\ . & . & & . \\ . & . & & . \\ . & . & & . \\ s_{K1} & s_{K2} & \cdots & s_K^{\ 2} \end{bmatrix} \qquad (2.14)$$

where its off-diagonal entries $s_{ij} = s_{ij}$ denote covariance between feature vectors $\overline{e_i}$ and $\overline{e}_j$, and the diagonal entries s_i^2 represents the variance of feature vectors $\overline{e_i}$. The correlation coefficient $r_{i,j}$ between the feature vectors $\overline{e_i}$ and $\overline{e}_j$ be defined as;

$$r_{i,j} = \frac{s_{i,j}}{\sqrt{s_i s_i}} \qquad (2.14)$$

The covariance matrix S_F can be transformed into a diagonal matrix Λ using similarity transformation;

$$\Lambda = U^T S_F U \quad = \begin{bmatrix} \lambda_1 & 0 & \cdots & 0 \\ 0 & \lambda_2 & \cdots & 0 \\ . & . & & . \\ . & . & & . \\ . & . & & . \\ 0 & 0 & \cdots & \lambda_K \end{bmatrix} \qquad (2.16)$$

where U is the modal matrix in the form of

$$U = [u_1 \quad u_2 \ldots\ldots\ldots\ldots u_K] \qquad (2.17)$$

with u_i's being the normalized eigenvectors corresponding to eigenvalues of the covariance matrix S_F. The eigenvalues λ_i are then solved from

$$\det(S_F - \lambda I) = 0 \qquad (2.18)$$

where I is the identity matrix of size K x K. Then, λ_i (eigenvalues) are ordered from the highest to the lowest. The corresponding eigenvectors t_i are solved from

$$[S_F - \lambda_i I]t_i = 0 \qquad i=1, 2,.....M \qquad (2.19)$$

These orthogonal eigenvectors are normalized for obtaining the orthonormal eigenvectors,

$$u_i = \frac{t_i}{\sqrt{t_i t_i^T}} = \frac{t_i}{|t_i|} \qquad (2.20)$$

to construct the matrix U that is used to transform the correlated feature vectors into a set of uncorrelated vectors, z_i for i=1,2, ...K

$$Z = \begin{bmatrix} z_1 \\ z_2 \\ \vdots \\ z_K \end{bmatrix} = U^T \begin{bmatrix} \overline{e}_1 - mean\ (\overline{e}_1) I_N \\ \overline{e}_2 - mean\ (\overline{e}_2) I_N \\ \vdots \\ \overline{e}_K - mean\ (\overline{e}_K) I_N \end{bmatrix} \qquad (2.21)$$

where I_N is a unity row vector of length N and the resulting matrix Z has a size of K x N same size with feature matrix F. z_i's will be called the principal components (PCs) of feature matrix F. Each PC vector has zero-mean, and variance of λ_i. The first PC of feature matrix F has the highest correlation coefficients with LTFVs $\overline{e_i}$ since λ_1 has the highest percentage in the summation of λ_i for i=1,2,.....,K as demonstrated in reference [3] and as to be examined in following chapter. Therefore, the first principal component can be regarded as the fused feature vector (FFV) of target by itself neglecting the other principal components.

If needed, the other principal components can be linearly combined to construct the FFV of the target by proper weighting factors ($\overline{\lambda_i}$) as described in Equation (2.23) below,

$$FFV = \sum_{i=1}^{K} \overline{\lambda_i} z_i \qquad (2.22)$$

where

$$\overline{\lambda_i} = \frac{\lambda_i}{\sum_{i=1}^{K} \lambda_i} \qquad (2.23)$$

CHAPTER III

APPLICATIONS

3.1. General

In this chapter, we will present the results for various classifiers which are constructed for perfectly conducting spheres of different sizes, dielectric spheres of exactly the same size but of slightly different permittivity values, dielectric coated perfectly conducting spheres of exactly the same external size but of different permittivity values and of different inner conducting part radius. Due to the presence of a large number of targets with high degree of similarities, the classification problem tackled here is more difficult then the classifier for dielectric only as targets discussed in [2] and [3]. The scattered responses of all these spherical targets can be easily computed from the available analytical solutions [34]. The classification technique employed in this thesis is the same technique as the one proposed in references [2] and [3]. In these references, the proposed technique is tested only to classify dielectric targets. In this work, however, we will discuss and test the performance of this technique to classify perfectly dielectric, conductor or coated conductor spheres. Even, all of these targets will be considered at once to form the catalog of a classifier.

For all the classifiers designed in this thesis the reference and test databases are constructed based on following basic rules:

1. As indicated in Figure 3.1, target responses are synthesized for a plane wave excitation that is linearly polarized in x-direction and propagates in z-direction.

2. By using the analytical solutions depicted in the reference [34] the far field scattered responses are computed at the $\Phi = \pi / 2$ plane for different values of the angle θ in the frequency domain from zero to a maximum frequency of 19.1 GHz at 512 frequency sample points, i.e. with frequency steps Δf= for 37.3 MHz.
3. Bistatic scattered data are synthesized for all targets in the frequency domain at thirteen different values of the bistatic aspect angle θ_b where $\theta_b = 180° - \theta$ and the angle θ assumes the values as follows: θ = 5º, 15º, 30º, 45º, 60º, 75º, 90º, 105º, 120º, 135º, 150º, 165º and 179º.

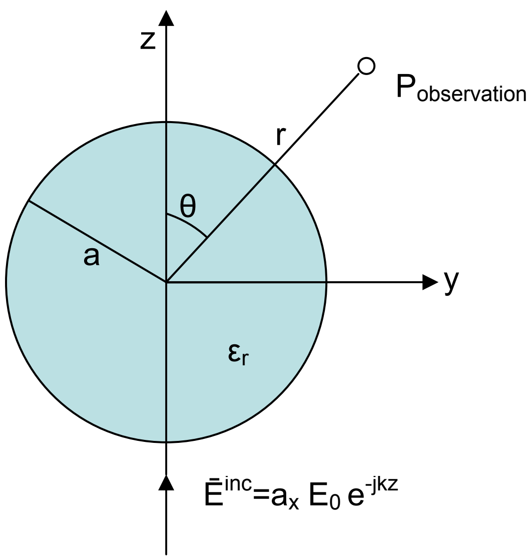

Figure 3.1 Problem geometry used to synthesize electromagnetic signals scattered from the spherical targets.

4. The scattered impulse response waveforms, which are the scattered impulse response waveforms in the approximate sense, are obtained by using the Inverse Fast Fourier Transformation (IFFT) of the windowed frequency-domain data, with 1024 sample points over a

total time span of T_0 = 26.81 nanoseconds i.e. with a time step of Δt=26.8 microseconds.

5. The resulting raw database is composed of "M_{tar} x 13" unprocessed scattered signals as M_{tar} is the number of targets in the classifiers catalog and each target is characterized at 13 bistatic aspects.
6. "M_{tar} x 5" of these signals are used to construct the reference feature database of this M_{tar}-target classifier while the remaining signals are used for testing.
7. Target features are extracted from time-domain scattered signals at five reference aspects θ=5º, 45º, 90º, 135º, 179º (located in aspects almost evenly by about 45 degrees separation).

3.2. Classifier Design for Perfectly Conducting Spheres

3.2.1. Construction of Classifier Database

In this section, three classifiers will be designed for nine different targets where the candidate targets are loss-free perfectly conducting spheres Tcon1, Tcon2, Tcon3, Tcon4, Tcon5, Tcon6, Tcon7, Tcon8, Tcon9 having different radii of 8, 8.5, 9, 9.5, 10, 10.5, 11, 11.5, 12 cm respectively.

The theoretical background of the natural resonance-based feature extraction technique is discussed in Chapter 2 and the basic rules followed for database construction are given in section 3.1.

Three different classifiers designed for the conductor targets are described below in Table 3.1. The design steps are given in detail next.

Table 3.1 classifier description for conductor targets.

Classifiers	Targets
CLCON1	Tcon1(r=8), Tcon5(r=10), Tcon9(r=12)
CLCON2	Tcon1(r=8), Tcon3(r=9), Tcon5(r=10), Tcon7(r=11), Tcon9(r=12)
CLCON3	Tcon1(r=8), Tcon2(r=8.5), Tcon3(r=9), Tcon4(r=9.5), Tcon5(r=10), Tcon6(r=10.5), Tcon7(r=11), Tcon8(r=11.5), Tcon9(r=12)

Step 1: Complex Frequency Responses (CFRs) are numerically synthesized for all targets at all aspects with basic assumptions listed in the section 3.1. As an example to the outputs the magnitude plots of CFRs for Tcon5 at 45, 90 and 165 degrees are plotted in Figure 3.2.

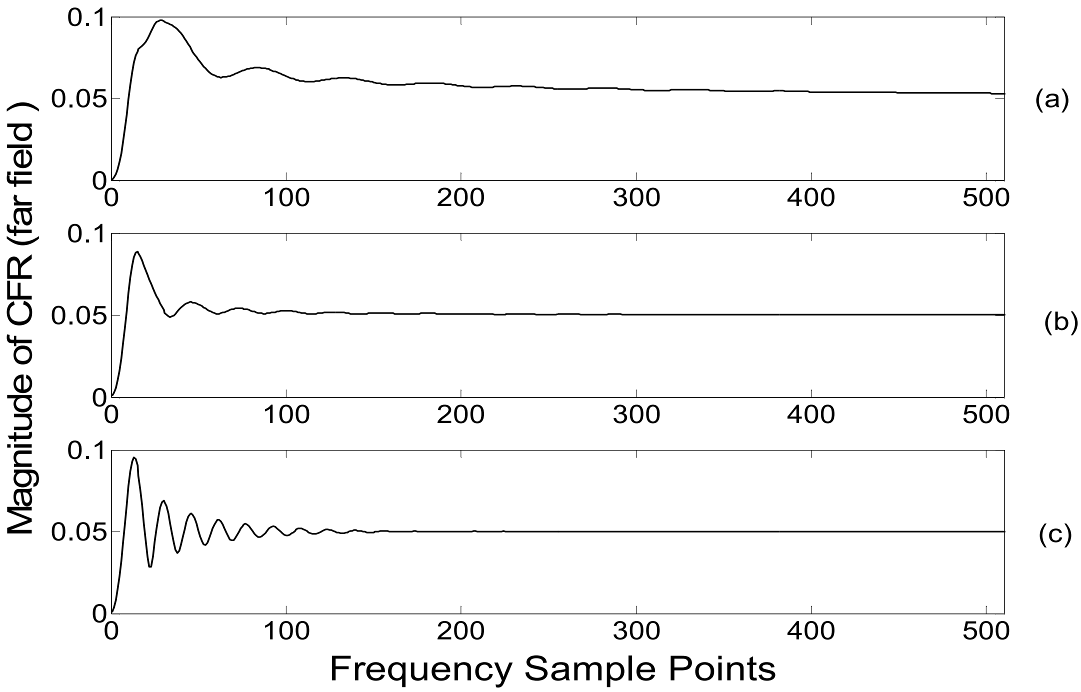

Figure 3.2 Magnitudes of CFRs for Tcon5 (a) 45º ; (b)90º; (c)165º

Step 2: Time-domain scattered responses are obtained from the CFRs by using the Inverse Fast Fourier Transformation (IFFT), with 1024 sample points over a total time span of T_0 = 26.81 nanoseconds. As an example to this step, the scattered responses of Tcon5 at 45, 90 and 165 degrees are shown in Figure 3.3 and Figure 3.4. Target features are extracted from time-domain scattered signals in various ways:

a) Choosing a suitable late time portion of the time domain responses.
b) Applying the PCA to the late-time scattered responses chosen in (a).
c) Applying the WD operation, next the PCA analysis to the late-time scattered response chosen in (a).

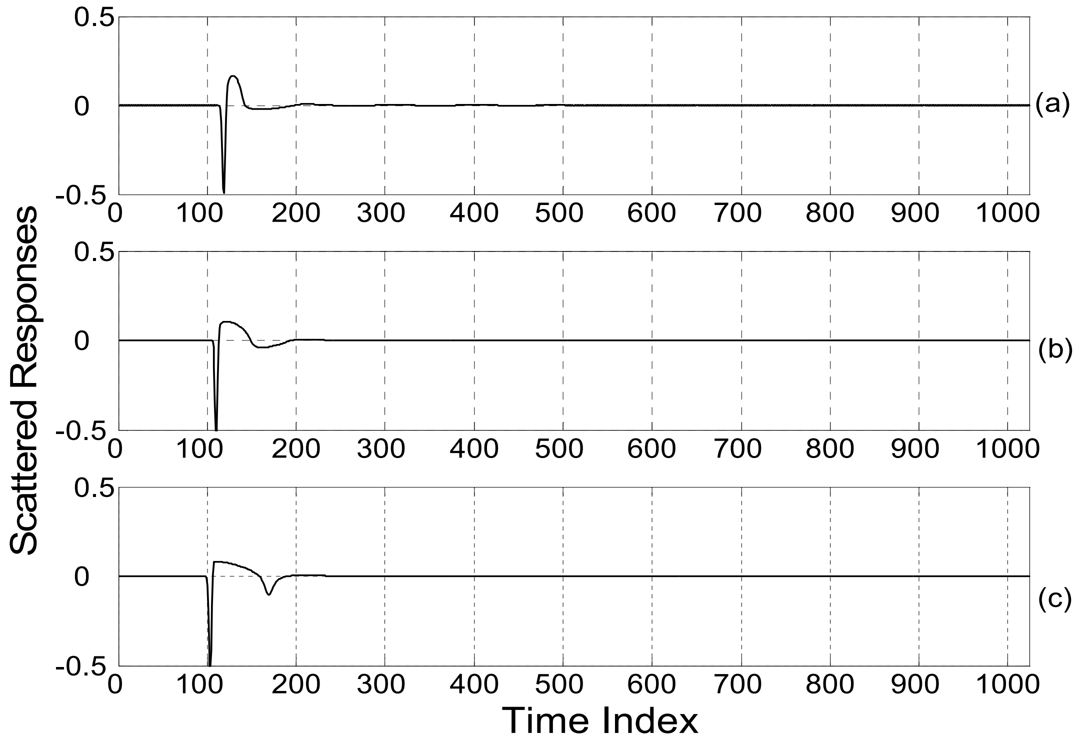

Figure 3.3 Time domain responses of Tcon5 (a) 45º; (b)90º; (c)165º

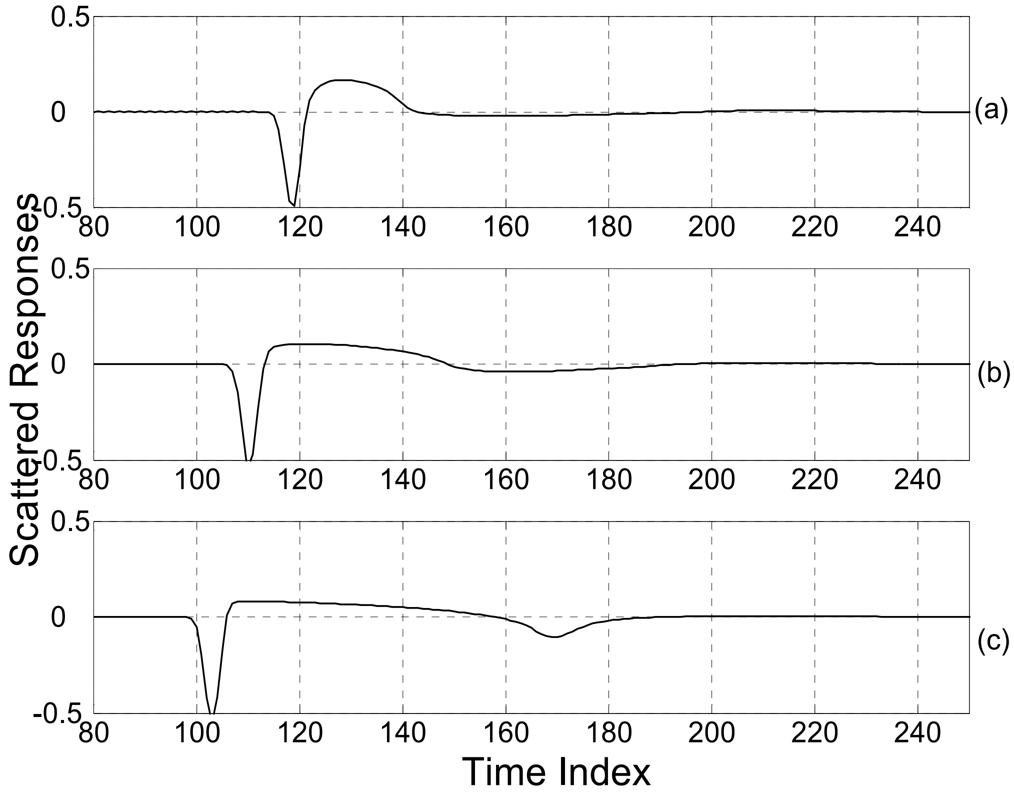

Figure 3.4 A focused view of time domain responses of Tcon5 (a) 45º; (b)90º; (c)165º

Step 3: The auto-WD matrix $\widetilde{w}_x$ of the discrete scattered signal x(t) is computed with N=1024. This step is repeated for all target classes at all five reference aspects. To display the behavior of these time-frequency images over aspect change, contour plots of the $\widetilde{w}_x$ matrices for the target Tcon5 at 45º, 90º and 165º reference aspects are presented in Figure 3.5.

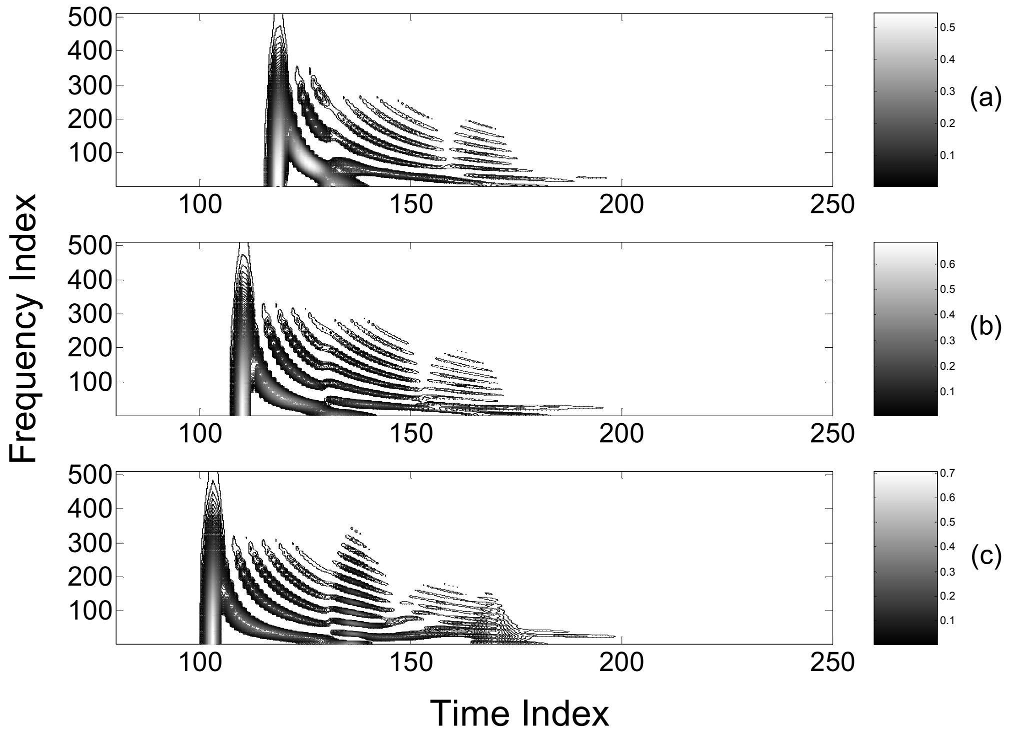

Figure 3.5 Contour plots of modified auto-Wigner distribution outputs for the target Tcon5 at (a) 45º; (b)90º; (c)165º.

Step 4: The optimum Q parameter is determined as discussed in Chapter II. The same procedure is repeated for all candidate targets of the classifier to make sure that the selected Q value is suitable for all targets. The correlation coefficients computed for the partitioned energy density vectors of the all targets at all 5 reference aspects are plotted in Figure 3.6, for the cases Q = 16, 32, 64, 128, 256 and 512 together with the correlation coefficients computed for the impulse response. As subintervals get wider or as Q value gets smaller, aspect dependency reduces. The optimal value of Q is chosen as 32 for the design of all three classifiers shown in Table 3.1.

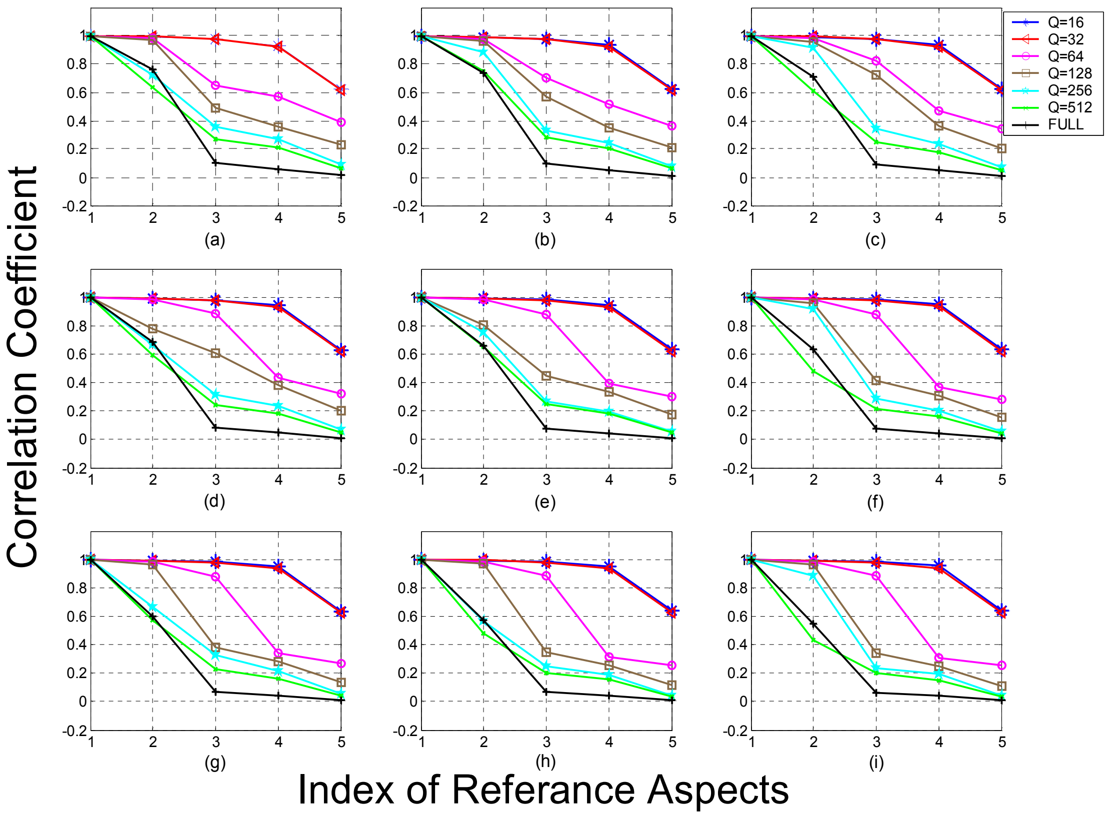

Figure 3.6 Correlation coefficients between the partitioned energy density vectors of the target (a)Tcon1 (b)Tcon2 (c)Tcon3 (d)Tcon4 (e)Tcon5 (f)Tcon6 (g)Tcon7 (h)Tcon8 (i)Tcon9 at the reference aspects computed against the partitioned energy density vector of the same target at 179 degrees, for different partition numbers Q and the full-time scattered signal. The indices 1 through 5 on the horizontal axis refer to the reference aspects of 179, 135, 90, 45 and 5 degrees.

Step 5: For the selected Q value, an optimal q* is determined. Correct Classification Factor (CCF) for each possible q* value ranging from 1 to Q-1 is computed, using the partitioned energy density vectors of all candidate targets extracted at all reference aspects. For this purpose, the CCF based on the reference database is defined as

$$CCF(q^*) = \frac{1}{(M_{tar}K^2)}\sum_{i,j} r_{i,j}^{matched} - \frac{1}{(M_{tar}^{\ 2} - M_{tar})K^2}\sum_{i,j} r_{i,j}^{mismatched} \qquad (3.1)$$

In this equation M_{tar} = 3 and K = 5 are the number of candidate targets and the number of reference aspects for the classifier CLCON1 respectively. M_{tar}=5 for the classifier CLCON2. Finally, M_{tar} = 9 for the classifier CLCON3. As seen from (3.1) CCF is the difference of total matched-case correlation coefficients and total mismatched-case correlation coefficients. To obtain high CCF, the first normalized summation should be much larger than the second one for a satisfactory target classification performance. So, the factor CCF must be as large as possible to satisfy our design objectives. The optimal value of q* is selected to get the largest CCF value without using the low SNR time zone of the data. The CCF versus q* results are displayed in the Figure 3.7 for CLCON1. As it can be realized from this figure the CCF has a maximum at q = 10. Since CCF is a statistical measure it gives an overall idea which may not work perfectly for all individual cases. In the application related to Figure 3.7 for instance, based on further manual inspection the parameter q* is chosen to be 9 instead of 10 to obtain 2-interval band as 9-10 instead of 10-11.

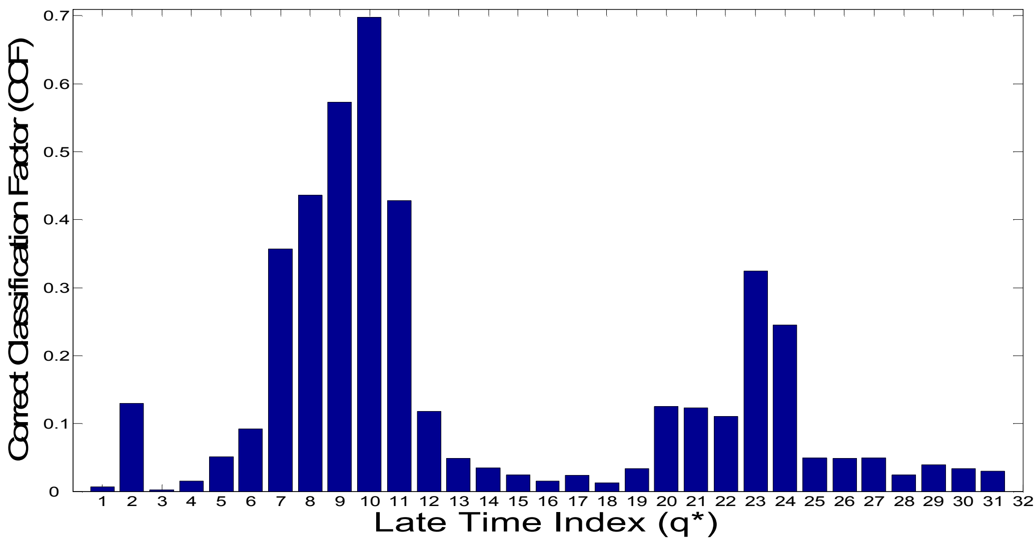

Figure 3.7 CCF plotted against q* to determine the optimal value of q* for CLCON1.

Step 6: The late-time feature vectors (LTFV) are extracted for all targets at all reference aspects over the selected late-time window that corresponds to the 9^{th} and 10^{th} time bands when Q=32, as discussed in Chapter II. LTFV of target Tcon5 at the reference aspects (θ_{ref}=5º, 45º, 90º, 135º, 179º) are plotted in Figure 3.8.

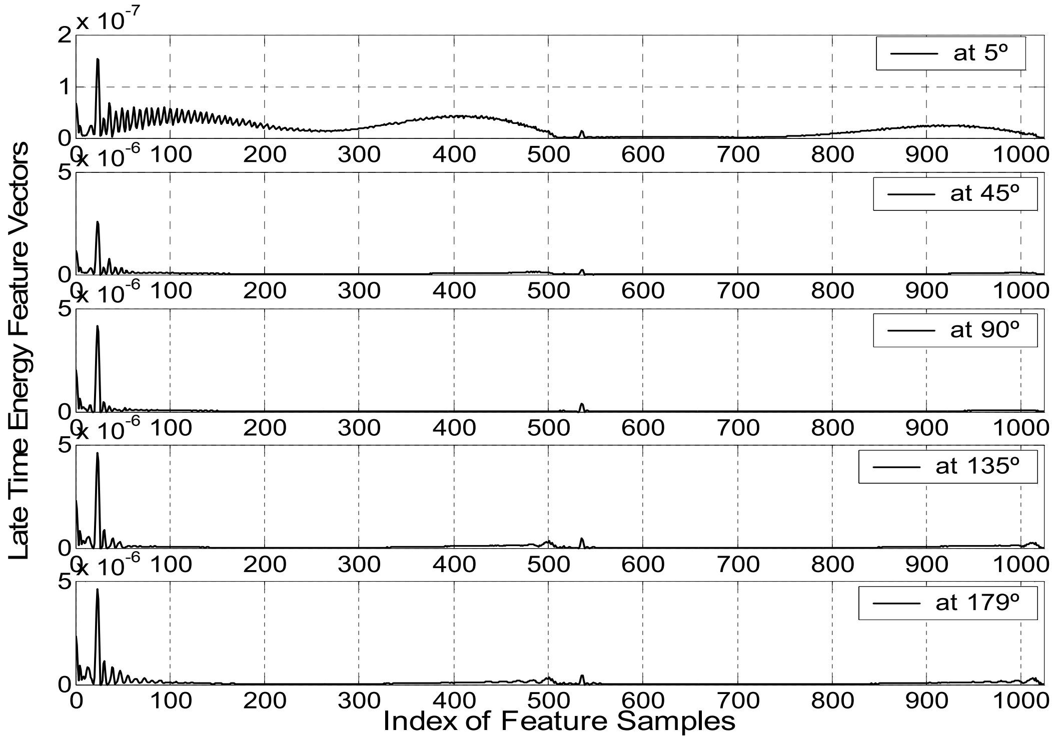

Figure 3.8 LTFV of Tcon5 extracted at the reference aspects.

The first set of 512 sample points of the horizontal axes of this figure represents the frequency sample points used in the WD calculations while the corresponding values on the vertical axes refer to the spectral energy values averaged over the 9^{th} time band while the second set of 512 sample points of the horizontal axes refers to the same set of sample frequencies but the corresponding values on the vertical axes give the spectral energy averaged over the 10^{th} time band. The shape and the magnitude of the LTFV change from the 9^{th} time band to the 10^{th} time band due to the fact that the natural resonance components exponentially decay in time at different rates.

Step 7: For each target, a feature matrix F, the principal components (PCs) of the matrix F and the related eigenvalues are computed using K=5 reference aspects as discussed in Chapter II. For the target Tcon5, the PCs based on the late-time energy feature vectors plotted in Figure 3.9. By applying the PCA technique to the set of LTFVs as explained in Chapter II, we have constructed the Fused Feature Vectors (FFVs) for each target in the classifier catalog.

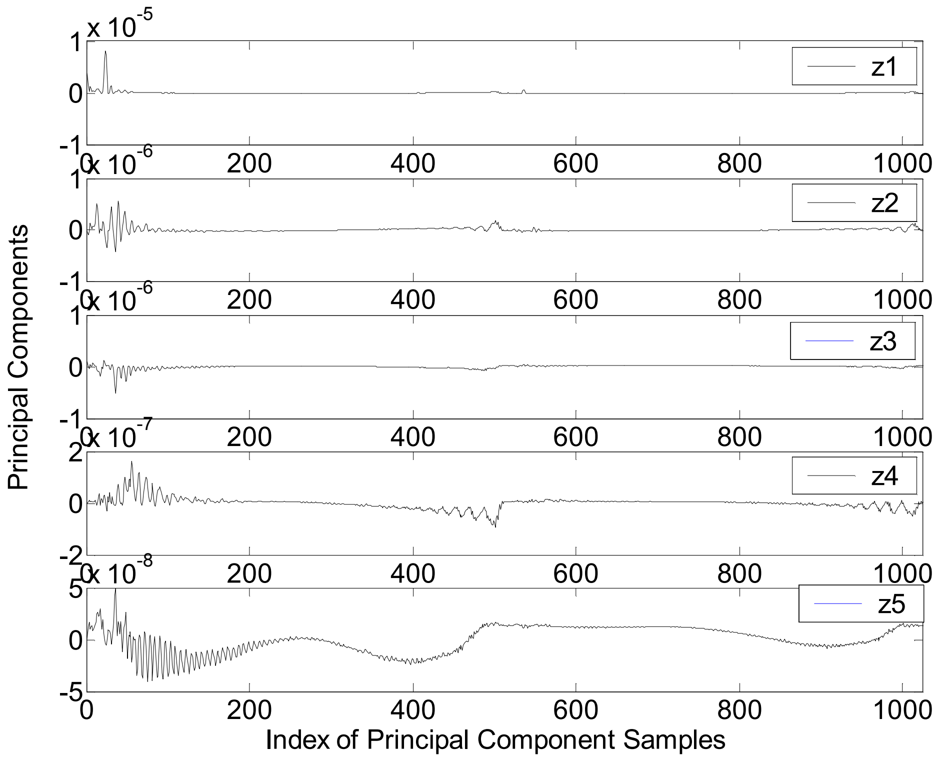

Figure 3.9 PCs for target Tcon5 based on LTFV extracted at five reference aspects.

Table 3.2 Correlation Coefficients between the reference LTFV's and the PC's for the target Tcon5 together with the associated eigenvalues. (to the classifier CLCON3 for FFV)

Eigenvalues		PCs	θ_{ref}				
λ_i (10^{-10})	$100\overline{\lambda_i}$		179º	135º	90º	45º	5º
0.5050	98.12%	z_1	0.9917	0.9975	0.9874	0.969	0.6311
0.0068	1.32%	z_2	0.1215	0.0178	-0.1498	-0.1744	-0.1737
0.0024	0.47%	z_3	-0.0384	0.0612	0.0379	-0.1700	-0.4413
0.0004	0.08%	z_4	0.0167	-0.0316	0.0332	-0.0408	0.1512
0.0001	0.02%	z_5	0.0024	-0.0047	0.0021	0.0049	-0.5949

Table 3.3 Correlation Coefficients between the reference LTSS's and the PC's for the target Tcon5 together with the associated eigenvalues. (to the classifier CLCON3 for FSS)

Eigenvalues		PCs	θ_{ref}				
λ_i (10^{-6})	$100\overline{\lambda_i}$		179º	135º	90º	45º	5º
0.8428	99.6%	z_1	0.9980	0.9997	0.9988	0.9943	0.9918
0.0031	0.4%	z_2	-0.0624	-0.0255	0.0488	0.1059	0.1256
0	0.0%	z_3	-0.0065	0.0059	0.0078	-0.0107	-0.0208
0	0.0%	z_4	0.0010	-0.0020	0.0018	-0.0009	-0.0050
0	0.0%	z_5	0.0000	0.0000	-0.0001	0.0003	-0.0028

The leading principal component z1 is very dominant as discussed in [3] and as seen in Table 3.2. and 3.3. (The eigenvalue λ_1 is noticeably larger than all other eigenvalues). Therefore, the leading principal component z1 is guaranteed to represent the major part of the variance across the whole reference data and hence safely characterizes the target Tcon5 at all aspects. In other words, the aspect dependent late-time behavior of the target Tcon5 can be represented by a single vector, $z_{FFV} \cong z_1$. LTFVs for each reference aspect and FFV of Tcon1 are shown in Figure 3.10. The FFV results obtained for the targets Tcon1, Tcon5 and Tcon9 are plotted in Figure 3.11. FFV results obtained for all conductor targets 3.12. Each FFV has the length N=1024, therefore, the total fused feature database of M_{tar}-target classifier can be stored in a matrix of size M_{tar}x1024. It uses a very small storage memory.

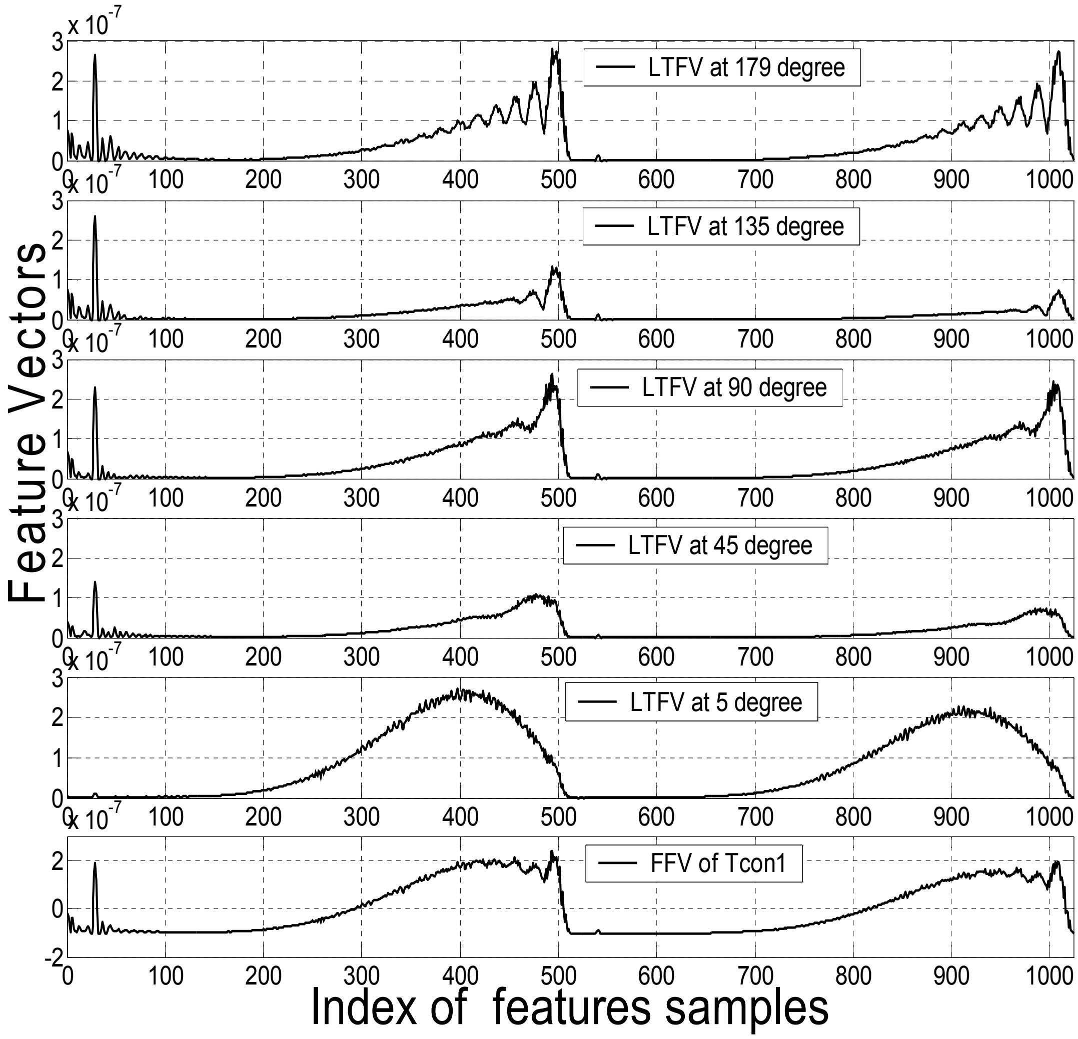

Figure 3.10 LTFVs for each reference aspect and the resulting FFV of the target Tcon1.

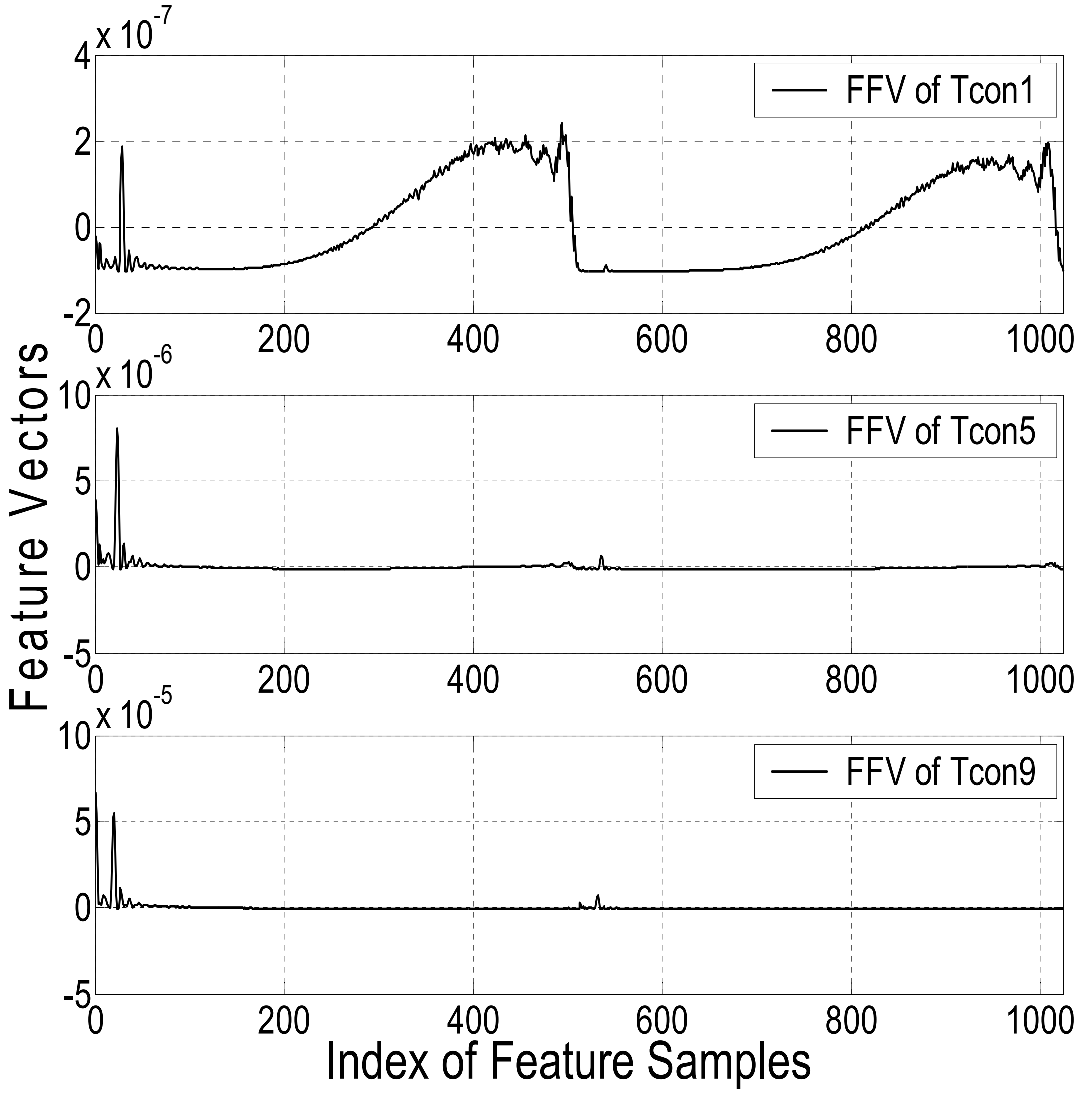

Figure 3.11 FFV of Tcon1, Tcon5 and Tcon9

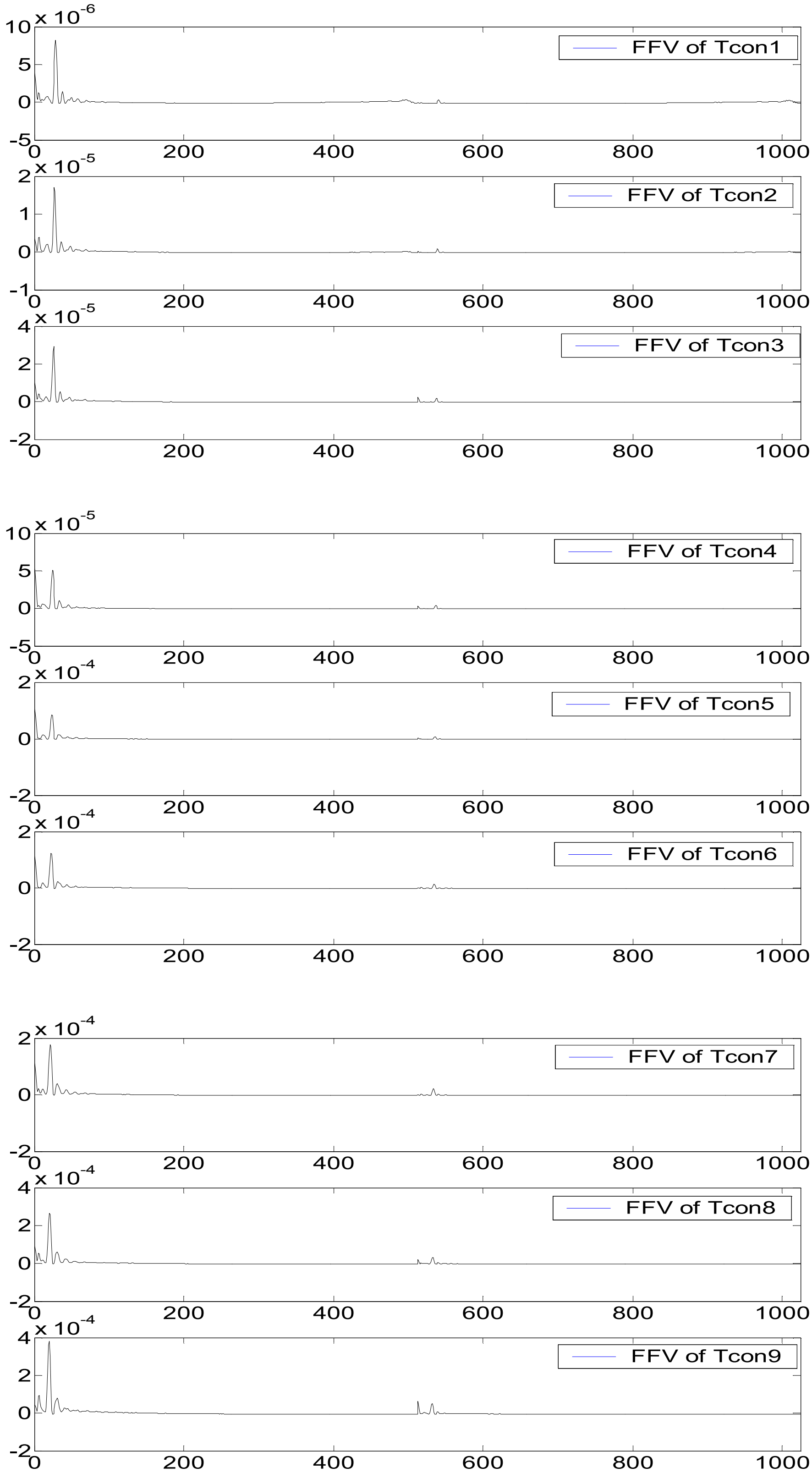

Figure 3.12 FFV of all conducting targets.

3.2.2. Performance verification of classifiers in noise free case

After constructing the feature databases for all three classifiers, in this part, the performance test of the classifiers are presented. The performances can be tested by using three different recognition criteria which are defined in reference [3] as;

1. Maximum reference match (MRM) criterion looks for the reference index that corresponds to the highest correlation coefficient between the tested signal/feature and the reference signals/ features. The classifier's decision is made in favor of the target class associated with this index.

2. Complete class match (CCM) criterion looks for a matching target class whose reference signals/features have the highest correlation coefficients with respect to the tested signal/feature at all reference aspects (i.e., all the other target classes at all reference aspects produce lower correlation coefficients).

3. Complete class match with at least 5 percent contrast margin (CCM-5%) criterion looks for the CCM criterion with an additional requirement that the maximum of the mismatched correlation coefficients is at least 5 percent lower than the minimum of the matched correlation coefficients to reduce decision uncertainty. If desired, this safety margin can be increased to test the robustness of the classifier for highly noisy data in particular.

Actually, MRM and CCM is the same for a FFV based classifier. The correct decision rate is then computed as the percentage of the number of correct decisions among the total number of decisions.

For, the first conductor classifier (CLCON1); since we have 3 targets and 13 test aspect (Φ (phi) =5, 15, 30, 45, 60, 75, 90, 105, 120, 135, 150, 165, 179 degrees) for each target, there are 39 (number of target x test aspects) test signals. The indices in the Figure 3.13, are arranged such that the indices 1 to 5 corresponds to target Tcon1, indices 6 to 10 corresponds to target Tcon5 and indices 11 to 15 corresponds to target Tcon9 for the horizontal axis; the indices 1 to 13 corresponds to test signals of target Tcon1, the indices 14 to 26 corresponds to test signals of target Tcon5, the indices 27 to 39 corresponds to test signals of target Tcon9 for the vertical axis. Obviously, in the figure, the horizontal axis indices are related to the reference information while the vertical indices are associated with the test signals/features. For other classifiers same methodology can be used to read figures Figure 3.14 and 3.15.

For the classifiers CLCON1, CLCON2 and CLCON3;

a. the correlation coefficient of each scattered test signal with respect to each scattered reference signal is computed to form a correlation coefficient matrix of size 39x15, 65x25 and 117x45, respectively, with the resulting contour plot given in Figure 3.13 (a), Figure 3.14 (a) and Figure 3.15 (a) together with a gray-scale bar to indicate the correlation levels. As seen in these figures, in all of them, the matched target blocks (the diagonal blocks) are completely lost as target classification is impossible simply based on the comparison of scattered signals.
b. Part (b)'s of Figure 3.13, Figure 3.14 and Figure 3.15 present the contour plots of the correlation coefficient matrices which are computed using the late-time scattered signals (LTSS) [6.70ns,8.38ns] (based on time bands 1 through 32 and q*=9) both as reference and testing. Matched and mismatched target blocks start to form in this case.

c. Figure 3.13(c), Figure 3.14(c) and Figure 3.15(c) show the contour plots for the correlation coefficients for the testing LTSSs against the fused scattered signals (FSSs).
d. Figure 3.13(d), Figure 3.14(d) and Figure 3.15(d) show the contour plots for each possible pair of full size (based on time bands 1 through 32) energy feature vectors for the test and reference data.
e. Figure 3.13(e), Figure 3.14(e) and Figure 3.15(e) show the contour plots for the correlation coefficient matrix computed for each possible pair of late-time feature vectors extracted from the information on the 9^{th} and 10^{th} time bands only.
f. The correlation coefficient of each LTFV (late-time test feature vector) with respect to each FFV (fused feature vector) is computed and plotted in Figure 3.13(f), Figure 3.14(f) and Figure 3.15(f) where for each target its FFV is assigned to all the reference aspects by definition.

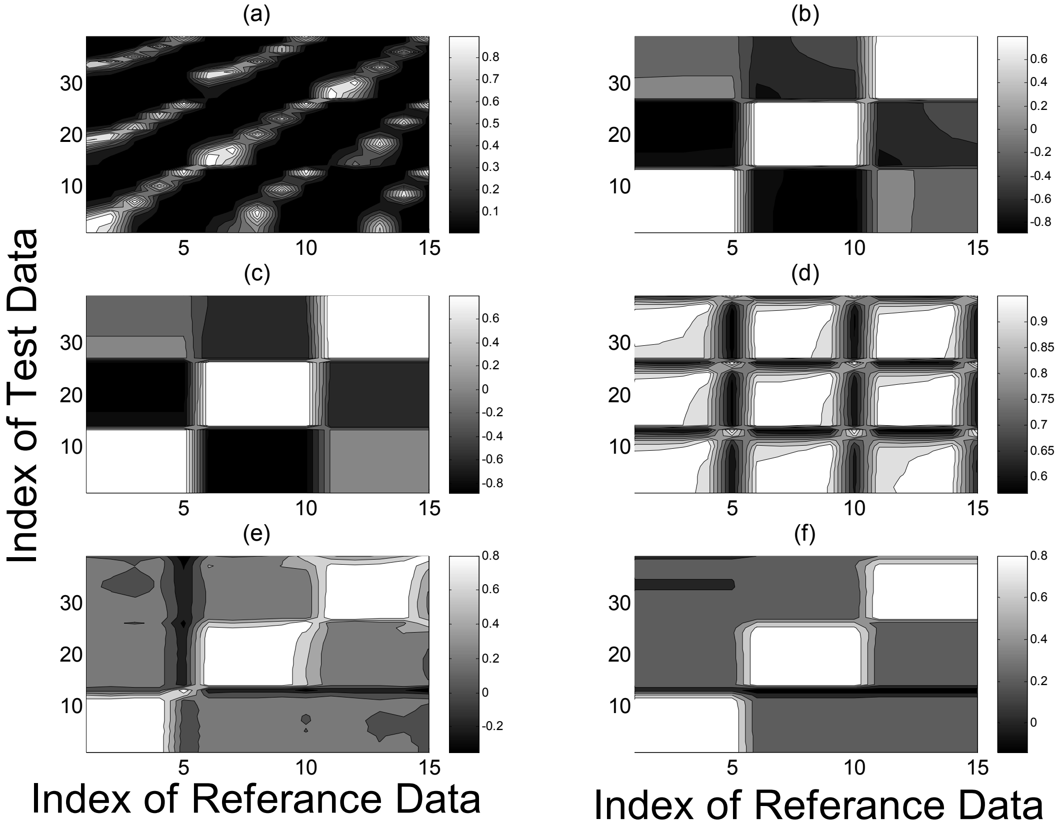

Figure 3.13 Contour plots of correlation coefficients computed for all possible pairs of the test data and the reference data for the classifier CLCON1 using (a) the unprocessed scattered signals, (b) late time scattered signals (LTSS) [6.70ns,8.38ns] (c) the testing LTSSs and fused scattered signals (FSSs) (d) the full-size energy feature vectors, (e) the late-time feature vectors (LTFVs) extracted on the late-time window [6.70ns,8.38ns] and (f) the testing LTFVs and the reference fused feature vectors (FFVs).

Correct decision rate (RDc) for CLCON1 is 100% based for LTSS, FSS and FFV based classifiers with the MRM and the CCM criterion. RDc is also 100% for the CCM-5% criterion with 5% safety margin. These values states that our classifiers based on LTSS, FSS and FFV have reached perfect decision rates. FSS based classifier has more safety margin.

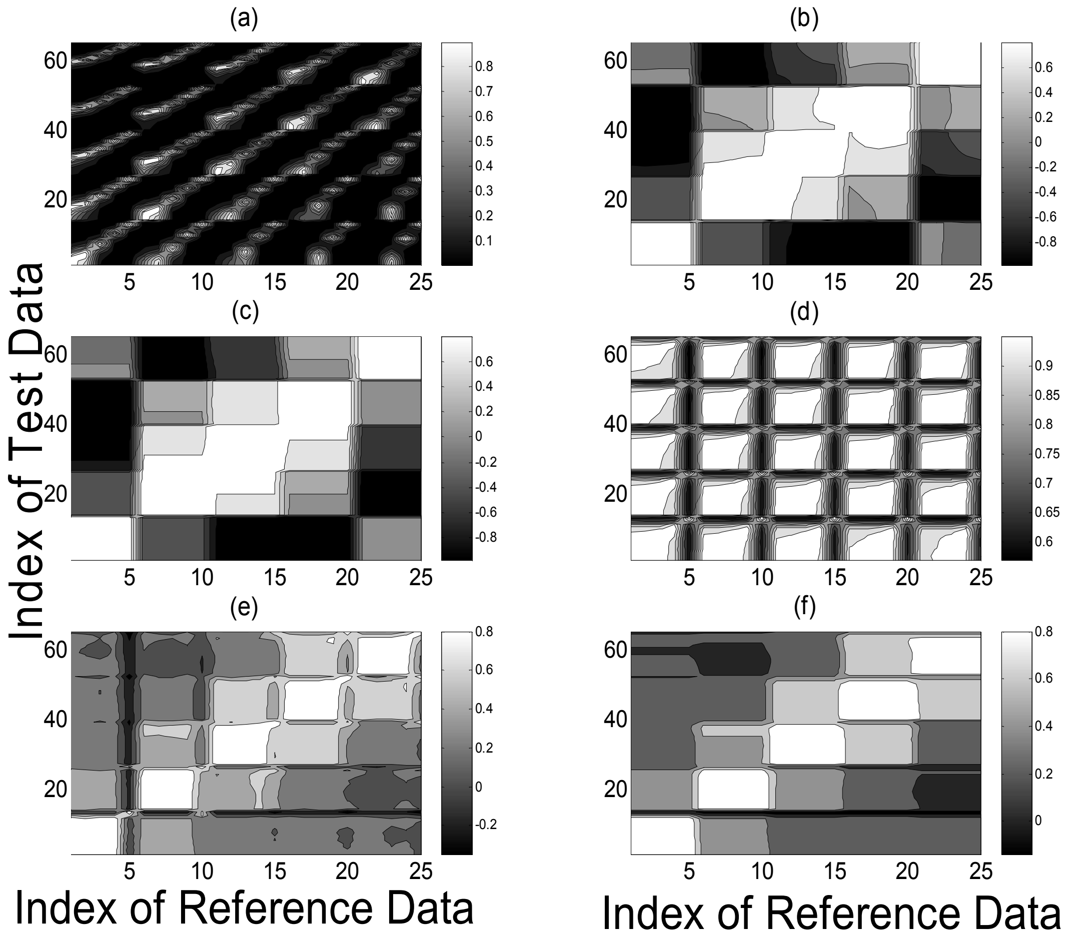

Figure 3.14 Contour plots of correlation coefficients computed for all possible pairs of the test data and the reference data for the classifier CLCON2 using (a) the unprocessed scattered signals, (b) late time scattered signals (LTSS) [6.70ns,8.38ns] (c) the testing LTSSs and fused scattered signals (FSSs) (d) the full-size energy feature vectors, (e) the late-time feature vectors (LTFVs) extracted on the late-time window [6.70ns,8.38 ns] and (f) the testing LTFVs and the reference fused feature vectors (FFVs).

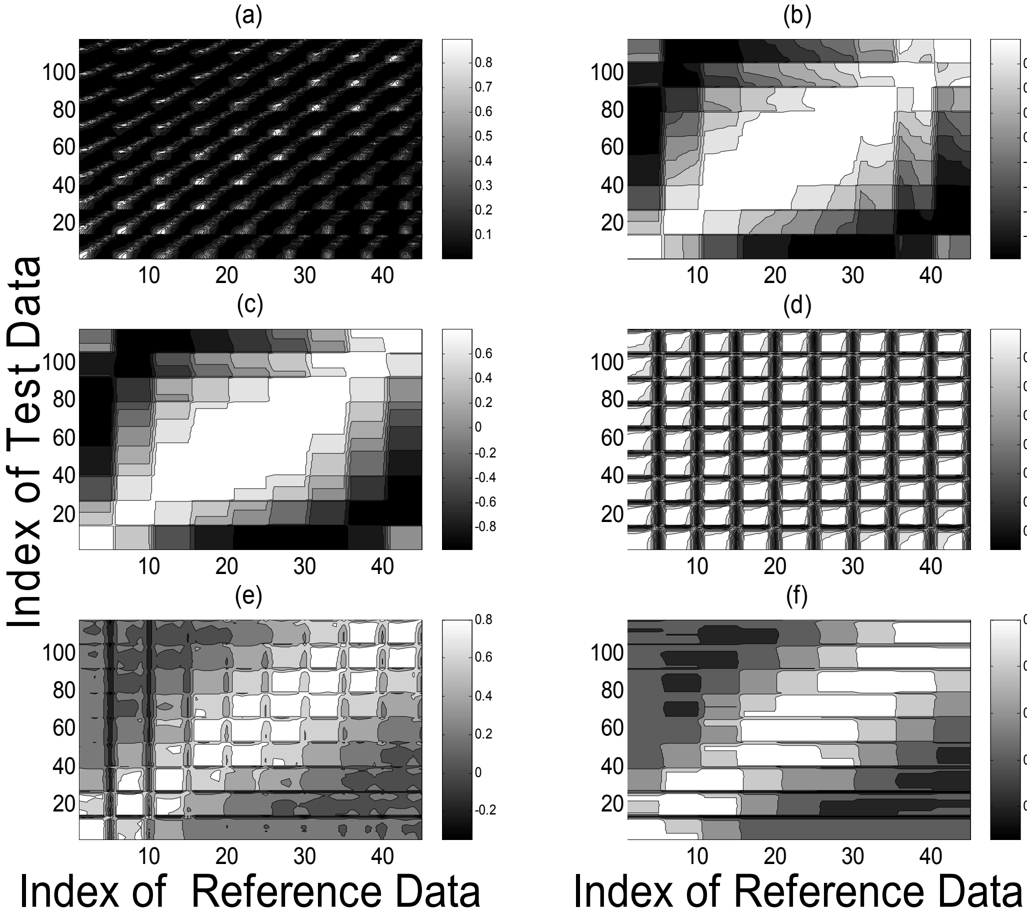

Figure 3.15 Contour plots of correlation coefficients computed for all possible pairs of the test data and the reference data for the classifier CLCON3 using (a) the unprocessed scattered signals, (b) late time scattered signals (LTSS) [6.70ns,8.38ns] (c) the testing LTSSs and fused scattered signals (FSSs) (d) the full-size energy feature vectors, (e) the late-time feature vectors (LTFVs) extracted on the late-time window [6.70ns,8.38ns] and (f) the testing LTFVs and the reference fused feature vectors (FFVs).

Table 3.4 Correct Decision Rates (RDc) of the LTSS-based, the LTFV-based and the FFV based classifiers by three different decision criteria: maximum reference match (MRM), complete class match (CCM)and the CCM with at least 5 percent contrast (CCM-5%) criteria.

	MRM			CCM			CCM-5%		
	CLCON1	CLCON2	CLCON3	CLCON1	CLCON2	CLCON3	CLCON1	CLCON2	CLCON3
LTSS-based [6.70ns,8.38 ns]	100%	100%	100%	100%	100%	92%	100%	100%	54%
FSS-based	100%	100%	100%	100%	100%	100%	100%	100%	73%
LTFV-based	100%	100%	100%	0%	0%	0%	0%	0%	0%
FFV-based	100%	100%	97%	100%	100%	97%	100%	100%	80%

As it can be realized from the figures 3.13, 3.14 and 3.15 and the table 3.4; although LTSS-based classifier results look good, its performance decreases if we measure it with the CCM with safety margin. FSS-based and FFV-based classifiers are more effective regarding both accuracy and robustness. LTFV based classifier gives high RDc with MRM criteria. Because of 5º reference aspects RDc goes to zero with the CCM and the CCM-5% crirteria. If we get rid of 5º reference aspect, we can also obtain higher decision rates for LTFV based classifier with the CCM and the CCM-5% criteria.

For demonstration of verification, a test signal which belongs to Tcon5 at 105 degree aspect is selected and the detection results of three classifiers are plotted in Figure 3.16.

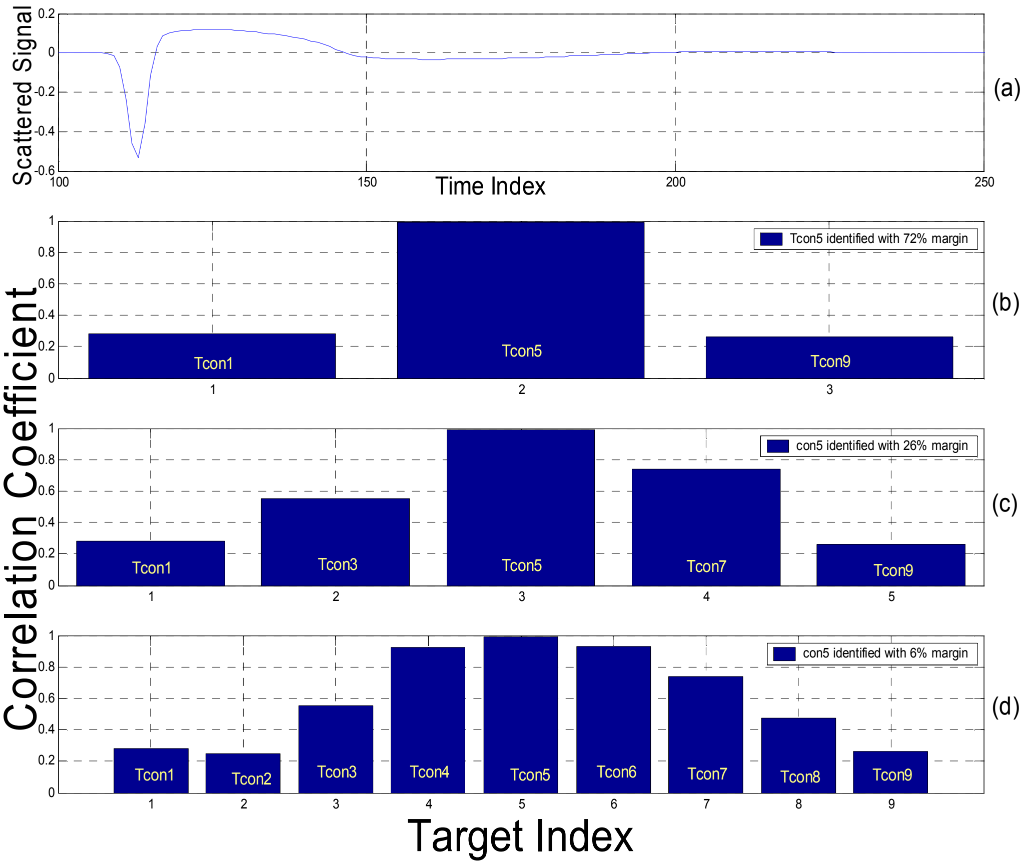

Figure 3.16 The FFV-based classifiers are tested with Tcon5 at 105 degree. The "unknown" scattered signal is plotted in (a) together with the bar chart results that show the correlation coefficients computed between the testing LTFV and the reference FFVs of the classifiers CLCON1 in (b), CLCON2 in (c) , CLCON3 in (d).

3.3. Classifier Design for Perfect Dielectric Spheres

3.3.1. Construction of Classifier Database

In this section we will design two different classifiers CLDIE1 and CLDIE2 for dielectric targets as defined in Table (3.5). All targets has same radius(r=10 cm), but different relative refractive indices (ε).

Table 3.5 Classifier description for dielectric type of targets

Classifiers	Targets
CLDIE1	Tdie1(ε =3), Tdie3(ε=4), Tdie5(ε=5), Tdie7(ε=6), Tdie8(ε=7).
CLDIE2	Tdie1(ε =3), Tdie2(ε=3.5), Tdie3(ε=4), Tdie4(ε=4.5), Tdie5(ε=5), Tdie6(ε=5.5), Tdie7(ε=6), Tdie8(ε=7).

These classifiers are designed using the same basic steps as followed in the design of classifiers for conductor targets as described in section 3.2.1.

Step 1: As an example, magnitude of CFRs for the target Tdie5 at the aspect angles of 45, 90 and 165 degrees are plotted in Figure 3.17.

Step 2: Time domain responses created using CFRs. Examples of scattered signals for Tcon5 at 45, 90 and 165 degrees are plotted in Figure 3.18.

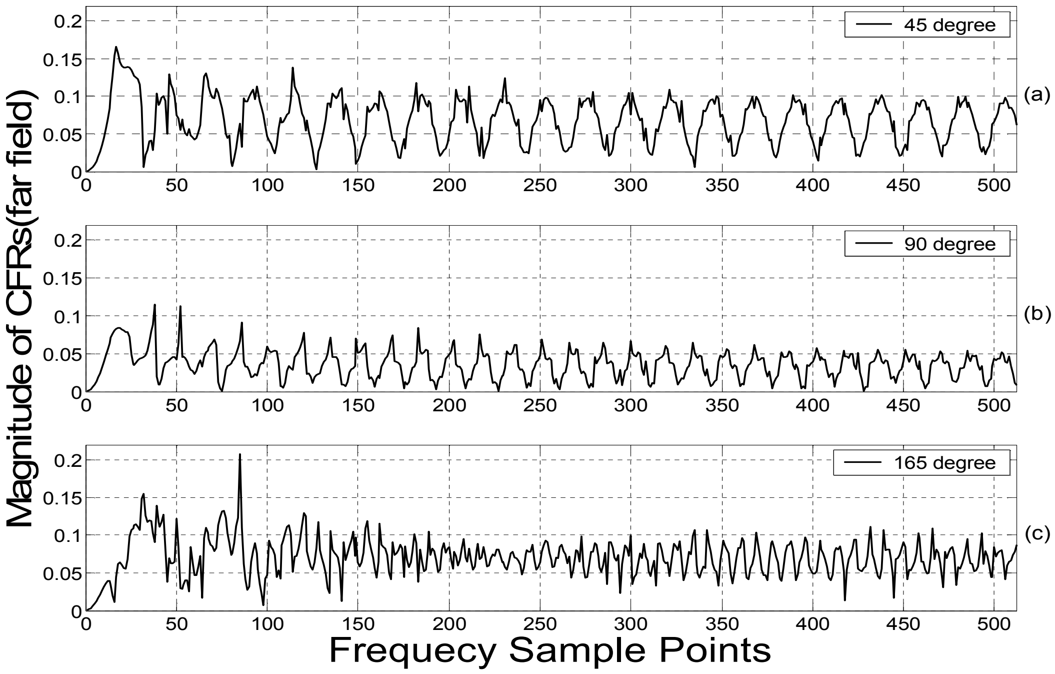

Figure 3.17 Magnitudes of CFRs for Tcon5 (a) 45º ; (b)90º; (c)165º

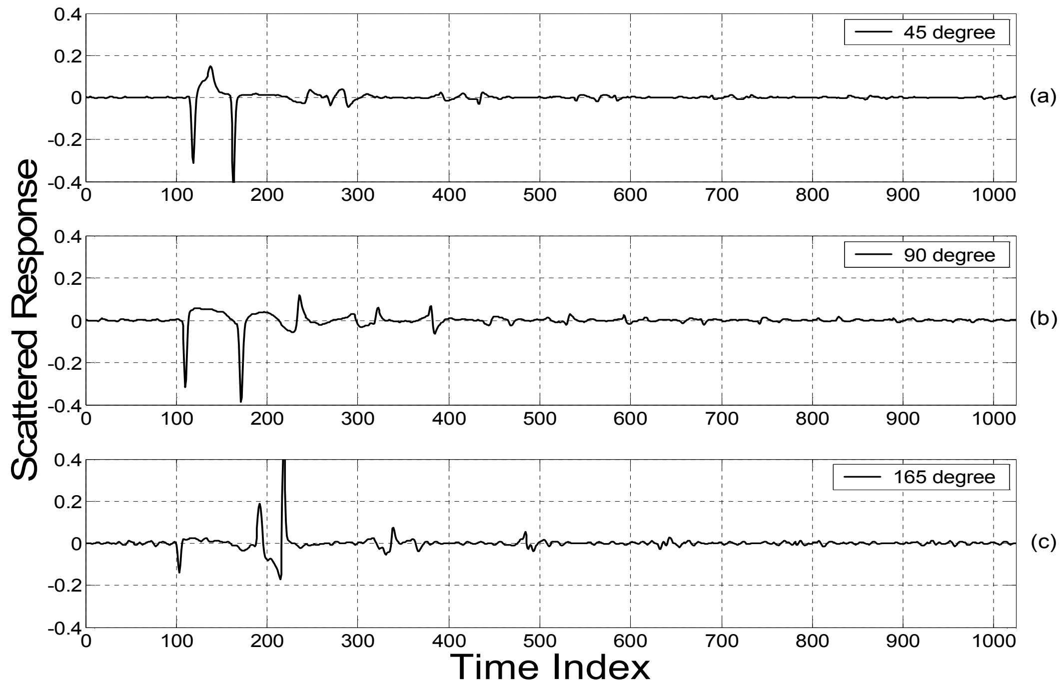

Figure 3.18 A focused wiev of Time Domain Responses (impulse responses) of Tcon5 (a) 45º; (b)90º; (c)165º

Step 3: The auto-WD matrix W_x of the discrete scattered signal x(t) is computed with N=1024 for all five reference aspects of all targets. As an example to the behavior of these time-frequency images over aspect change, contour plots of the magnitudes of the W_x matrices for the target Tdie5 at 45º, 90º and 165º reference aspects are presented in Figure 3.19.

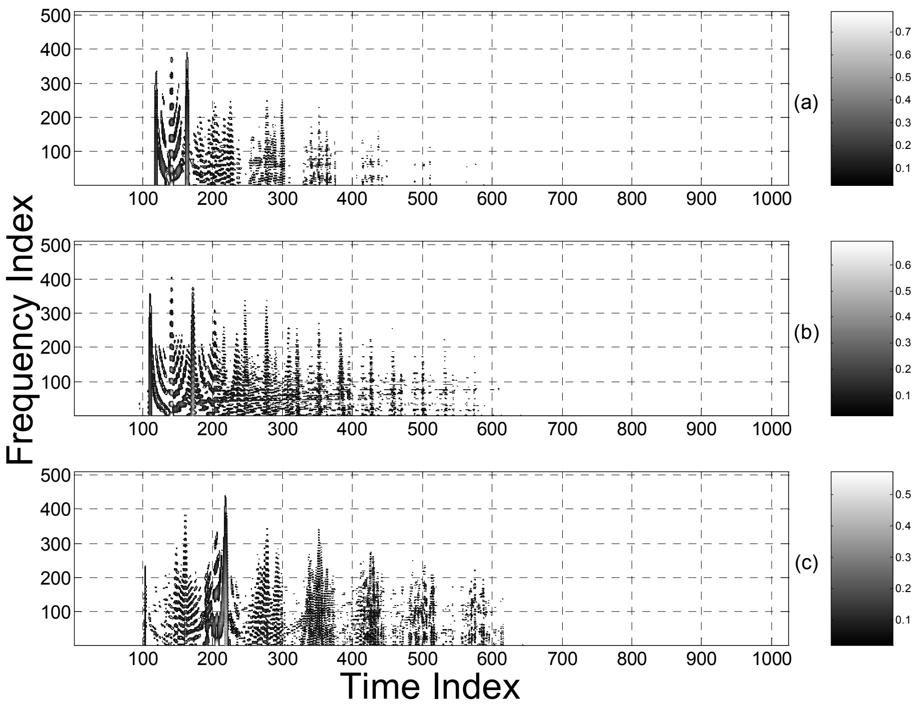

Figure 3.19 Contour plots of the magnitude of the modified auto-Wigner distribution outputs for the target Tdie5 at (a) 45º; (b)90º; (c)165º.

Step 4: Optimum Q is determined. The correlation coefficients computed for the partitioned energy density vectors of all the targets at 5 reference aspects are plotted in Figure 3.20, for the cases Q = 8, 16, 32 and 64 together with the correlation coefficients computed for the impulse responses. As subintervals get wider or as Q value gets smaller, aspect dependency reduces. The optimal value of Q is chosen as 16 for both classifier designs.

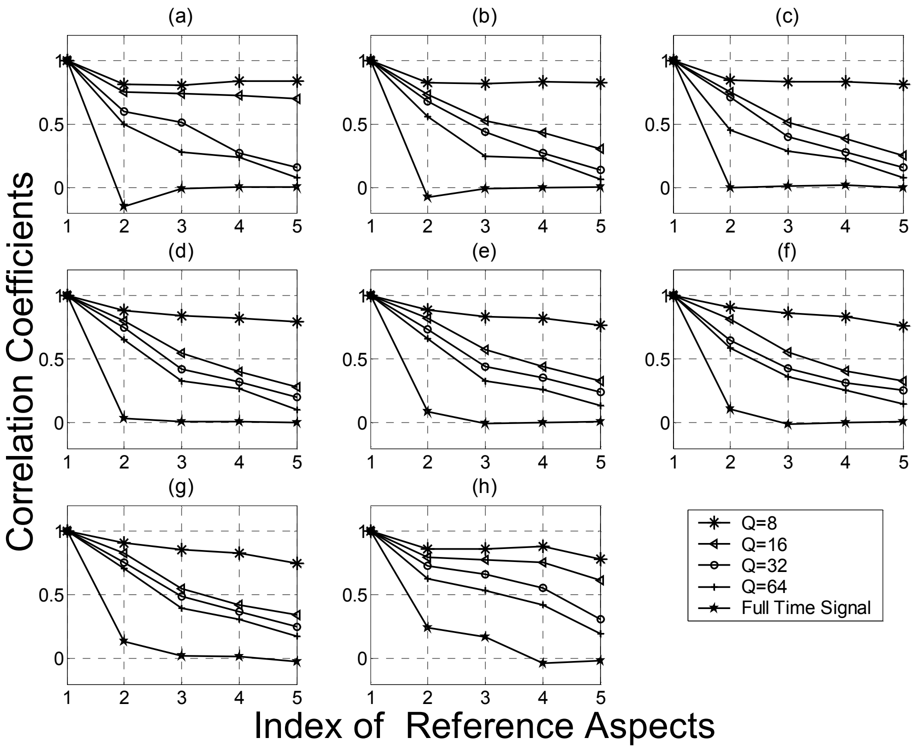

Figure 3.20 Correlation coefficients between the partitioned energy density vectors of the target (a)Tdie1 (b)Tdie2 (c)Tdie3 (d)Tdie4 (e)Tdie5 (f)Tdie6 (g)Tdie7 (h)Tdie8 at the reference aspects computed against the partitioned energy density vector of the same target at 179 degrees, for different partition numbers Q and the full-time scattered signal. The indices 1 through 5 on the horizontal axis refer to the reference aspects of 179, 135, 90, 45 and 5 degrees.

Step 5: For selected Q value, an optimal q* is determined. q*=12 case is selected as optimum band. (Figure 3.21)

Step 6: The late-time feature vectors (LTFV) are extracted for all targets at all reference aspects over the selected latetime window that corresponds to the 12^{th} and 13^{th} time bands when Q=16. LTFV of target Tdie5 at the reference aspects (θ_{ref}=5º, 45º, 90º, 135º, 179º) are plotted in Figure 3.22

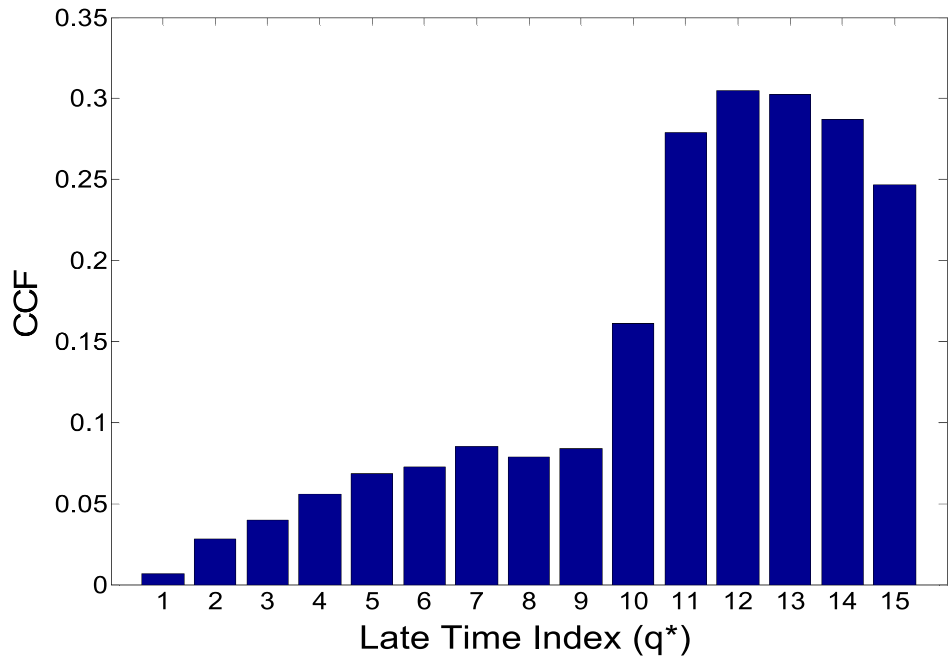

Figure 3.21 CCF plotted against q* to determine the optimal value of q* for CLDIE2.

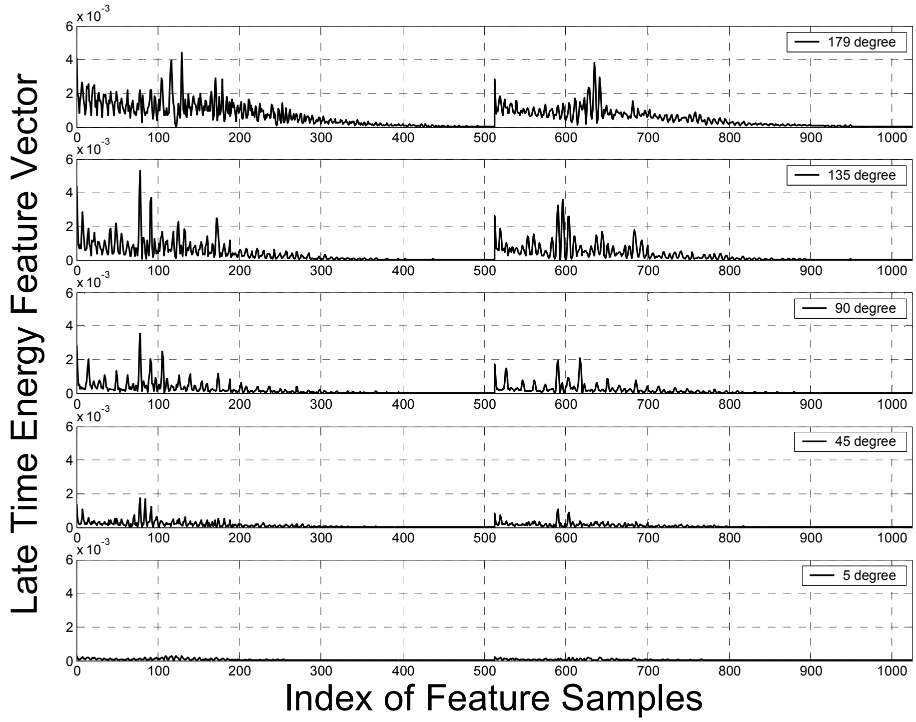

Figure 3.22 LTFV of Tdie5 extracted at the reference aspects.

Step 7: For each target, a feature matrix F, the principal components (PCs) of the matrix F and the related eigenvalues are formed at K=5 reference aspects as discussed in Chapter II. For the target Tdie5, PCs based on the late-time energy feature vectors plotted in Figure 3.23. By applying PCA on LTFV, we have constructed Fused Feature Vectors (FFVs) of each target.

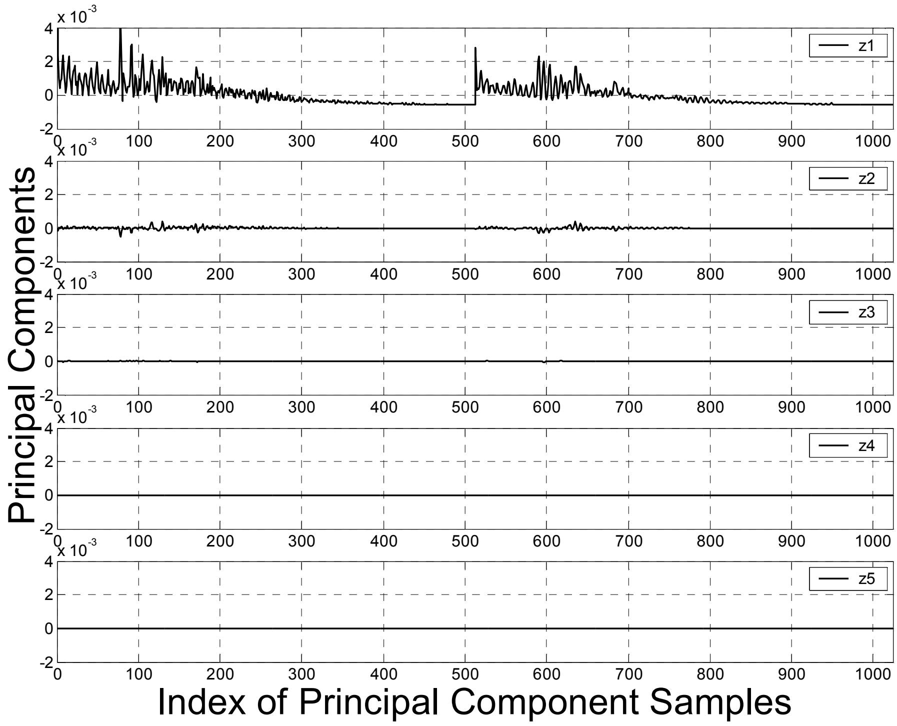

Figure 3.23 PCs for target Tdie5 based on LTFV extracted at five reference aspects.

Table 3.6 Correlation Coefficients between the reference LTFV and PCs for Tdie5 together with the associated eigenvalues.

Eigenvalues		PCs	θ_{ref}				
$\lambda_i\,(10^{-6})$	$100\bar{\lambda}_i$		179º	135º	90º	45º	5º
0.6871	78.30%	z_1	0.9086	0.8939	0.7930	0.7807	0.7906
0.1442	16.43 %	z_2	0.4175	-0.4187	-0.3471	-0.2841	0.1789
0.0365	4.16%	z_3	-0.0048	-0.1584	0.4983	0.1032	0.0308
0.0089	1.01%	z_4	0.0038	0.0228	0.0490	-0.5468	-0.1361
0.0008	0.09%	z_5	-0.0021	-0.0001	-0.0002	-0.0128	0.5687

The leading principal component z_1 is very dominant as discussed in [3] and as seen in Table 3.6. λ_1 is much larger than the variances of all other PCs.

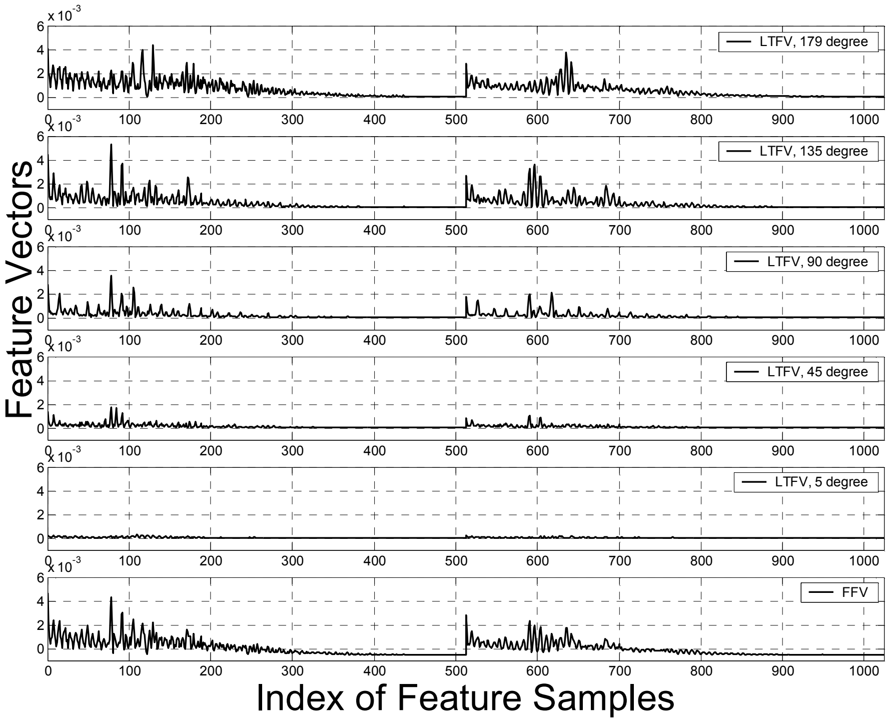

Figure 3.24 LTFVs for each reference aspect and FFV of Tdie5

The FFV results obtained for the dielectric targets are plotted in Figure 3.25. Each FFV has the length N=1024, therefore, the total fused feature database of M_{tar}-target classifier can be stored in a matrix of size M_{tar}x1024. It uses a very small storage memory.

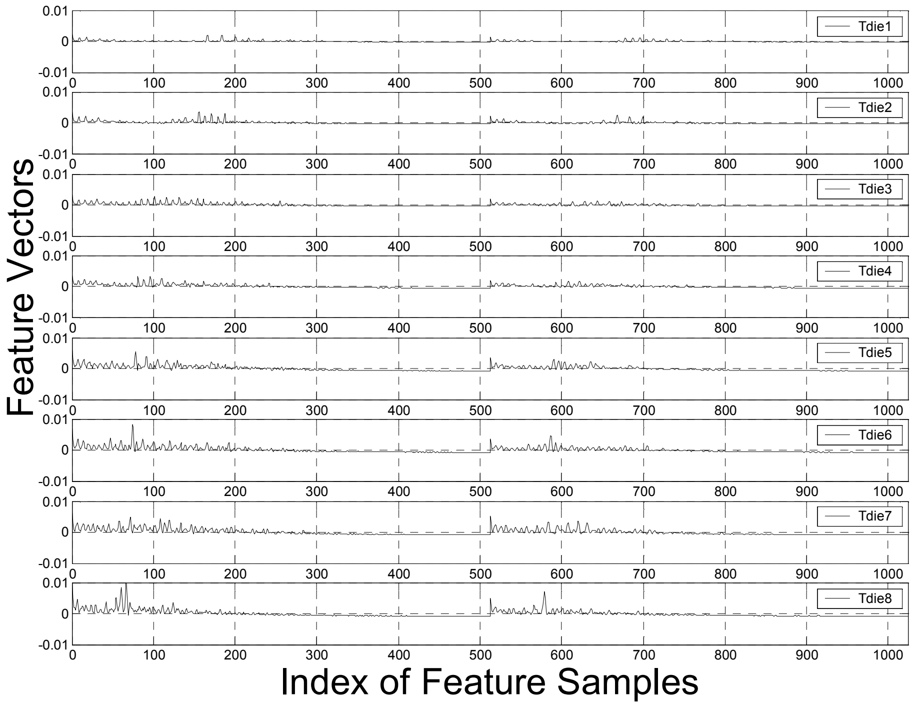

Figure 3.25 FFV of dielectric targets.

3.3.2. Performance verification of dielectric classifiers in noise free case

After constructing the reference databases of both dielectric classifiers, classifiers are tested for their correct classification performance in this part. The approach introduced for performance testing in section 3.2.2 is also used here.

For the first dielectric classifier (CLDIE1); since, we have 5 targets and 13 test aspects (Φ (phi) =5, 15, 30, 45, 60, 75, 90, 105, 120, 135, 150, 165, 179 degrees) for each target, there are (number of target x test aspects =)

65 test signals. The indices in Figure 3.26, are arranged such that the indices 1 to 5 corresponds to target Tdie1, indices 6 to 10 corresponds to target Tdie3 and indices 11 to 15 corresponds to target Tdie5 and so on for the horizontal axis; the indices 1 to 13 corresponds to test signals of target Tdie1, the indices 14 to 26 corresponds to test signals of target Tdie3, the indices 27 to 39 corresponds to test signals of target Tdie5 and so on for the vertical axis. For the other classifier same methodology can be used to read the similar Figure 3.27.

For both classifiers CLDIE1 and CLDIE2;

a. The correlation coefficient of each scattered test signal with respect to each scattered reference signal is computed to form correlation coefficient matrices of size 65x25 and 104x40 for the classifiers CLDIE1 and CLDIE2 respectively whose contour plots are given in Figure 3.26 (a) and Figure 3.27 (a) together with colorbars bar to indicate the correlation levels.
b. Similar plots are given in Figure 3.26 (b), Figure and 3.27 (b) where the correlation coefficient matrices are computed for late time scattered signals (LTSS) [18.43ns, 21.78 ns] (based on time bands 1 through 16 and q*=12)
c. Figure 3.26 (c) and Figure 3.27 (c) plot correlation coefficients for the testing LTSSs and fused scattered signals (FSSs).
d. Figure 3.26 (d) and Figure 3.27(d) plot each possible pair of full size (based on time bands 1 through 16) energy feature vectors for the test and reference data.
e. Figure 3.26 (e) and Figure 3.27 (e) plot the correlation coefficient matrices computed for each possible pair of late-time feature vectors extracted from the information on the 12^{th} and 13^{th} time bands only.
f. The correlation coefficient of each LTFV (late-time test feature vector) with respect to each FFV (fused feature vector) is computed

and plotted in Figure 3.26 (f) and Figure 3.27 (f) where for each target its FFV is assigned to all the reference aspects by definition.

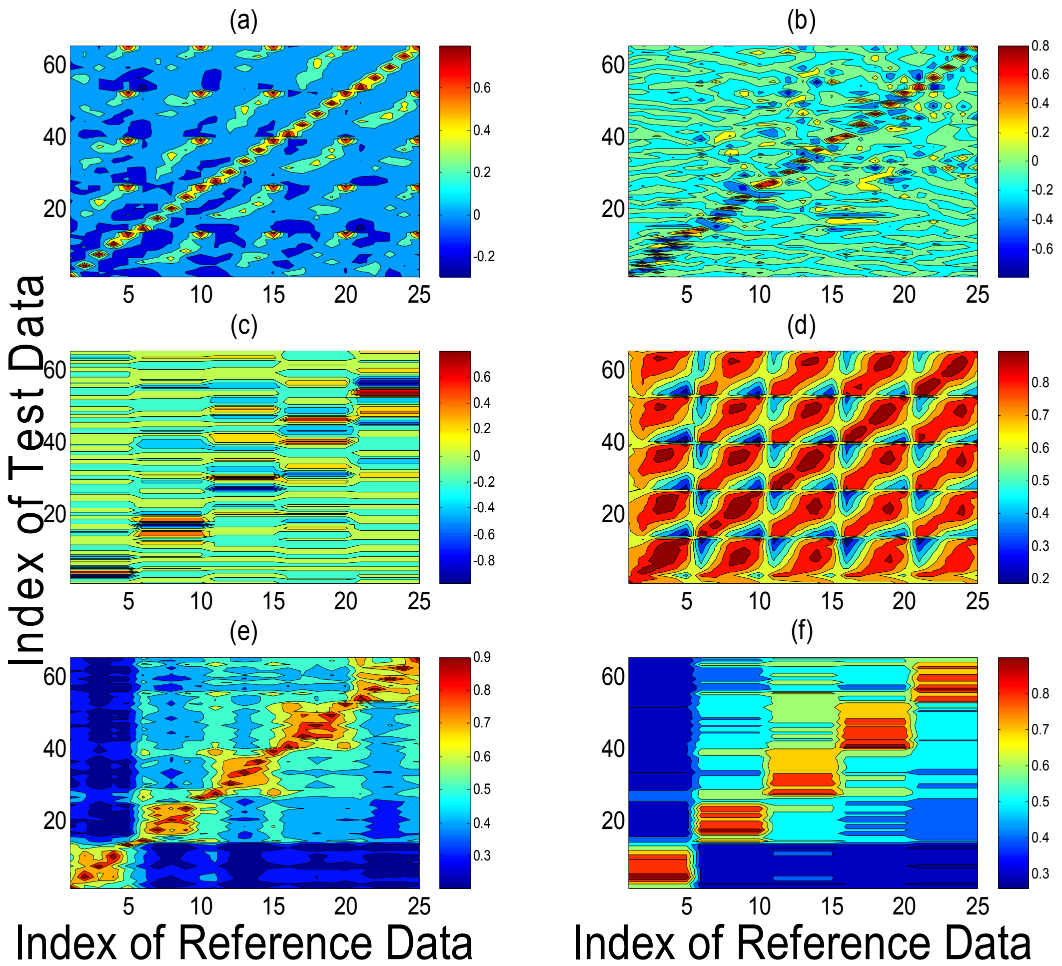

Figure 3.26 Contour plots of correlation coefficient matrices computed for all possible pairs of the test data and the reference data for the classifier CLDIE1 using (a) the unprocessed scattered signals, (b) late time scattered signals (LTSS) [18.43ns, 21.78ns], (c) the testing LTSSs and fused scattered signals (FSSs), (d) the full-size energy feature vectors, (e) the late-time feature vectors (LTFVs) extracted on the late-time window [18.43ns, 21.78ns] and (f) the testing LTFVs and the reference fused feature vectors (FFVs).

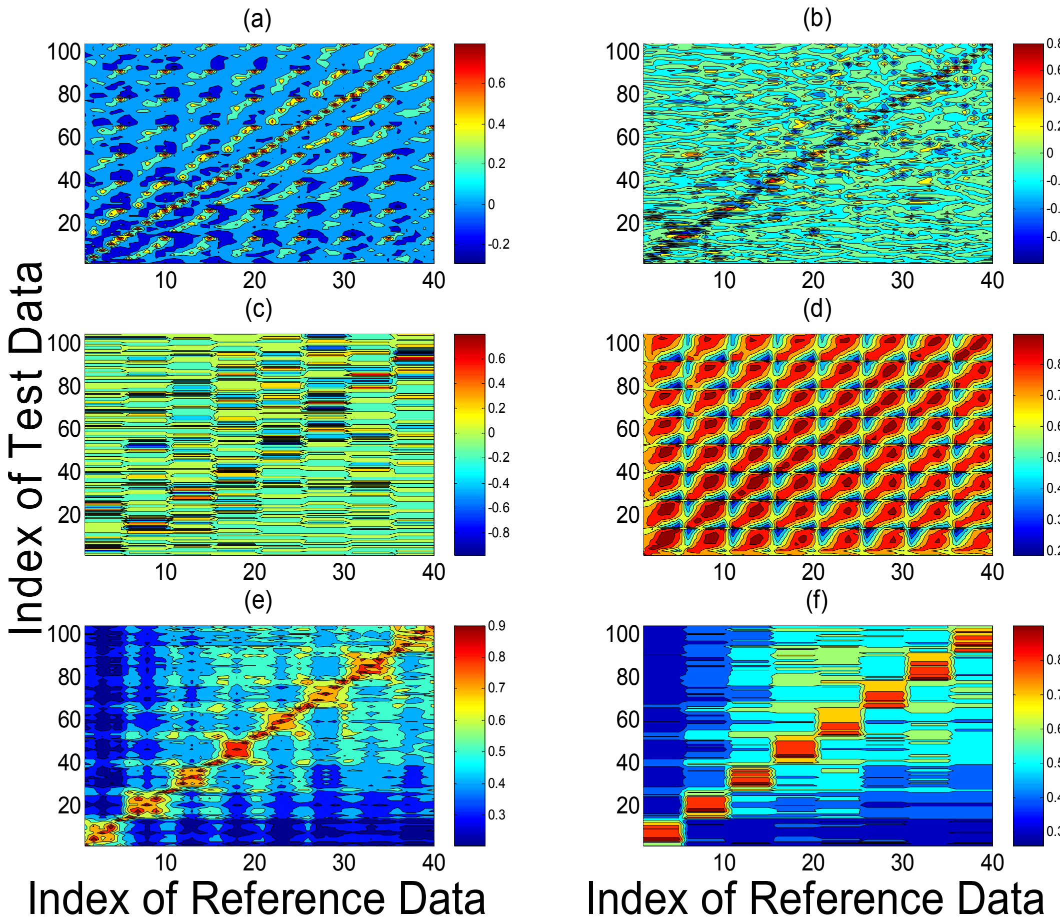

Figure 3.27 Contour plots of correlation coefficient matrices computed for all possible pairs of the test data and the reference data for the classifier CLDIE2 using (a) the unprocessed scattered signals, (b) late time scattered signals (LTSS) [18.43ns, 21.78 ns] (c) the testing LTSSs and fused scattered signals (FSSs) (d) the full-size energy feature vectors, (e) the late-time feature vectors (LTFVs) extracted on the late-time window [18.43ns, 21.78 ns] and (f) the testing LTFVs and the reference fused feature vectors (FFVs).

Table 3.7 Correct Decision Rates (RDc) of the LTSS-based, the LTFV-based and the FFV based classifiers by three different decision criteria: maximum reference match (MRM), complete class match (CCM)and the CCM with at least 5 percent contrast (CCM-5%) criteria.

	MRM		CCM		CCM-5%	
Classifier Name	CLDIE1	CLDIE2	CLDIE1	CLDIE2	CLDIE1	CLDIE2
LTSS-based [18.43ns, 21.78 ns]	68%	57%	0	0	0	0
FSS-based	34%	28%	34%	28%	34%	28%
LTFV-based	100%	100%	63.08%	50%	55.39%	34.62%
FFV-based	100%	100%	100%	100%	98.46%	98.08%

As it can be realized from the last two figures and table above, the FFV-based classifier performs for better in terms of accuracy and robustness as compared to the LTSS-based, FSS-based, and LTFV-based classifiers.

3.4. Classifier Design for Dielectric Coated Conductors

3.4.1. Construction of Classifier Database

In this section we will design six different classifiers for dielectric coated conductor spheres. These classifiers and the related candidate targets are defined in Table 3.8 below. All the targets in this study has the same outer radii(r=10 cm), but different inner radii as well as different relative refractive indices (ε).

Table 3.8 Classifier description for dielectric coated conductor type of targets.

Classifiers	Targets
CLCOA1	Tcoa1(r_{in}=2 ε =3), Tcoa4(r_{in}=4 ε =3), Tcoa7(r_{in}=7 ε =3), Tcoa10(r_{in}=8 ε =3), Tcoa13(r_{in}=9ε =3).
CLCOA2	Tcoa1(r_{in}=2 ε =5), Tcoa4(r_{in}=4 ε =5), Tcoa7(r_{in}=7 ε =5), Tcoa10(r_{in}=8 ε =5), Tcoa13(r_{in}=9ε =5).
CLCOA3	Tcoa1(r_{in}=2 ε =7), Tcoa4(r_{in}=4 ε =7), Tcoa7(r_{in}=7 ε =7), Tcoa10(r_{in}=8 ε =7), Tcoa13(r_{in}=9ε =7).
CLCOA4	Tcoa1(r_{in}=2 ε =3), Tcoa2(r_{in}=2 ε =5), Tcoa3(r_{in}=2 ε =7), Tcoa4(r_{in}=4 ε =3), Tcoa5(r_{in}=4 ε =5), Tcoa6(r_{in}=4 ε =7),
CLCOA5	Tcoa7(r_{in}=7 ε =3), Tcoa8(r_{in}=7 ε =5), Tcoa9(r_{in}=7 ε =7), Tcoa10(r_{in}=8 ε =3), Tcoa11(r_{in}=8 ε =5), Tcoa12(r_{in}=8 ε =7), Tcoa13(r_{in}=9ε =3), Tcoa14(r_{in}=9 ε =5), Tcoa15(r_{in}=9 ε =7).
CLCOA6	Tcoa1(r_{in}=2 ε =3), Tcoa2(r_{in}=2 ε =5), Tcoa3(r_{in}=2 ε =7), Tcoa4(r_{in}=4 ε =3), Tcoa5(r_{in}=4 ε =5), Tcoa6(r_{in}=4 ε =7), Tcoa7(r_{in}=7 ε =3), Tcoa8(r_{in}=7 ε =5), Tcoa9(r_{in}=7 ε =7), Tcoa10(r_{in}=8 ε =3), Tcoa11(r_{in}=8 ε =5), Tcoa12(r_{in}=8 ε =7), Tcoa13(r_{in}=9ε =3), Tcoa14(r_{in}=9 ε =5), Tcoa15(r_{in}=9 ε =7).

The design steps used for the classifiers shown in Table 3.8 are the same as the steps used for the design of classifiers for conductors (as described in section 3.2.) and dielectrics (in section 3.3.)

Step 1: As an example, magnitude of the CFRs for the target Tcoa5 at the aspect angles of 45, 90 and 165 degrees are plotted in Figure 3.28.

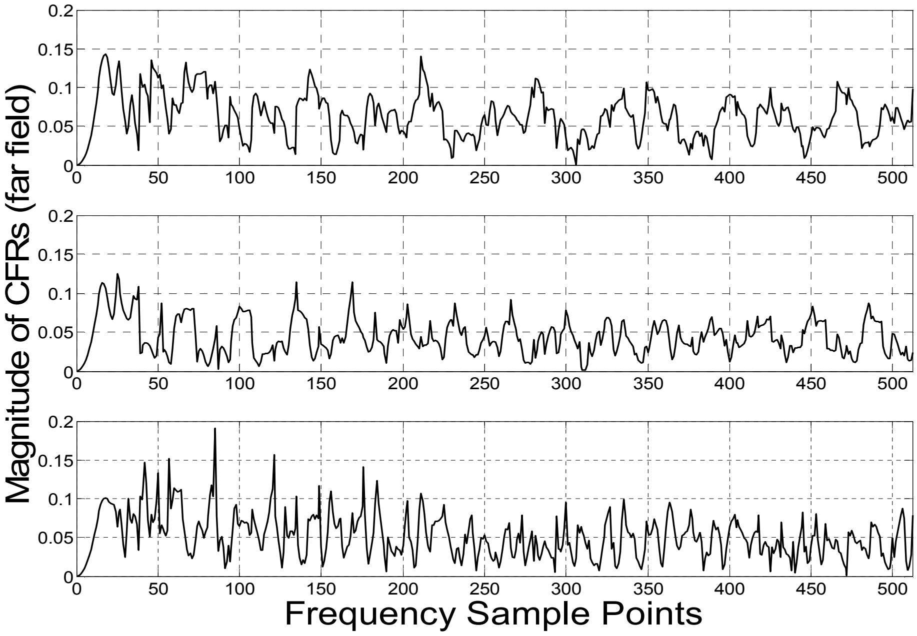

Figure 3.28 Magnitudes of CFRs for Tcoa5 (a) 45º ; (b)90º; (c)165º

Step 2: Time domain responses are synthesized using the CFRs. Examples of scattered signals for Tcoa5 at 45, 90 and 165 degrees are plotted in Figure 3.29.

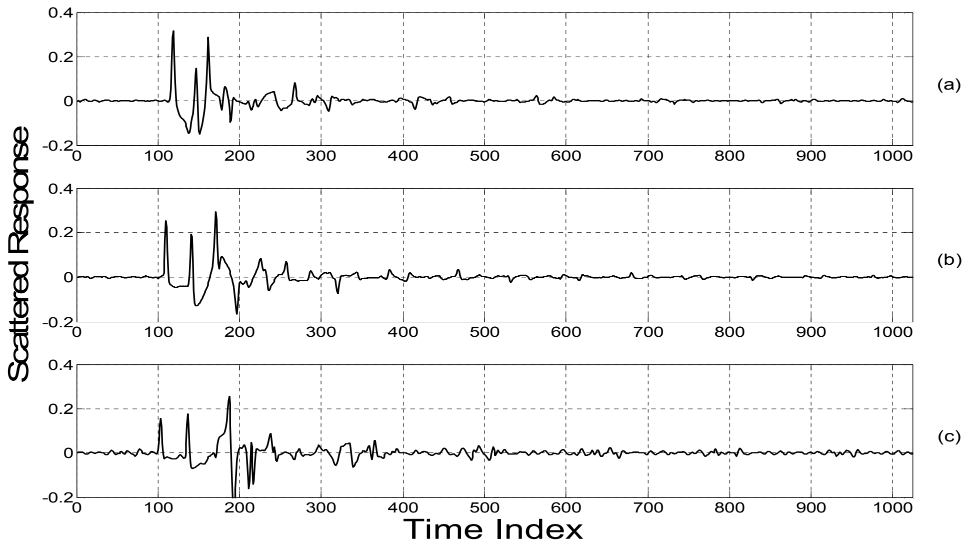

Figure 3.29 Time Domain Responses of at the aspects Tcoa5 (a) 45º; (b)90º; (c)165º

Step 3: The auto-WD matrix W_x of the discrete scattered signal x(t) is computed with N=1024 for all five reference aspects of all targets. As an example to the behavior of these time-frequency images over aspect change, contour plots of the magnitude of W_x matrices for the target Tcoa5 at 45º, 90º and 165º reference aspects are presented in Figure 3.30.

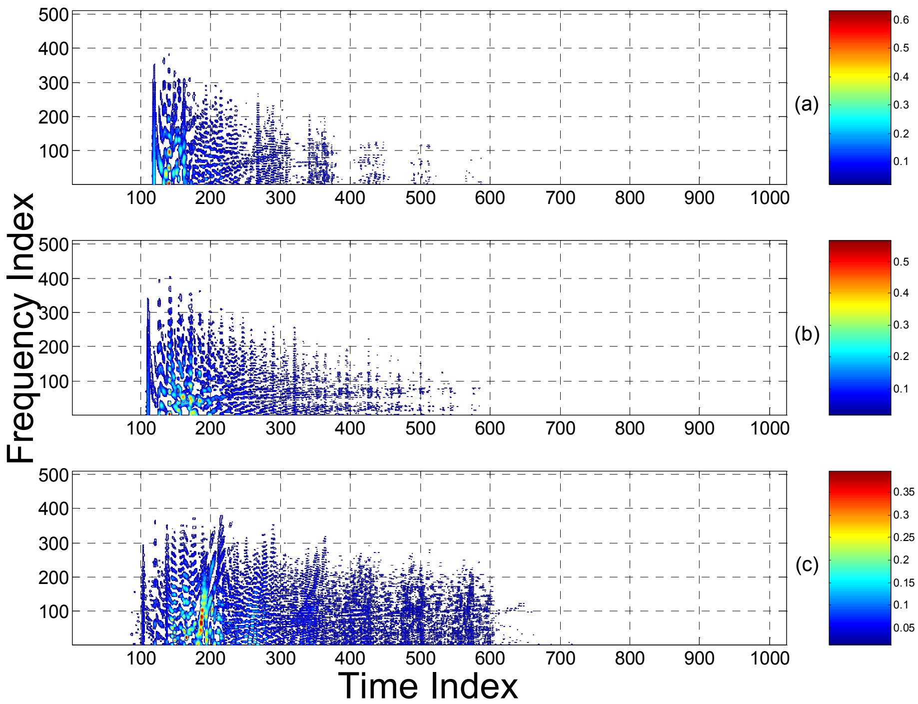

Figure 3.30 Contour plots of the magnitude of the modified auto-Wigner distribution outputs for the target Tcoa5 at (a) 45º; (b)90º; (c)165º.

Step 4: Optimum Q is determined. The correlation coefficients computed for the partitioned energy density vectors of the all targets at 5 reference aspects are plotted in Figure 3.31, for the cases Q = 8, 16, 32 and 64 together with the correlation coefficients computed for the impulse response. As subintervals get wider or as Q value gets smaller, aspect dependency reduces. The optimal value of Q is chosen as 16 for all classifiers design.

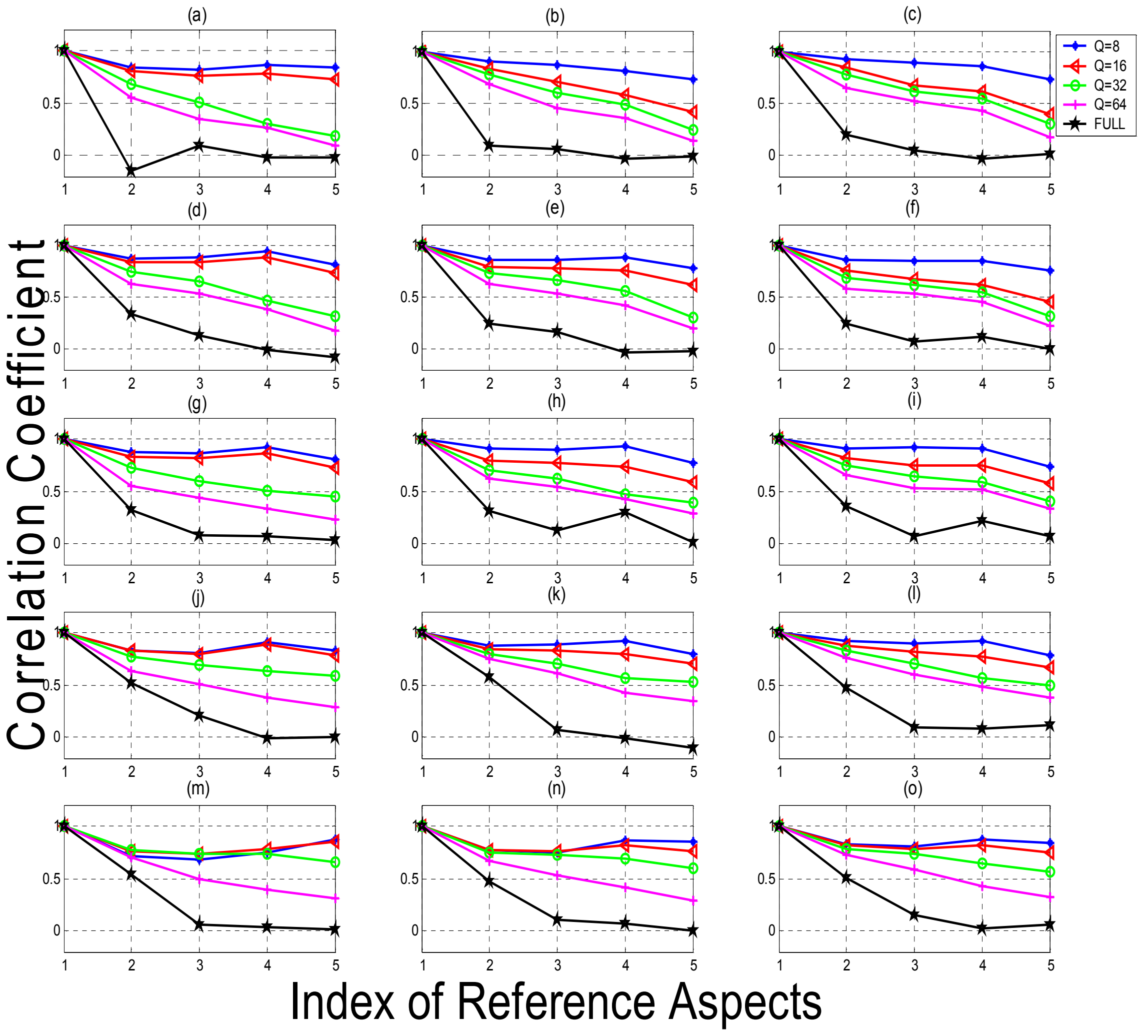

Figure 3.31 Correlation coefficients between the partitioned energy density vectors of the target (a)Tcoa1 (b)Tcoa2 (c)Tcoa3 (d)Tcoa4 (e)Tcoa5 (f)Tcoa6 (g)Tcoa7 (h)Tcoa8 (i)Tcoa9 (j)Tcoa10 (k)Tcoa11 (l)Tcoa12 (m)Tcoa13 (n)Tcoa14 (o)Tcoa15 at the reference aspects computed against the partitioned energy density vector of the same target at 179 degrees, for different partition numbers Q and the full-time scattered signal. The indices 1 through 5 on the horizontal axis refer to the reference aspects of 179, 135, 90, 45 and 5 degrees.

Step 5: For selected Q value, an optimal q* is determined for each classifier. q*=11 case is selected as optimum band.

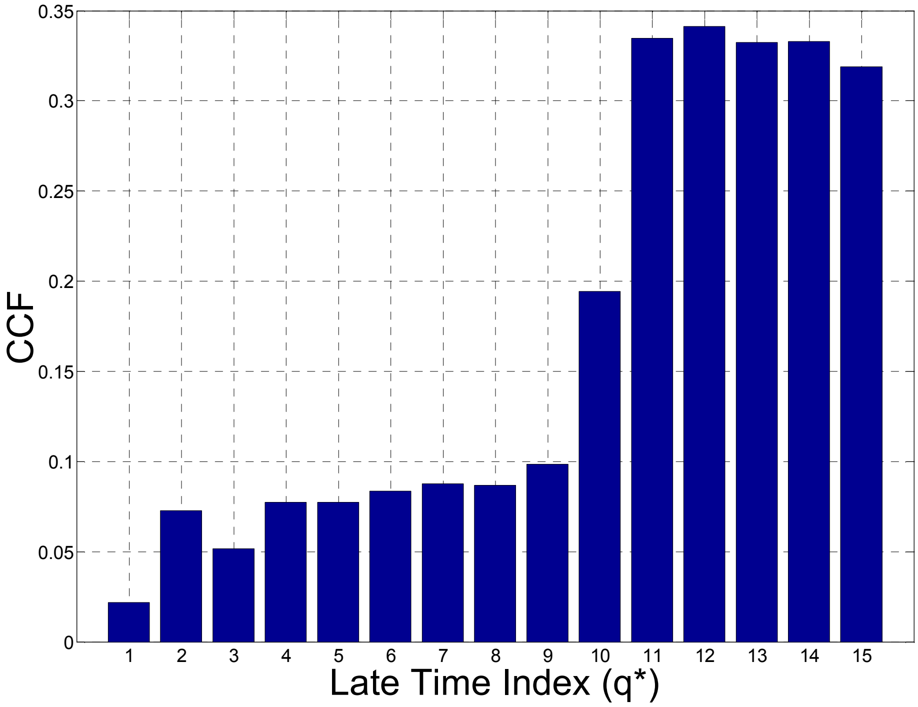

Figure 3.32 CCF plotted against q* to determine the optimal value of q* for CLCOA2.

Step 6: The late-time feature vectors (LTFV) are extracted for all targets at all reference aspects over the selected late-time window that corresponds to the 11th and 12th time bands when Q=16. LTFV of the target Tcoa5 at the reference aspects (θ_{ref}=5º, 45º, 90º, 135º, 179º) are plotted in Figure 3.33.

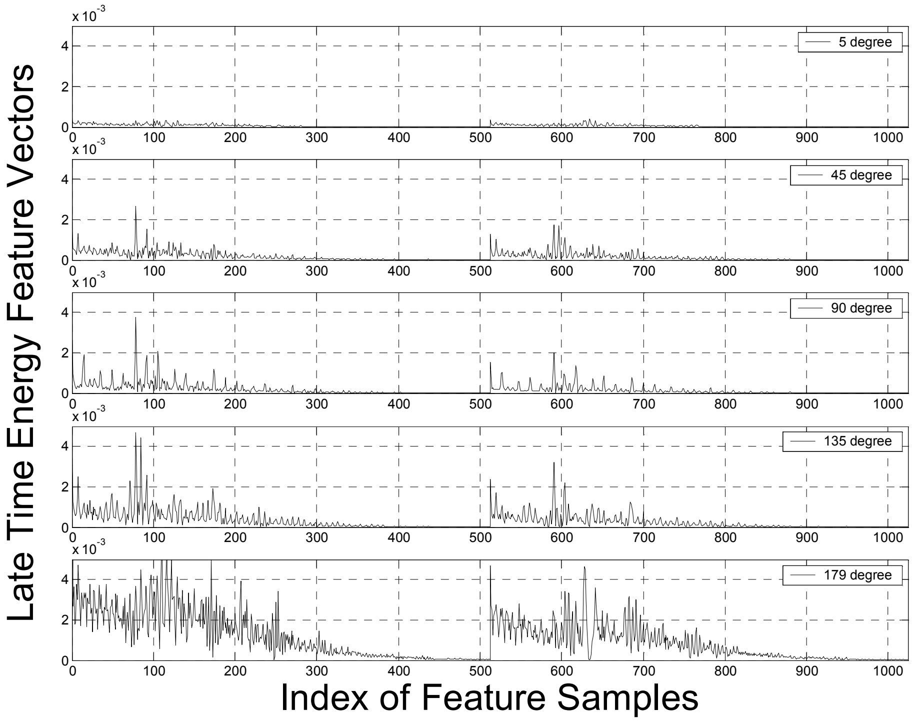

Figure 3.33 LTFVs of Tcoa5 extracted at the reference aspects.

Step 7: For each target, a feature matrix F, the principal components (PCs) of the matrix F and the related eigenvalues are formed at K=5 reference aspects as discussed in Chapter II. For the target Tdie5, the PCs based on the late-time energy feature vectors are plotted in Figure 3.34. By applying the PCA on LTFVs, we have constructed the Fused Feature Vectors (FFVs) of each target.

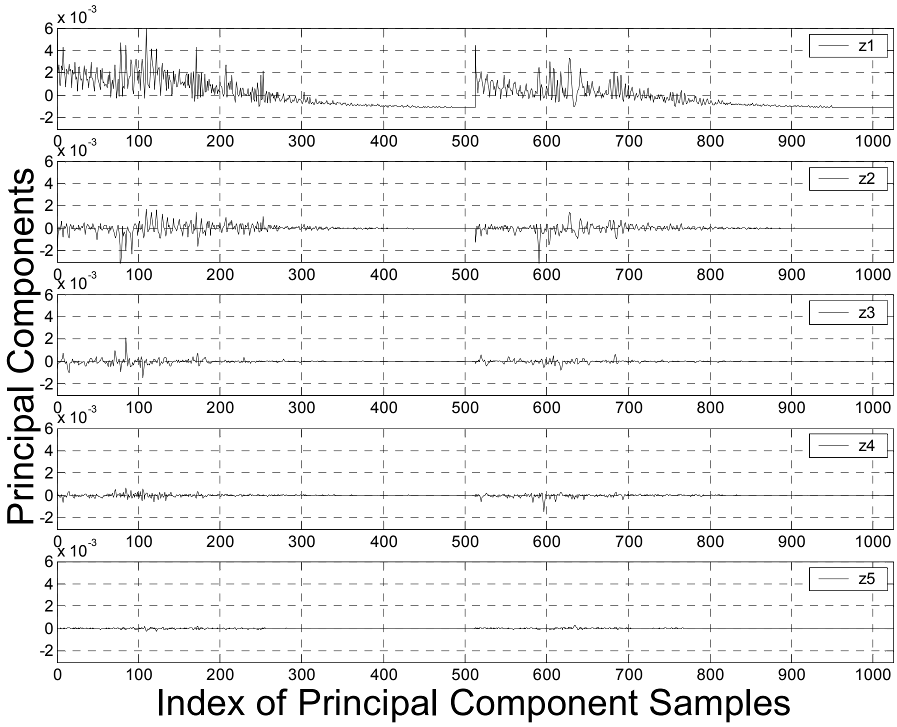

Figure 3.34 PCs for the target Tcoa5 based on LTFV extracted at five reference aspects.

Table 3.9 Correlation Coefficients between the reference LTFV and PCs for target Tcoa5 together with the associated eigenvalues.

Eigenvalues		PCs	θ_{ref}				
λ_i (10^{-5})	$100\overline{\lambda}_i$		179º	135º	90º	45º	5º
0.1319	87.76	z_1	0.9919	0.7493	0.6516	0.7125	0.7864
0.0141	9.38	z_2	0.1270	-0.6265	-0.5944	-0.5041	-0.0711
0.0028	1.86	z_3	-0.0007	0.2122	-0.4442	-0.1905	-0.0760
0.0013	0.86	z_4	0.0030	0.0332	0.1577	-0.4487	-0.2016
0.0002	0.13	z_5	-0.0013	0.0009	0.0015	-0.0217	0.5746

The leading principal component z_1 is very dominant as discussed in [3] and as seen in Table 3.8. λ_i is much larger than the variance of all other PCs.

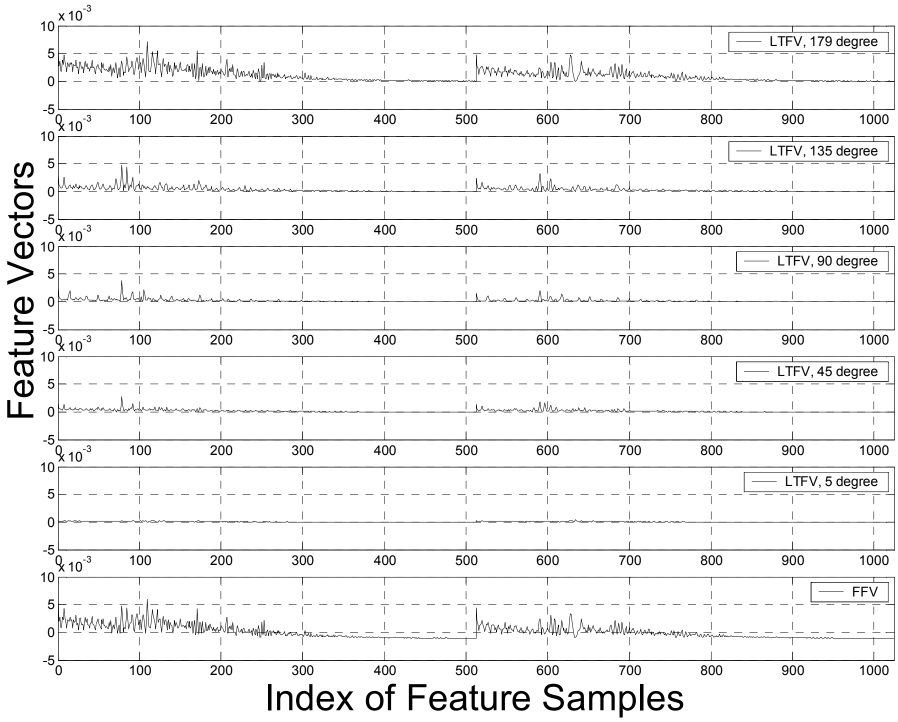

Figure 3.35 LTFVs for each reference aspect and the FFV of Tcoa5.

The FFV results are obtained for all the targets. Each FFV has the length N=1024, therefore, the total fused feature database of M_{tar}-target classifier can be stored in a matrix of size M_{tar}x1024. It uses a very small storage memory.

3.4.2. Performance verification of classifiers in noise free case

After constructing reference databases of all six classifiers, they are tested for performance concerning their decision accuracy using the same approach as used for the performance testing of previously designed conductor classifier (see section 3.2.2.) and dielectric classifiers (see section 3.3.2.)

For all these classifiers;

a. The correlation coefficient of each scattered test signal with respect to each scattered reference signal is computed to form correlation coefficient matrices whose contour plots are given in Figure 3.36 (a) through Figure 3.41 (a) together with proper colorbar to indicate the correlation levels.
b. Similar plots are given in Figure 3.36 (b) through Figure 3.41 (b) where the correlation coefficient matrices are computed for late time scattered signals (LTSS) (based on time bands 1 through 16 and $q^*=11$)
c. Figure 3.36 (c) through Figure 3.41 (c) show the contour plot for the correlation coefficient matrices for the testing LTSSs and fused scattered signals (FSSs).
d. Figure 3.36 (d) through Figure 3.41 (d) show similar plots each possible pair of full size (based on time bands 1 through 16) energy feature vectors for the test and reference data.
e. Figure 3.36 (e) through Figure 3.41 (e) show the contour plots for the correlation coefficient matrices computed for each possible pair of late-time feature vectors extracted from the information on the 11^{th} and 12^{th} time bands only.
f. The correlation coefficient of each LTFV (late-time test feature vector) with respect to each FFV (fused feature vector) is computed for each classifier and are plotted in Figure 3.36 (f) through Figure 3.41 (f) where for each target its FFV is assigned to all the reference aspects by definition.

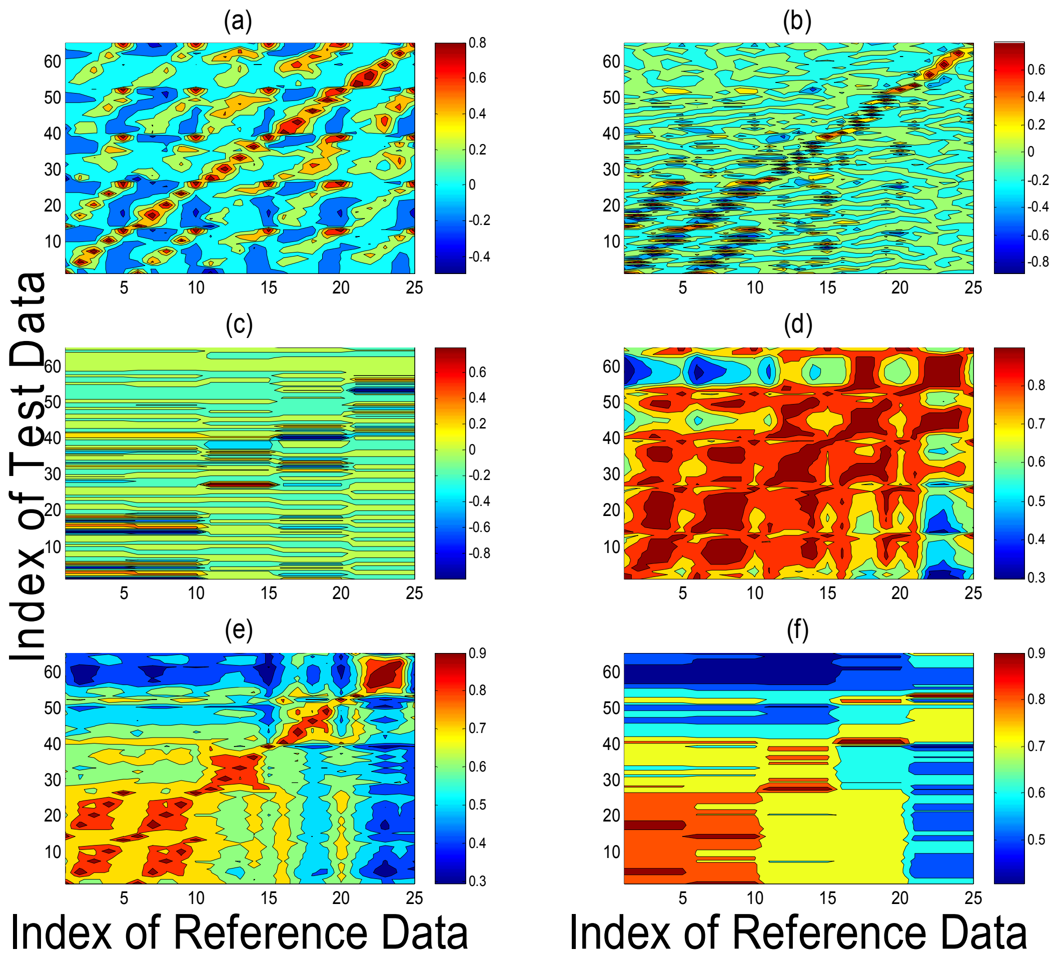

Figure 3.36 Contour plots of correlation coefficient matrices computed for all possible pairs of the test data and the reference data for the classifier CLCOA1 using (a) the unprocessed scattered signals, (b) late time scattered signals (LTSS) (c) the testing LTSSs and fused scattered signals (FSSs) (d) the full-size energy feature vectors, (e) the late-time feature vectors (LTFVs) extracted on the late-time window and (f) the testing LTFVs and the reference fused feature vectors (FFVs).

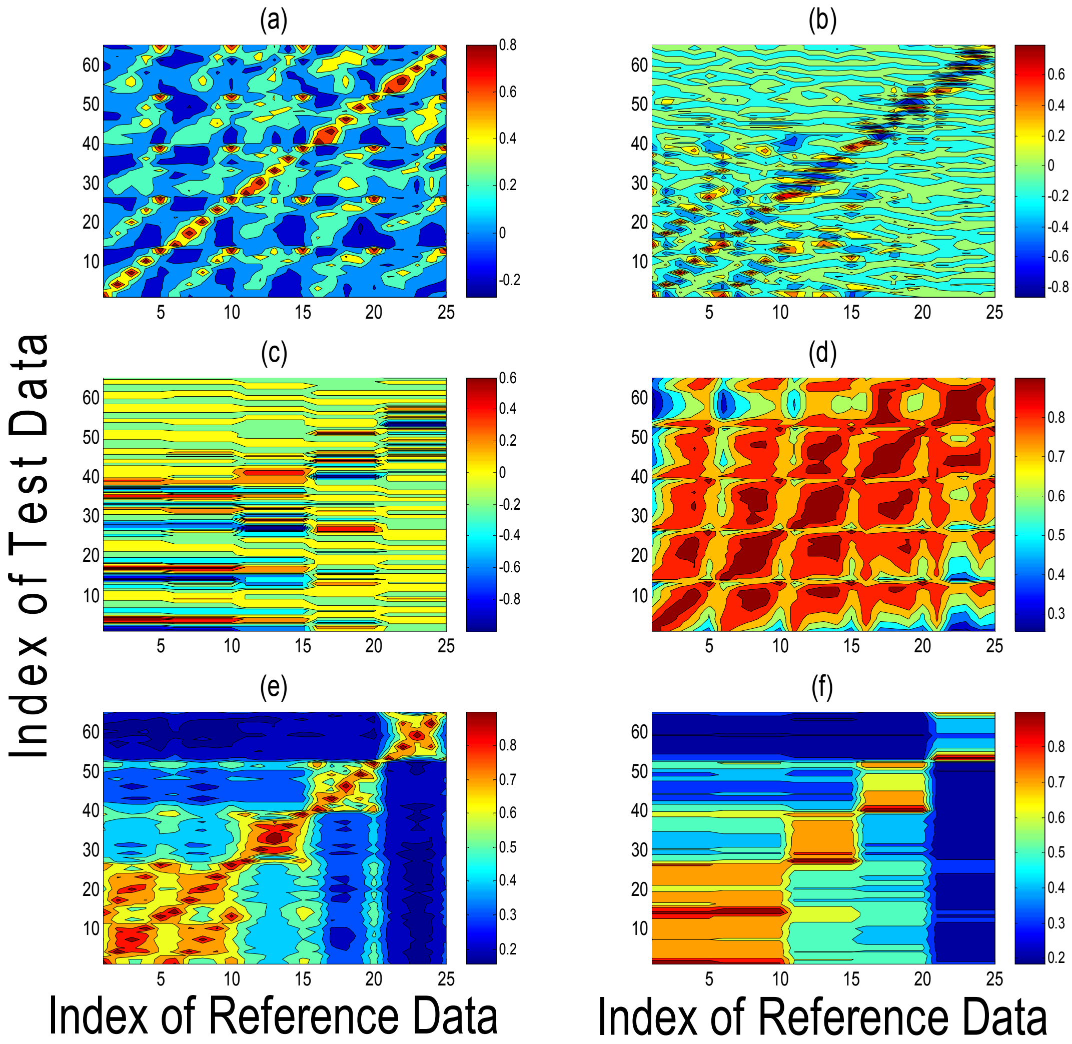

Figure 3.37 Contour plots of correlation coefficient matrices computed for all possible pairs of the test data and the reference data for the classifier CLCOA2 using (a) the unprocessed scattered signals, (b) late time scattered signals (LTSS) (c) the testing LTSSs and fused scattered signals (FSSs) (d) the full-size energy feature vectors, (e) the late-time feature vectors (LTFVs) extracted on the late-time window and (f) the testing LTFVs and the reference fused feature vectors (FFVs).

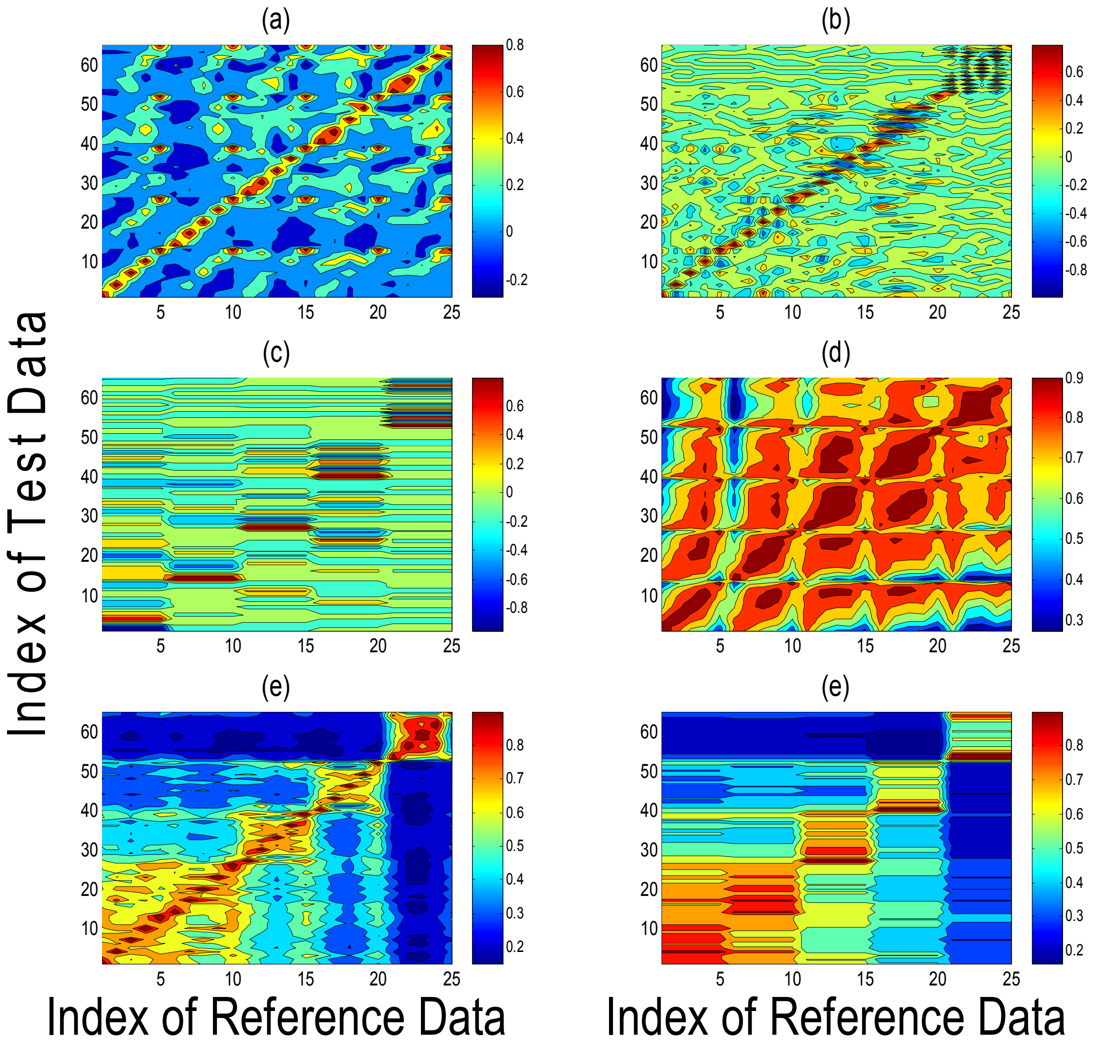

Figure 3.38 Contour plots of correlation coefficient matrices computed for all possible pairs of the test data and the reference data for the classifier CLCOA3 using (a) the unprocessed scattered signals, (b) late time scattered signals (LTSS) [18.43ns, 21.78 ns] (c) the testing LTSSs and fused scattered signals (FSSs) (d) the full-size energy feature vectors, (e) the late-time feature vectors (LTFVs) extracted on the late-time window [18.43ns, 21.78 ns] and (f) the testing LTFVs and the reference fused feature vectors (FFVs).

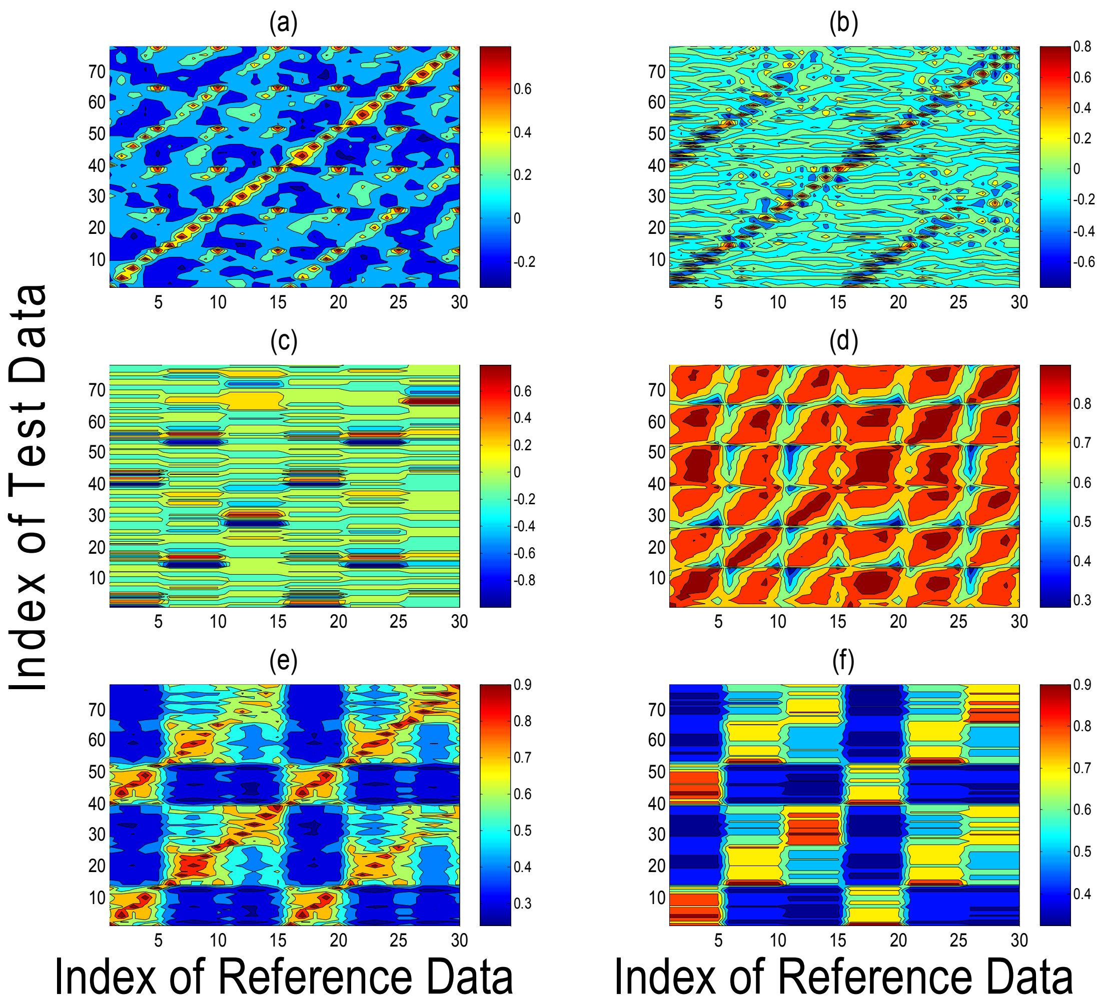

Figure 3.39 Contour plots of correlation coefficient matrices computed for all possible pairs of the test data and the reference data for the CLCOA4 using (a) the unprocessed scattered signals, (b) late time scattered signals (LTSS) (c) the testing LTSSs and fused scattered signals (FSSs) (d) the full-size energy feature vectors, (e) the late-time feature vectors (LTFVs) extracted on the late-time window and (f) the testing LTFVs and the reference fused feature vectors (FFVs).

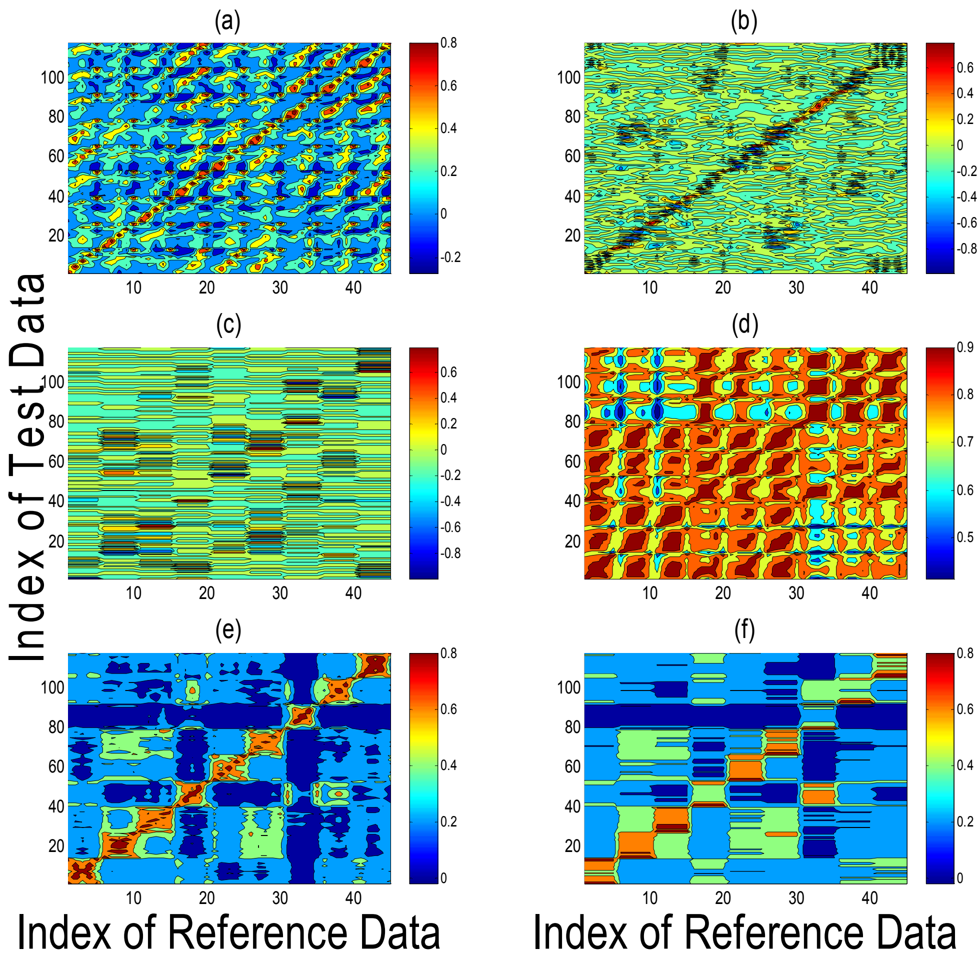

Figure 3.40 Contour plots of correlation coefficient matrices computed for all possible pairs of the test data and the reference data for the classifier CLCOA5 using (a) the unprocessed scattered signals, (b) late time scattered signals (LTSS) (c) the testing LTSSs and fused scattered signals (FSSs) (d) the full-size energy feature vectors, (e) the late-time feature vectors (LTFVs) extracted on the late-time window and (f) the testing LTFVs and the reference fused feature vectors (FFVs).

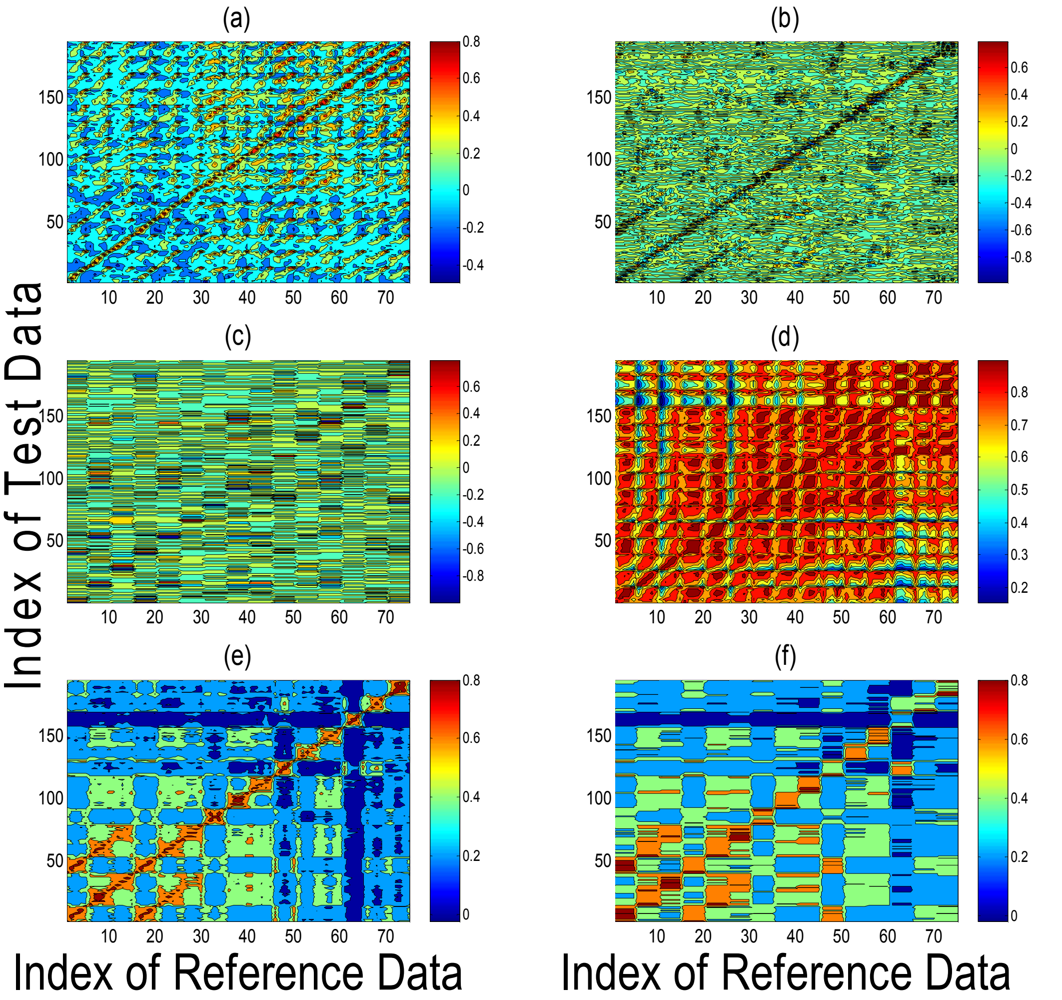

Figure 3.41 Contour plots of correlation coefficient matrices computed for all possible pairs of the test data and the reference data for the classifier CLCOA6 using (a) the unprocessed scattered signals, (b) late time scattered signals (LTSS) (c) the testing LTSSs and fused scattered signals (FSSs) (d) the full-size energy feature vectors, (e) the late-time feature vectors (LTFVs) extracted on the late-time window and (f) the testing LTFVs and the reference fused feature vectors (FFVs).

Table 3.10 Correct Decision Rates (RDc) of the LTSS-based, FSS-based LTFV-based and FFV based classifiers by three different decision criteria: maximum reference match (MRM), complete class match (CCM)and the CCM with at least 5 percent contrast (CCM-5%) criteria.

	MRM					
	CLCOA1	CLCOA2	CLCOA3	CLCOA4	CLCOA5	CLCOA6
LTSS	63%	60%	85%	64%	68%	59%
FSS	22%	20%	38%	21%	26%	17%
LTFV	85%	94%	100%	86%	100%	93%
FFV	65%	92%	98%	77%	86%	82%
	CCM					
LTSS	0%	0%	0%	0%	0%	0%
FSS	22%	20%	38%	21%	26%	17%
LTFV	15%	34%	49%	3%	56%	24%
FFV	65%	92%	98%	77%	86%	82%
	CCM-5%					
LTSS	0%	0%	0%	0%	0%	0%
FSS	20%	20%	38%	21%	26%	16%
LTFV	14%	32%	46%	1%	48%	19%
FFV	63%	66%	95%	50%	85%	70%

As it can be realized from the last six figures and table above, the FFV-based classifiers are more effective regarding both accuracy and robustness.

3.5. Classifier Design for The Whole Group of Perfect Dielectrics, Perfect Conductors and Dielectric Coated Conductors.

3.5.1. Construction of The Classifier Database

In this section, we will design a new classifier (CLMIX1) whose database includes a total of 27 targets such that we have considered three dielectric spheres, nine conducting spheres and fifteen dielectric coated conducting spheres as described in Table 3.11. All the targets have the same radii of 10 cm except conducting spheres.

Table 3.11 classifier description.

Classifiers	Targets
CLMIX1	Tdie1(ε =3), Tdie5(ε=5), Tdie8(ε=7), Tcon1(r=8), Tcon2(r=8.5), Tcon3(r=9), Tcon4(r=9.5), Tcon5(r=10), Tcon6(r=10.5), Tcon7(r=11), Tcon8(r=11.5), Tcon9(r=12), Tcoa1(r_{in}=2 ε =3), Tcoa2(r_{in}=2 ε =5), Tcoa3(r_{in}=2 ε =7), Tcoa4(r_{in}=4 ε =3), Tcoa5(r_{in}=4 ε =5), Tcoa6(r_{in}=4 ε =7), Tcoa7(r_{in}=7 ε =3), Tcoa8(r_{in}=7 ε =5), Tcoa9(r_{in}=7 ε =7), Tcoa10(r_{in}=8 ε =3), Tcoa11(r_{in}=8 ε =5), Tcoa12(r_{in}=8 ε =7), Tcoa13(r_{in}=9ε =3), Tcoa14(r_{in}=9 ε =5), Tcoa15(r_{in}=9 ε =7).

In this classifier design simulation, we find it useful to examine the behaviour of cumulative energy curves of scattered signals for different target types. After normalizing a scattered time domain signals to have unit total energy (as we have already done at the beginning of our design procedure, in general) the cumulative normalized energy curve $\overline{e}(t)$ associated with a scattered signal x(t) is defined as

$$\overline{e}_x(t) = \int_0^t \left|\overline{x}(\tau)\right|^2 d\tau \qquad (3.1)$$

where

$$\bar{x}(t) = \frac{x(t)}{\left[\int_0^\infty |x(\tau)|^2 d\tau\right]^{1/2}} \tag{3.2}$$

is the normalized scattered signal in time domain.

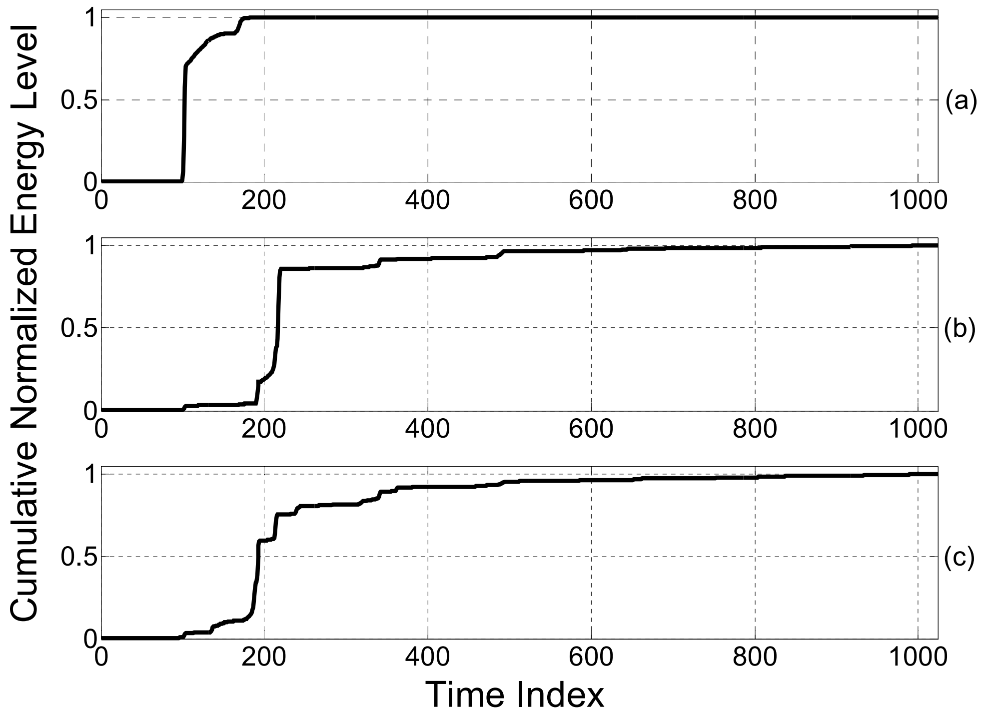

Figure 3.42 Energy figures of (a) Condunting sphere Tcon5 at 179º(b) Dielectric sphere Tdie5 at 179º(c) Dielectic coated conducting sphere Tcoa5 at 179º.

It is known that a perfectly conducting sphere is a very high Q (quality factor) target whose natural response decays very quickly due to very high real parts of sphere poles. Therefore, the maximum normalized energy level of unity is attained at much earlier time for a conducting sphere as compared to dielectric sphere or a dielectric coated conducting sphere of the similar overall size as seen from Figure 3.42. Due to the internal resonance mechanism happening in the dielectric material, these later type of targets have long lasting late-time natural responses in their impulse response type scattered data. These facts are reflected in Figure 3.43 where the time indices at which each scattered signal attains the 99.999 percent of its maximum normalized energy level is plotted against 416 different scattered test data indices. In this figure, we considered a total of 32 targets (8 dielectric spheres, 15 dielectric coated conducting spheres and 9 conducting spheres) at 13 different bistatik aspect angles each. We have used the time domain scattered signals generatedso far in this study at 1024 time domain sample points. As it can be seen in this figure normalized energy curves of spherical conductor type targets reach their maximum value before the time index 300 while the other targets show this behaviour between the indices 870 and 1024.

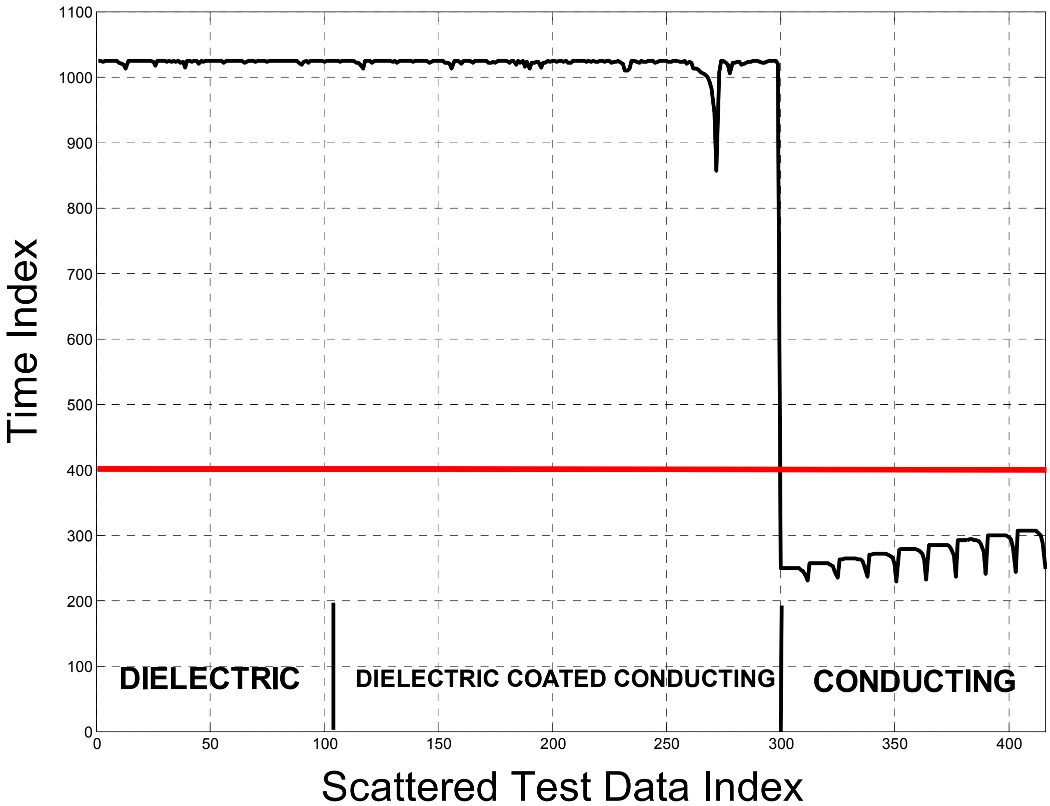

Figure 3.43 Energy separation figure

Using the observations, it is obviously possible to classify a test signal coming from a perfectly conducting sphere at very beginning just by examining its normalized energy curve. By using a threshold level at the time index 400, for example, the conducting spheres can be easily recognized, then a classifier which is the same as the CLCON3 classifier (designed in section 3.2) can be used to identify the size of the conducting sphere. For the other targets a new classifier will be designed as summarized below. Note that after recognizing the conducting sphere separately using the tresholding method and CLCON3 classifier, we are left with 3 dielectric spheres and 15 dielectric coated spheres (a total of 18 targets) for this new classifier. Therefore, we have 18x5=90 reference signals and 18x13=234 test signals to be used in the evaluation of this classifier.

Since all the data needed for this classifier design are ready to use we can continue from step 4.

Step 4: Optimum Q can be chosen as 16 using Figure 3.20 and Figure 3.31.

Step 5: For the selected Q value, an optimal q* is determined as q*=12. As the optimum band indexbased on the result shown in Figure 3.44 below.

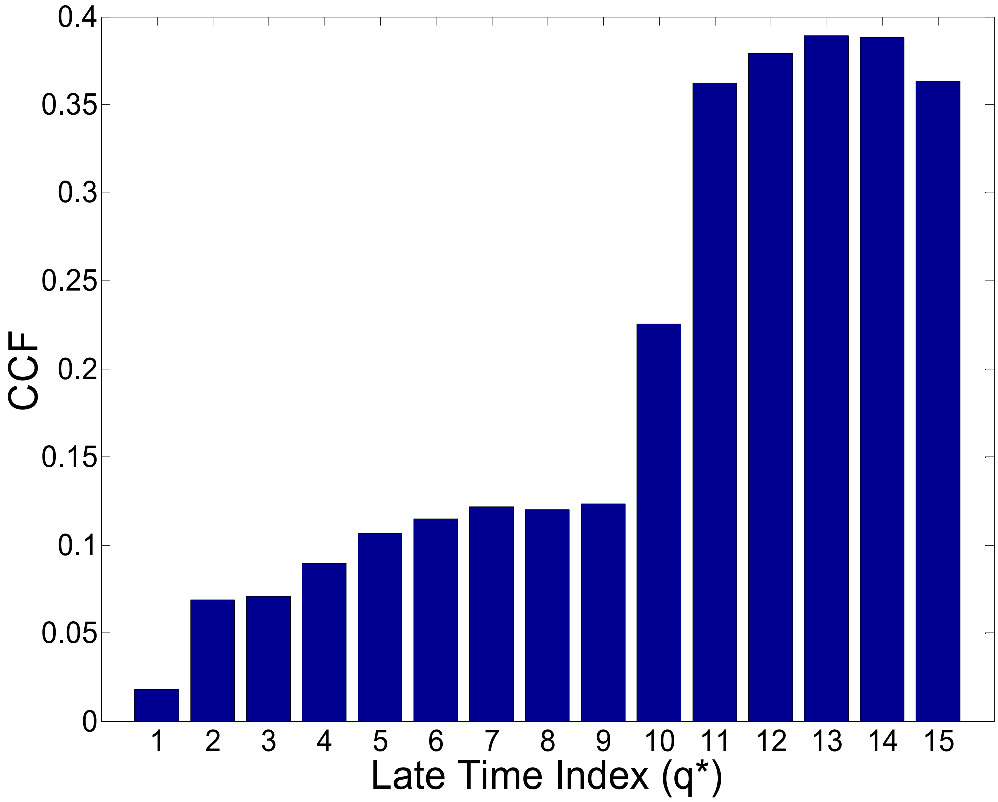

Figure 3.44 CCF plotted against q* to determine the optimal value of q* for CLMIX1.

Step 6: The late-time feature vectors (LTFV) are extracted for all targets at all reference aspects over the selected late time window that corresponds to the 12th and 13th time bands when Q=16.

Step 7: For each target, a feature matrix F, the principal components (PCs) of the matrix F and the related eigenvalues are formed at K=5 reference aspects as discussed in Chapter II. By applying PCA on LTFV, we have constructed Fused Feature Vectors (FFVs) of each target.

3.5.2. Performance verification of the classifier CLMIX1 in noise free case

The performance of the classifier designed for dielectric and dielectric coated conductor targets (as a part of the the classifier CLMIX1) can be summarized as follows:

a. The correlation coefficient of each scattered test signal with respect to each scattered reference signal is computed to form a correlation coefficient matrix of size, 234x90 whose contour plot is given in Figure 3.45 (a) together with a colorbar to indicate the correlation levels.
b. A similar plot is given in Figure 3.45 (b) where the correlation coefficient matrix is computed for late time scattered signals (LTSS) (based on time bands 1 through 16 and q*=12)
c. Figure 3.45 (c) plots correlation coefficients for the testing LTSSs and fused scattered signals (FSSs).
d. Figure 3.45 (d) plots each possible pair of full size (based on time bands 1 through 16) energy feature vectors for the test and reference data.
e. Figure 3.45 (e) plots the correlation coefficient matrix computed for each possible pair of late-time feature vectors extracted from the information on the 12^{th} and 13^{th} time bands only.
f. The correlation coefficient of each LTFV (late-time test feature vector) with respect to each FFV (fused feature vector) is computed for each classifier and are plotted in Figure 3.45 (f) where for each target its FFV is assigned to all the reference aspects by definition.

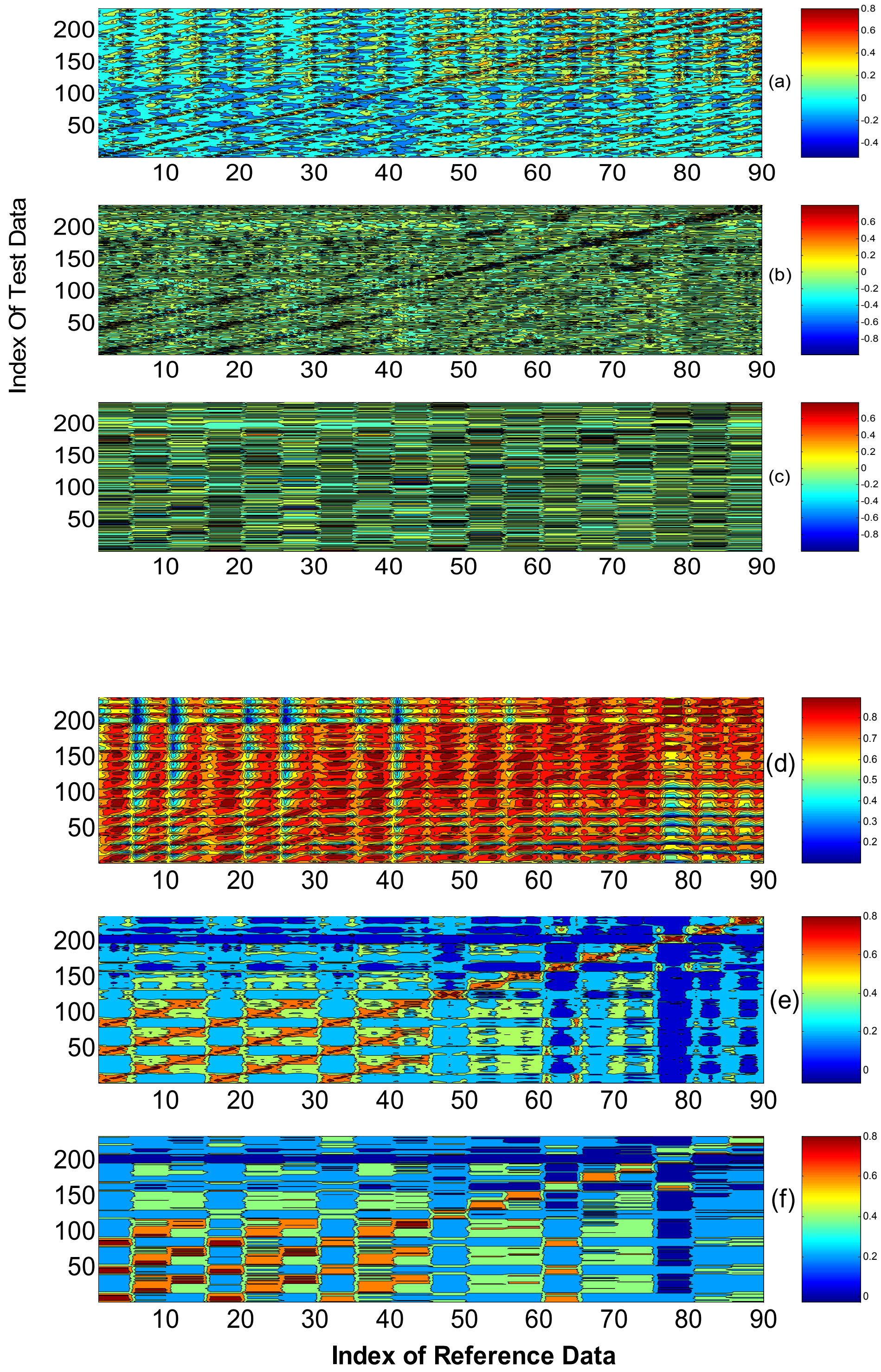

Figure 3.45 Contour plots of correlation coefficient matrices computed for all possible pairs of the test data and the reference data for the classifier CLMIX1.

Table 3.12 Correct Decision Rates (RDc) of the LTSS-based, Fss-based, LTFV-based and FFV based classifiers by three different decision criteria: maximum reference match (MRM), complete class match (CCM)and the CCM with at least 5 percent contrast (CCM-5%) criteria results for only dielectric and dielectric coated conductor type targets.

	MRM	CCM	CCM-5%
(LTSS)	56	0	0
(FSSs)	18	18	15
(LTFV)	88	21	17
FFV based	66	66	53

Table 3.13 Correct Decision Rates (RDc) of the LTSS-based, Fss-based, LTFV-based and FFV based classifiers by three different decision criteria: maximum reference match (MRM), complete class match (CCM)and the CCM with at least 5 percent contrast (CCM-5%) criteria results for all targets in the CLMIX1 databese.

	MRM	CCM	CCM-5%
(LTSS)	71%	31%	18%
(FSSs)	45%	45%	34%
(LTFV)	92%	47%	45%
(FFV)	77%	77%	62%
(FFV/FSS)	77%	77%	60%

As it can be realized from Figure 3.45 and Table 3.12, the FFV-based classifier is more effective for dielectric containing targets considering both accuracy and robustness. Remember we have determined earlier in section 3.2, for conducting targets that FSS-based and FFV-based classifiers are both found suitable leading to almost the same correct decision rates for noise-free analysis. If we combine the correct desicion rates of FFV for dielectric containing targets and the correct desicion rates of FSS for perfectly conductor targets, we and up with 77% overall correct decision rate for MRM and CCM cases and 60% for CCM-5% case for the CLMIX1 classifier as shown in Table 3.13.

3.6. Noise Performance Analysis of the Selected Classifiers

In this section, noise performance of two sets of classifiers will be investigated. First, the classifier CLCOA3 (designed for dielectric coated conducting sphere classification) will be tested at varying signal to noise ratio (SNR) levels. The performances of the LTSS-based, FSS-based, LTFV-based and FFV-based versions of the classifier CLCON2 will be compared in detail. Next, the same noise analysis will be repeated for the classifier CLCON2, which is previously designed for the conducting spheres at varying SNR levels. Since similar analyses were already performed for a dielectric classifier Turhan-Sayan in [3], noise performance analysis of a dielectric sphere classifier is not repeated in this thesis.

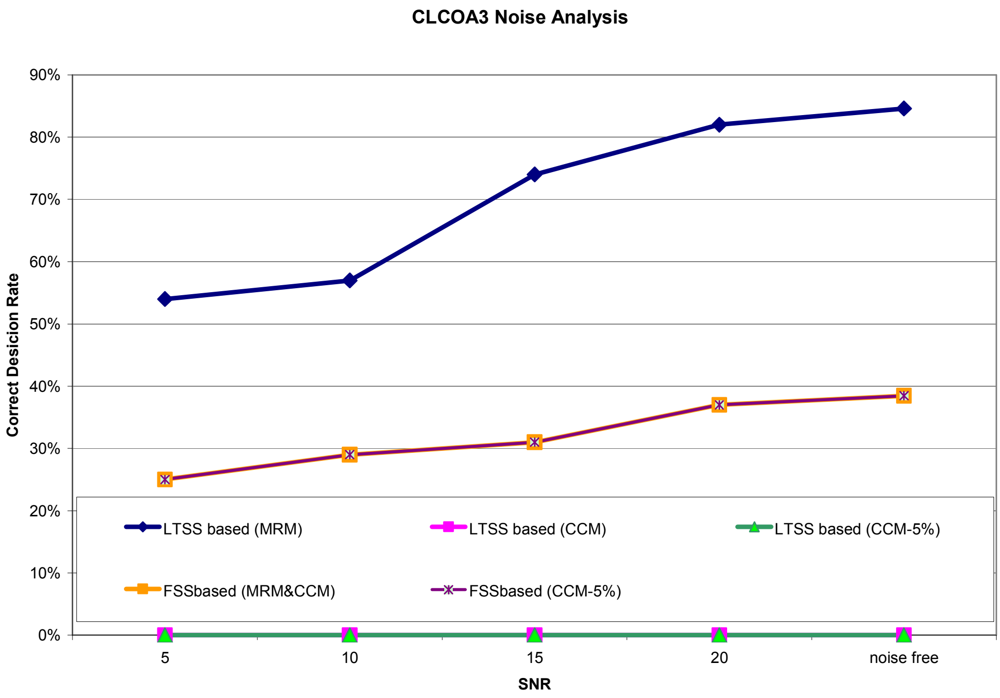

Figure 3.46 Correct Desicion Rates vs. for CLCOA3 noise analysis.

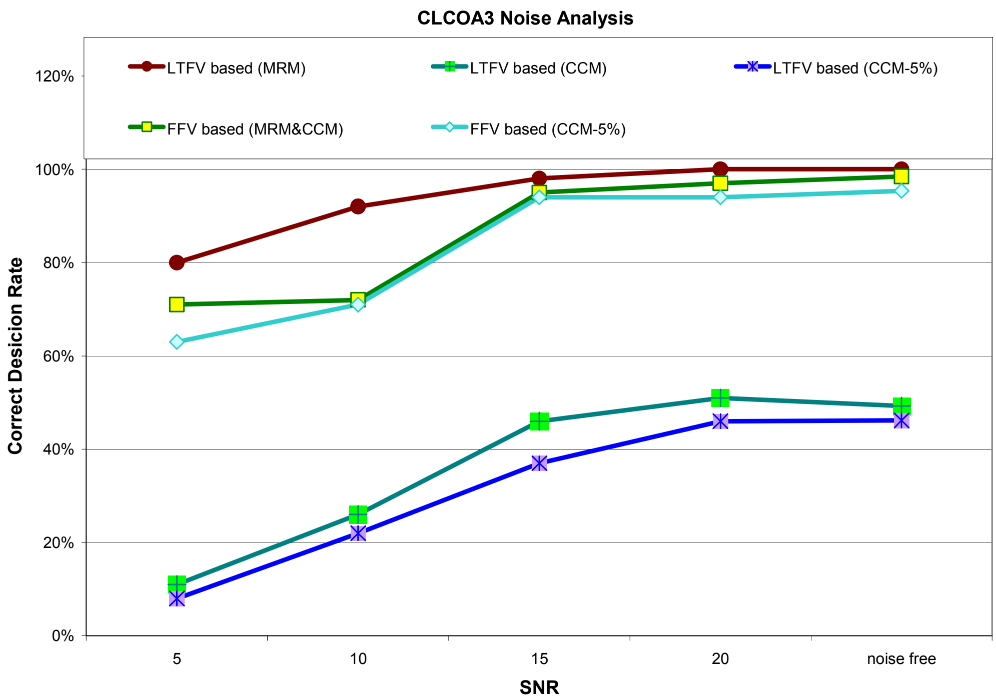

Figure 3.47 Correct Desicion Rates vs. for CLCOA3 noise analysis.

The noise performance analysis done for the classifier CLCOA3 can be summarized as follows: The noise performances of the LTSS based, FSS based, LTFV based and FFV based classifiers are compared at the SNR levels of 20 dB, 15 dB, 10 dB and 5 dB using the test database of CLCOA3. The correct decision rates for these classifiers are computed based on each of the decision criteria MRM, CCM and CCM-5 % and plotted in Figure 3.46 and Figure 3.47. As sees Figure 3.47 curves of correct decision rates for the FFV-based classifier (using the MRM/CCM and CCM-5% criteria) and for the LTFV-based classifier (using the MRM criterion only) change very similarly from 100% to about 65%-70% level as the SNR of the test signal gets down to 5 dB. The LTFV-based classifier performs poorly for the CCM and CCM-5% criteria with correct decision rates falling from 45%-50% level to 10% level on the SNR drops from infinity (noise free case) to 5 dB level. The performances of the LTSS-based and FSS-based classifiers are summarized in Figure 3.46, similarly. It is observed in this figure that the correct decision rate for the LTSS-based classifier with MRM criteria changes from to 85% to 55% as SNR decreases down to 5 dB. LTSS-based classifier for CCM and CCM-5% criteria makes no correct desicion. As a result, the FFV-based classifier is proven to be the only acceptable solution when a robust decision scheme with minimized decision uncertainty is also required in addition to high correct decision rate, short decision time, small storage memory and satisfactory noise performance even at very low SNR levels.

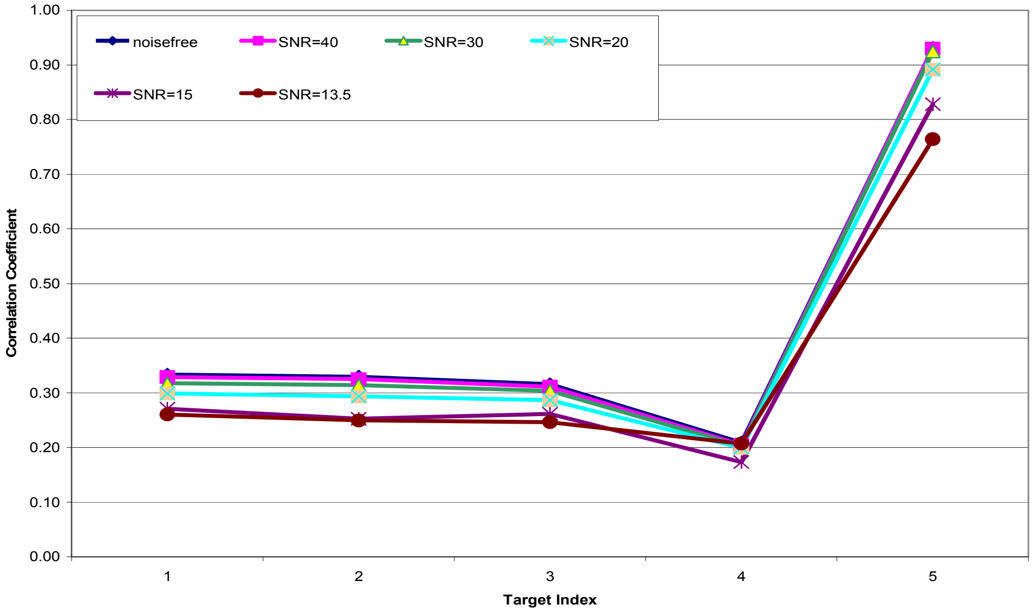

Figure 3.48. The FFV-based CLCOA3 classifier is tested by the "unknown" target Tcoa15 at 165 degrees at 6 different SNR levels changing from infinity to 13.5 dB.

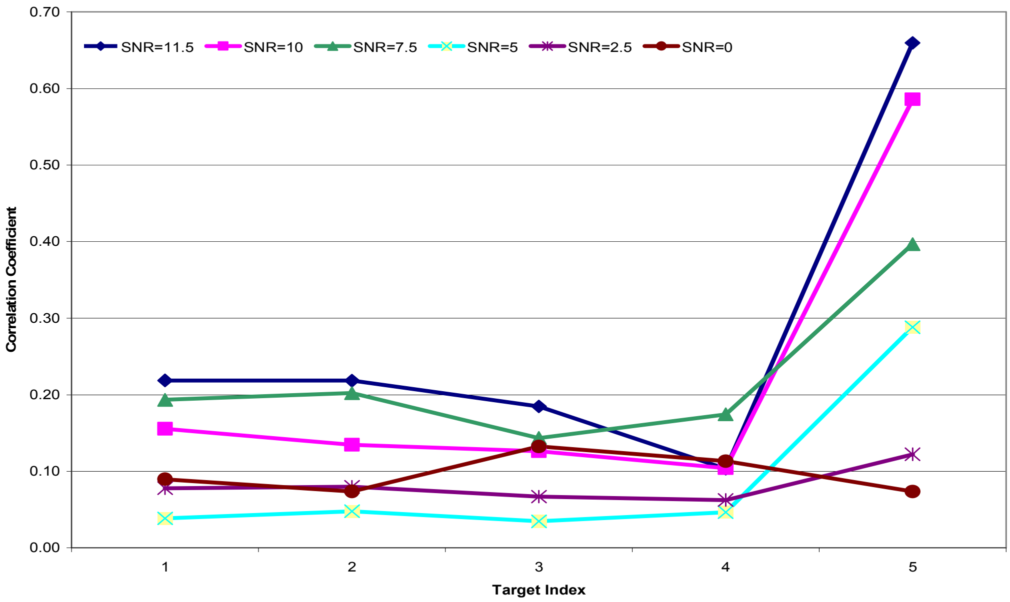

Figure 3.49. The FFV-based CLCOA3 classifier is tested by the "unknown" target Tcoa15 at 165 degrees at 6 different SNR levels changing from 11.5 dB to zero decibel.

For a randomly selected test signal which happens to be the test signal for the target Tcoa15 at 165 degree aspect angle, a set of noisy test signals are synthesized by adding white Gaussian noise to the noise-free scattered time domain signal at the overall SNR levels of 40, 30, 20, 15, 13.5, 11.5, 10, 7.5, 5, 2.5 and 0 dB levels. In view of the fact that the proposed feature extraction process essentially use the scattered information over the 11^{th} and 12^{th} time bands only, the corresponding effective SNR levels over this late-time window are computed as 26.78 dB, 16.72 dB, 6.24 dB, 1.47 dB, -0.10 dB, -2.70 dB, -3.78 dB, -5.63 dB, -9.10 dB, -11.76 dB and -13.90 dB, respectively. The correlation coefficient values for FFV based classifier are plotted in Figure 3.48 for the first six SNR levels starting from the noise-free case for which the SNR is infinite down to SNR is infinite down to SNR=13.5dB level. The rest of the results for the SNR levels of 11.5 dB to zero decibel are reported separately (for clarity) in Figure 3.49.

The test target Tcoa15 (corresponding to the target index value of 5 in the horizontal axis of Figure 3.48 and Figure 3.49) is correctly classified at the overall SNR levels as low as 2.5 dB that corresponds to the effective SNR of -11.76 dB in the selected late-time zone. In other words, even when the noise power is about 15 times larger than the signal power over the 11^{th} and 12^{th} time bands, the test target can still be correctly identified with a contrast margin of about 36 percent. At the zero dB overall SNR case finally, the target is incorrectly classified to be the target Tcoa9 corresponding to target index 3 in Figure 3.48 and Figure 3.49. It is also observed in these figures that the correlation coefficient curve tends to shift to lower values with a smaller dynamical range as the SNR of the test signal gets lower, as expected.

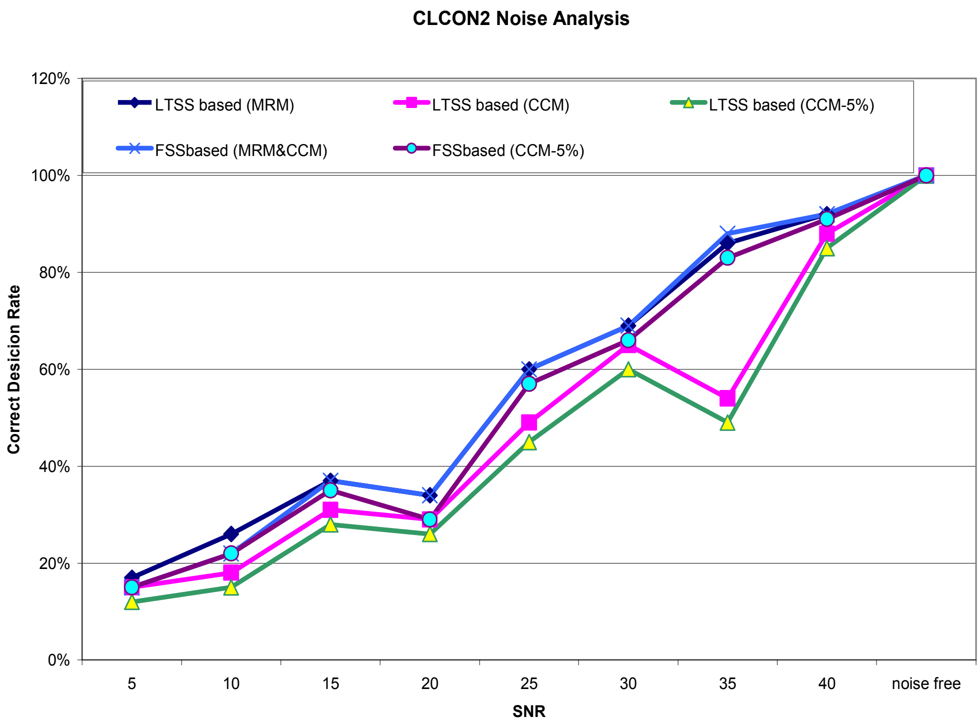

Figure 3.50 Correct Desicion Rates vs. for CLCON2 noise analysis.

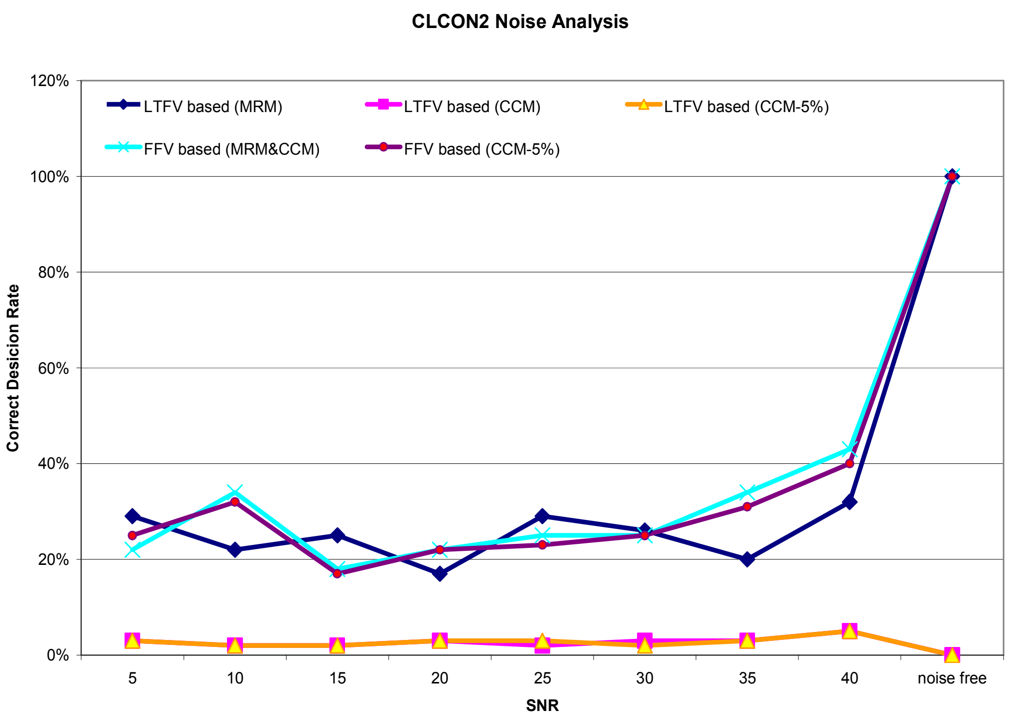

Figure 3.51 Correct Desicion Rates vs. for CLCON2 noise analysis

Secondly, the noise performance analysis results for the classifier CLCON2 can be summarized as follows: The noise performances of the LTSS based, FSS based, LTFV based and FFV based classifiers are compared at the SNR levels of 40 dB, 35 dB, 30 dB, 25 dB, 20 dB, 15 dB, 10 dB and 5 dB using the test database of the classifier CLCON2. The correct decision rates for these classifiers are computed based on each of the decision criteria MRM, CCM and CCM-5 % and plotted in Figure 3.50 and Figure 3.51.

As seen in Figure 3.50 curves of correct decision rates for the FSS-based classifier (using the MRM/CCM and CCM-5% criteria) and for the LTSS-based classifier (using the MRM criterion only) change very similarly and slowly from 100% to 15% as the SNR gets down to 5 dB level. The LTSS-based results classifiers for the CCM and CCM-5% criteria drop more sharply around the 35 dB level. As observed in Figure 3.51, on the other hand, the recognition performance of the LTFV and FFV based classifiers drop below the 40% level even for a very high SNR of 40 dB. In summary, the FSS-based classifier provides best solution compared to the other type of CLCON2 classifiers, but none of the classifiers examined here gives a robust decision scheme with the SNR levels below 25 dB. In other words, the noise performance of the target classifiers designed for conducting spheres is found to be poor.

At a randomly selected target/aspect combination of Tcon9 at 165 degree, a set of noisy test signals are synthesized by adding white Gaussian noise to the noise-free scattered time domain signal at the overall SNR levels of 40 dB, 35 dB, 33.5 dB, 31.5 dB, 30 dB, 27.5 dB, 25 dB, 23.5 dB, 21.5 dB, 20 dB, 18.5 dB, 16.5 dB, 15 dB, 13.5 dB, 11.5 dB, 10 dB, 7.5 dB, 5 dB, 2.5 dB and 0 dB. In view of the fact that the proposed feature extraction process essentially use the scattered information over the 9th and 10th time bands only, the corresponding effective SNR levels over this late-time window are computed as 7.84 dB, 1.23 dB, 0.62 dB, -1.05 dB, -2.71 dB, -5.41 dB, -8.54 dB, -8.82 dB, -10.59 dB, -12.64 dB, -14.48 dB, -15.98 dB, -19.75 dB, -18.27 dB, -21.67 dB, -22.67 dB, -25.53 dB, -27.59 dB, -31.29 dB and -32.18 dB, respectively. The correlation coefficient values for the LTSS based and the FSS based classifiers are plotted in Figure 3.52 and Figure 3.53 for all mentioned SNR levels including the noise-free case for which the SNR is infinite.

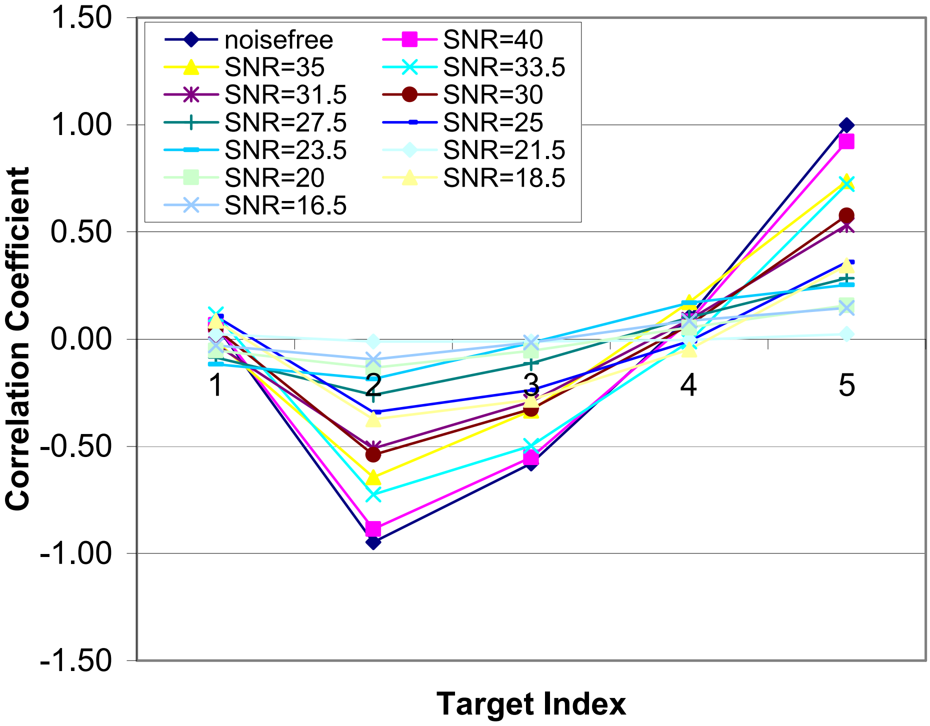

Figure 3.52 The FSS-based classifier is tested by the "unknown" target Tcon9 at 165 degrees at 13 different SNR levels changing from infinity to 16.5 decibel.

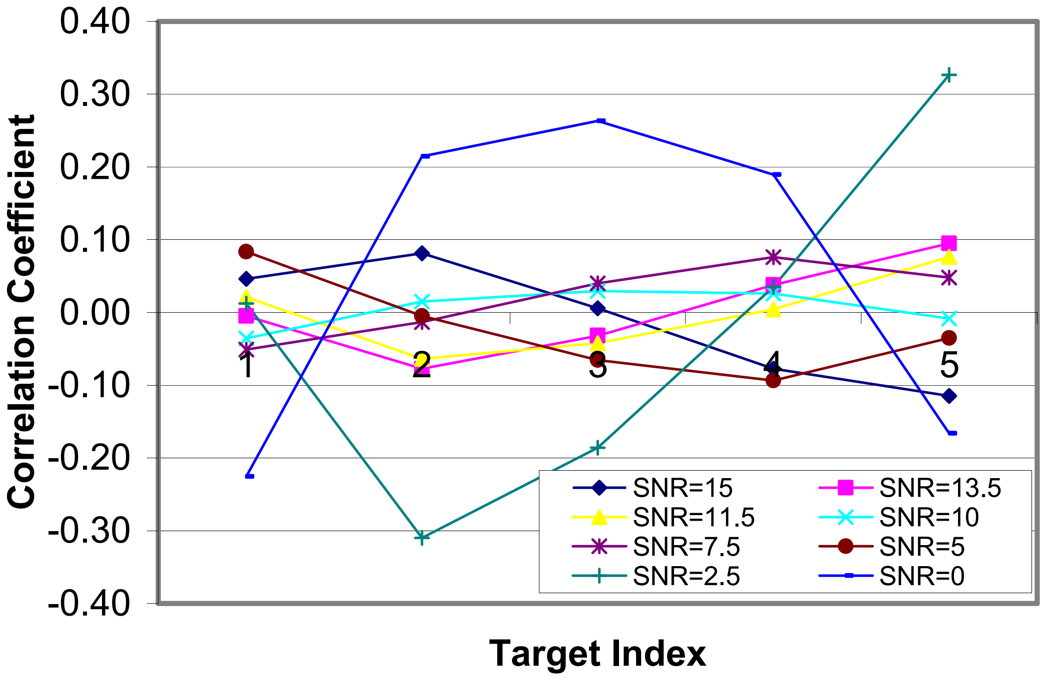

Figure 3.53 The FSS-based classifier is tested by the "unknown" target Tcon9 at 165 degrees at 8 different SNR levels changing from 15 decibel to zero decibel.

The test target Tcon9 (corresponding to the target index value of 5 in the horizontal axis of Figure 3.50 and 3.51) is correctly classified at the overall SNR levels from infinity down to 15 dB that corresponds to the effective SNR of -19.75 dB. For lower SNR levels classification is coincidental.

CHAPTER IV

CONCLUSION

This thesis has been focused in designing electromagnetic target classifiers using a natural resonance based design technique, which aims the formation of a minimal size classifier database via extraction and fusion of target features from the reference data scattered at only a few aspects not only for dielectric or perfectly conducting spheres but for also dielectric coated conducting spheres and mixture of all these targets. The classification problem tackled here is difficult to solve as the targets have basically the same geometrical shape and the same overall size but slightly different material composition leading to similar target pole patterns. This similarity becomes stronger among the dielectric containing targets. The technique used for classifier design was originally introduced by Turhan-Sayan [2,3] and demonstrated for dielectric spheres. The application of the same technique was reported for perfectly conducting wire target structures just recently in [13]. In this thesis, the aim has been to solve more complicated classification problems regarding the material composition of the targets as well as the size and variety of target classes used in classification. Classification catalogs containing a large number of targets are formed for the simulation problems. In some of the classifier design simulations, both loss-free dielectric spherical targets and dielectric coated conducting spheres are used as candidate targets. Even perfectly conducting spherical targets are included into these extended target sets in the last classifier design problem presented. It should be also mentioned that the classifier design technique introduced in references [2] and [3] is applied to dielectric coated conducting targets for the first time in this thesis.

Main objective of the above mentioned core technique is to represent each target class by a single fused feature vector to be used at any possible testing aspect with sufficient accuracy. To fulfill this objective, it is obviously necessary to minimize the aspect dependency of the reference feature database. The Wigner-Ville Distribution (WD) and the Principal Component Analysis (PCA) are the main signal processing tools employed in the core technique for this purpose. Using the WD, the natural resonance-related late-time energy feature vectors are extracted from the scattered data. After then, feature vectors belonging to a few different reference aspect angles are fused by using the PCA technique.

Applied design technique is successfully demonstrated for different classifiers where the targets are perfectly conducting spheres whose sizes slightly vary, equal-size dielectric spheres whose relative permittivities slightly vary from one to another, equally large dielectric coated conducting spheres whose relative permittivities and/or inner radius slightly vary from one to another. The reference databases of the classifiers are constructed using scattered data at five distant aspect angles. Real-time classification decisions in a test case can be completed in less than a second for worst case (with the largest database), using a laptop computer with a microprocessor of 2.2 GHz speed and in MATLAB 6.1 programming environment.

Based on the simulation results, it is observed that for larger relative permittivity (ε_r) values used for coating, better classification results are obtained. When the ε_r gets smaller, it becomes more and more difficult to differentiate coated spherical conductors from each other based on the differences in their inner conductor radii. The perfectly conducting spheres (with their infinitely large ε_r), on the other hand, can be easily recognized as they display a noticeably different late-time behavior as compared to dielectric and/or dielectric coated conducting targets.

For small bistatic aspect angles (see Figure 3.1) correct decision rates are almost perfect, for larger bistatic angles approaching to 180 degres false identification is more likely due to reduced signal (i.e. worse SNR) levels. Considering typical radar operations, return signals from reasonably small bistatic aspect angles or at monostatic aspects are needed. So, the classification technique is suitable for bi-static radar or electronic warfare (EW) systems, not for the conventional high frequency, narrow band radars but for the ultrawide band (UWB) radars of the future generation.

Advantages of classifiers designed in this thesis are mainly high correct decision rate, very high decision speed, low memory requirements, need for reduced amount of reference data, simplicity, repeatability and computational efficiency.

As indicated in [13] the electromagnetic target classifier design technique suggested in references [2] & [3] can be further simplified in the case of perfectly conducting structures such that the WD computation and LTFV extraction steps can be skipped altogether. Instead, the PCA fusion technique can be directly applied to the suitably chosen late-time portions of the conducting target responses to construct the final form of the classifier's fused feature database.

REFERENCES

[1] G.Turhan-Sayan, K. Leblebicioglu, and T. Ince, “Electromagnetic target classification using time-frequency analysis and neural networks,” Microw. Opt. Technol. Lett., vol. 21, pp. 63–69, 1999

[2] G.Turhan-Sayan, "Natural resonance-based feature extraction with reduced aspect sensitivity for electromagnetic target classification," Pattern Recognition, Vol.36, No. 7, pp. 1449-1466, July 2003.

[3] G.Turhan-Sayan, “Real Time Electromagnetic Target Classification Using a Novel Feature Extraction Technique with PCA-Based Fusion” IEEE Transactions On Antennas and Propagation, Vol. 53, No.2, February 2005.

[4] G.Turhan-Sayan and T. İnce, “Neural Network techniques in Electromagnetic Target Classification: A Comparison Study,” 1999 IEEE AP-S International Symposium and UNSC/URSI National Radio Science Meeting, AP proceedings, Vol.3, pp. 2222-2225, July 1999, Orlando, Florida, USA.

[5] G. Turhan-Sayan, K. Leblebicioğlu and S. İnan, “Input signal shaping for target identification using genetic algorithms,” Microwave and Optical Technology Letters, vol.17, no.2, pp.128-132, Feb. 1998.

[6] G. Turhan-Sayan and M. Kuzuoglu, "Pole Estimation for Arbitrarily-Shaped Dielectric Targets by a Genetic Algorithm-Based Resonance Annihilation Technique," IEE Electronics Letters, vol. 37, no. 6, pp.380-381, March 2001.

[7] V. C. Chen and S. Qian, “Joint time-frequency transform for radar range-Doppler imaging,” IEEE Trans. Aerosp. Electron. Syst., vol. 34, pp. 486–499, Apr. 1998.

[8] C. Delfs and F. Jondral, “Classification of piano sounds using time-frequency signal analysis,” Proc. IEEE Int. Conf. Acoust., Speech, Signal Process., vol. 3, pp. 2093–2096, 1997.

[9] V. C. Chen and H. Ling, “Joint time-frequency analysis for radar signal and image processing,” IEEE Signal Processing Mag., vol. 16, pp. 81–93, Mar. 1999.

[10] S. Qian and D. Chen, “Joint time-frequency analysis,” IEEE Signal Processing Mag., vol. 16, pp. 52–67, Mar. 1999.

[11] H. Dickhaus and H. Heinrich, “Classifying biosignals with wavelet networks,” IEEE Eng. Med. Biol. Mag., vol. 15, pp. 103–111, 1996.

[12] Y. Shi and X.-D. Zhang, "A Gabor atom network for signal classification with application in radar target recognition," IEEE Trans. Signal Processing, vol. 49, no. 12, pp. 2994-3004, Dec. 2001. 23

[13] M.Okan Ersoy “Application Of A Natural-Resonance Based Feature Extraction Technique To Small-Scale Aircraft Modeled By Conducting Wires For Electromagnetic Target Classification” M.S. thesis METU September 2004.

[14] S. S. Abeysekera and B. Boashash, “Methods of signal classification using the images produced by the Wigner-Ville distribution,” Pattern Recogn. Lett., vol. 12, pp. 717–729, 1991.

[15] G. C. Gaunaurd and H. C. Strifors, “Signal analysis by means of time frequency (Wigner-type) distributions—Applications to sonar and radar echoes,” Proc. IEEE, vol. 84, pp. 1231–1248, Sept. 1996.

[16] D.L.Moffatt and R.K.Mains, “Detection and Discrimination of Radar Targets”, IEEE Transactions on Antennas and Propagation, vol. AP-23, pp. 358-367, May 1975.

[17] D.P.Nyquist, K.M.Chen, E.Rothwell and B.Drachman, “Radar Target Discrimination using the Extinction-Pulse Technique”, IEEE

Transaction on Antennas and Propagation, vol. AP-33, pp. 929-937, Sept. 1985.

[18] C.W.Chuang and D.L.Moffatt, “Natural resonances via Prony’s method and target discrimination”, IEEE Transactions on Aerosp. Electron. Syst., vol. AES-12, 1976.

[19] E.M.Kennaugh, “The K-Pulse Concept”, IEEE Transaction on Antennas and Propagation, vol. AP-29, pp. 327-331, March 1981.

[20] K.T.Kim, I.S.Choi, and H.T.Kim, “Efficient radar target classification using adaptive joint time-frequency processing”, IEEE Trans. Antennas Propagat., vol. 48, no. 12, pp. 1789-1801, Dec. 2000.

[21] Xi Miao; Azimi-Sadjadi, M.R.; Bin Tan; Dubey, A.C.; Witherspoon “Detection of mines and mine-like targets using principal component and neural-network methods”, Neural Networks, IEEE Transactions on, Volume: 9, Issue: 3, May 1998 Pages:454 – 463.

[22] Jouny.I, Garber.F.D, Ahalt,S.C “Classification of radar targets using synthetic neural networks”, Aerospace and Electronic Systems, IEEE Transactions on , Volume: 29 , Issue: 2 , April 1993 Pages:336 – 344.

[23] Azimi-Sadjadi.M.R, De Yao, QiangHuang, Dobeck.G.J, “Underwater target classification using wavelet packets and neural networks”, Neural Networks, IEEE Transactions on , Volume: 11 , Issue: 3 , May 2000 Pages:784 – 794.

[24] C. E. Baum, E.J. Rothwell, K.M. Chen, et al., "The singularity expansion method and its application to target identification," Proc. IEEE vol. 79, no.10, pp.1481-1492, 1991.

[25] E.M. Kennaugh, D.L. Moffatt, "Transient and impulse response approximations," Proc. IEEE vol. 53, no.8, pp. 893-901, Aug. 1965.

[26] P. Ilavarasan, E.J. Rothwell, K.M. Chen and D.P. Nyquist, "Natural resonance extraction from multiple data sets using physical constraints," Radio Science, vol.29, no.1, pp.1-7, Jan.1994.

[27] C. Chen and L. Peters, "Buried unexploded ordnance identification via complex natural resonances," IEEE Trans. Antennas Propagat., vol.45, no.11, pp.1645-1654, Nov. 1997.

[28] C. Chen, "Electromagnetic resonances of immersed dielectric spheres," IEEE Trans. Antennas Propagat., vol. 46, no.7, pp. 1074-1083, July 1998.

[29] H.T. Kim, N.Wang and D.L. Moffatt, "K-pulse for a thin circular loop," IEEE Trans. Antennas Propagat., vol.33, no.12, pp. 1403-1407, Dec. 1985.

[30] F.Y.S. Fok, D.L. Moffatt and N. Wang, "K-pulse estimation from the impulse response of a target," IEEE Trans. Antennas Propagat., vol.35, no.8, Aug. 1987.

[31] K.M. Chen, D.P. Nyquist, E.J. Rothwell, L.L. Webb and B. Drachman,"Radar target discrimination by convolution of radar returns with extinction pulses and single-mode extraction signals," IEEE Trans. Antennas Propagat., vol.34, no.7, pp.896-904, July 1986.

[32] F. Hlawatsch and G.F. Boudreaux-Bartels, "Linear and quadratic time-frequency signal representations," IEEE Signal Processing Mag., vol. 9, no. 2, pp. 21-67, Apr. 1992.

[33] J. E. Jackson, A User's Guide to Principal Components. New York: John Wiley & Sons, Inc., 1991.

[34] M. Kerker, The Scattering of Light, and Other Electromagnetic Radiation. New York: Academic Press, 1969.

[35] C.E.Baum, “Toward an engineering theory of electromagnetic scattering: the singularity and eigenmode expansion methods”, in: P.L.E. Uslenghi (Ed.), Transient Electromagnetic Fields, Academic Press, New York, 1978 (Chapter 15).

[36] Baum,C.E. “Signature-based target identification and pattern recognition”, Antennas and Propagation Magazine, IEEE ,Volume: 36, Issue: 3 , Jun 1994 Pages:44 – 51.

[37] L. Cohen, Time–Frequency Analysis, Prentice-Hall, Englewood CliBs, NJ, 1995.